PREPARATION AND THERMOCHEMICAL PROPERTIES OF ALKALI-METAL DIURANATES (VI) AND DINEPTUNATES (VI)

Austin Ian Judge

(Ph.D. Thesis)

1985

PREPARATION AND THERMOCHEMICAL PROPERTIES OF ALKALI-METAL DIURANATES (VI) AND DINEPTUNATES (VI)

CONTENTS

List of Tables

List of Figures

PREPARATION AND THERMOCHEMICAL PROPERTIES OF ALKALI-METAL DIURANATES (VI) AND DINEPTUNATES (VI)

Austin Ian Judge

(Ph.D. Thesis)

Department of Chemistry
University of Leicester
Leicester LE1 7RH

1985

A B S T R A C T

Alkali-metal diuranates (VI) and dineptunates (VI) have been prepared by controlled thermal decomposition of well-characterised alkali-metal uranyl (VI) and neptunyl (VI) triacetates having the desired stoicheiometric alkali-metal to actinide ratio. The compounds in the series $M^{I}_2M^{VI}_2O_7$ (M^{I} = Na - Cs incl., M^{VI} = U or Np) have been obtained in this way. This preparative method failed to provide further evidence for the existence of the controversial ternary oxide, $Li_2U_2O_7$. Isolation of the analogous neptunium complex, $Li_2Np_2O_7$, was not achieved.

Enthalpies of formation have been derived from the enthalpies of solution in 1 mol dm^{-3}HCl and auxiliary thermodynamic data.

The values for $Na_2U_2O_7$ and $Cs_2U_2O_7$ are in good agreement with those assessed by Cordfunke and O'Hare and thus confirm the reliability of the method of preparation of such mixed oxides, as compared to the 'classical' methods which involve heating an actinide oxide with an alkali-metal binary oxide, nitrate or carbonate. The values for $K_2U_2O_7$ and $Rb_2U_2O_7$ are previously unreported.

Confirmation of an earlier assessment of the enthalpy of formation of $Na_2Np_2O_7$ and preliminary values for the enthalpies of formation of $K_2Np_2O_7$, $Rb_2Np_2O_7$ and $Cs_2Np_2O_7$ have been obtained.

ACKNOWLEDGEMENTS

First and foremost I would like to thank Dr. David Brown, Prof. Jean Fuger and Dr. John Holloway for their expert supervision and encouragement during my research and thesis preparation.

Additionally, thanks are due to the many people who provided excellent technical tuition and support at both the Chemistry Division, A.E.R.E. Harwell and the Radiochemical Centre of the University of Liege. To Mr. Roger Wiltshire and Dr. Brian Whittaker and their staff for invaluable help and encouragement, often over cups of tea but specifically with α-spectrometry. M. Watelet and M. Robert Gens for much assistance particularly with the calorimetric measurements. Mr. Neville Bridger for d.t.a and t.g.a. studies. Mr. Brian Bellamy for guidance in Guinier X-ray powder diffraction techniques. Messrs. Frank Birks, Alan Morton, Steve Firkin and Denzil Brown for alkali-metal analyses. Mr. John Pollock and his Health-Physics staff for excellent safety support throughout my years at Harwell. Mrs. Margaret Johnson and the staff of Type & Print for their tremendous efforts slaving over typewriters.

I would also like to thank Dr. John Berry, Mr. Martin Plews and Mr. Paul Stone who had the misfortune of having to share an office and laboratory with me but who were nevertheless an unending source of assistance and humour. Special thanks are due to Dr. Tze Chung Tso who guided my first faltering steps into the field of Actinide Chemistry and provided such an excellent example in the laboratory. I am also endebted to him for his patience in explaining many experimental techniques.

Penultimately, I acknowledge with thanks the financial support of the S.E.R.C., who provided me with a C.A.S.E. award, and the Chemistry Division, A.E.R.E. Harwell.

Finally, many thanks go to my wife, Yvette, for looking after me whilst I struggled through my thesis preparation and without whose encouragement and support this may never have been completed.

1. INTRODUCTION

1.1 THE ACTINIDE ELEMENTS

The actinide series comprises the fourteen elements following actinium in the Periodic Table. The increase in atomic number from 89 to 103 corresponds to the progressive filling of the 5f orbital shell. This is analogous to the lanthanide series where the 4f shell is progressively filled. An indication of the similarities between the actinide elements and their lanthanide counterparts is illustrated by comparing their respective gaseous state electronic configurations. These configurations, which result mainly from the interpretation of electronic spectra, are listed in Table 1:1.

Although most of the later actinides have a stable oxidation state of +3 in aqueous solution, as do the lanthanides, the earlier actinides exhibit a variety of oxidation states. The stability of the +3 oxidation state is not due to a common electronic configuration but depends on thermodynamic factors. These being that, in aqueous solution, the difference between the enthalpies of hydration of the tripositive and dipositive ions is numerically greater than the third ionization potential whilst the fourth ionization potential is numerically greater than the difference between the enthalpies of hydration of the tetrapositive and tripositive ions.

Table 1:1 Electronic Configurations for Gaseous Atoms of the Lanthanide and Actinide Elements[1]

Lanthanide Series					Actinide Series				
Z	Symbol	Electronic Configuration *a*			Z	Symbol	Electronic Configuration *b*		
57	La		$5d^1$	$6s^2$	89	Ac		$6d^1$	$7s^2$
58	Ce	$4f^1$	$5d^1$	$6s^2$	90	Th		$6d^2$	$7s^2$
59	Pr	$4f^3$		$6s^2$	91	Pa	$5f^2$	$6d^1$	$7s^2$
60	Nd	$4f^4$		$6s^2$	92	U	$5f^3$	$6d^1$	$7s^2$
61	Pm	$4f^5$		$6s^2$	93	Np	$5f^4$	$6d^1$	$7s^2$
62	Sm	$4f^6$		$6s^2$	94	Pu	$5f^6$		$7s^2$
63	Eu	$4f^7$		$6s^2$	95	Am	$5f^7$		$7s^2$
64	Gd	$4f^7$	$5d^1$	$6s^2$	96	Cm	$5f^7$	$6d^1$	$7s^2$
65	Tb	$4f^9$		$6s^2$	97	Bk	$5f^8$	$6d^1$	$7s^2$
66	Dy	$4f^{10}$		$6s^2$	98	Cf	$5f^{10}$		$7s^2$
67	Ho	$4f^{11}$		$6s^2$	99	Es	$5f^{11}$		$7s^2$
68	Er	$4f^{12}$		$6s^2$	100	Fm	$5f^{12}$		$7s^2$
69	Tm	$4f^{13}$		$6s^2$	101	Md	$5f^{13}$		$7s^2$
70	Yb	$4f^{14}$		$6s^2$	102	No	$5f^{14}$		$7s^2$
71	Lu	$4f^{14}$	$5d^1$	$6s^2$	103	Lr	$5f^{14}$	$6d^1$	$7s^2$

a plus xenon (Xe) core: $1s^2 2s^2 2p^6 3s^2 3p^6 3d^{10} 4s^2 4p^6 4d^{10} 5s^2 5p^6$
b plus radon (Ra) core: $1s^2 2s^2 2p^6 3s^2 3p^6 3d^{10} 4s^2 4p^6 4d^{10} 5s^2 5p^6 5d^{10} 6s^2 6p^6$

The variety of oxidation states exhibited by the actinides up to and including americium, as shown in Table 1:2, can be explained in two ways. Firstly, based on the assumption that the differences in ionization potential between the 4f and 5f series are similar to those between the 3d and 4d transition elements, it is possible that the effective nuclear charge experienced by the 5f electrons of actinides at the start of the series is less than that experienced by the analogous 4f electrons in the lanthanides. This effect decreases with increasing atomic number due to the actinide contraction, this being a contraction of the whole f shell caused by poor screening of one f electron by another. Secondly, because of the almost comparable energies of the 5f, 6d, 7s and 7p orbitals and their spatial overlap it is possible that bonding can involve any or all of these orbitals thus allowing complex formation.

Table 1:2 Oxidation States *a* for the Elements Thorium to Americium

Th	Pa	U	Np	Pu	Am
					2
	3	3	3	3	*3*
4	4	4	4	*4*	4
	5	5	*5*	5	5
		6	6	6	6
			7	7	

a The most stable oxidation states in aqueous solution are given in italics.

It should be noted that although the common oxidation state for most of the later actinides in aqueous solution is +3, as previously discussed, the stable oxidation state of nobelium is the dipositive state, presumably due to the filled f shell electron configuration of the No^{2+} ion.

All the known isotopes of the actinide elements are radioactive and the consequences of this in connection with this work are discussed in Section 2:1.

1:2 ACTINIDE OXIDE USE AND RESEARCH

A considerable amount of research into the actinide elements and their compounds was stimulated by the development of early atomic weapons and also

the development of electricity generation by nuclear fission.

Today an important technological use of oxides of two actinides, uranium and plutonium, is as nuclear fuels. With respect to the safe operation of nuclear power stations it is necessary to have as complete an understanding of these materials and their properties as possible.

One of the chemical problems arising from the use of actinide oxides as nuclear fuels is the potential formation of complex oxides[2] during burn up of these fuels as a result of their reaction either with fission products such as caesium[3] and strontium or with coolant or cladding materials such as sodium, chronium and zirconium. With this in mind, it is perhaps not surprising that research has been carried out to determine accurate thermodunamic data for actinide mixed oxide systems such as Na/U/O, Cs/U/O and U/Pu/O.

A particular area of interest is that of the liquid metal fast breeder reactor (LMFBR) which has a mixed uranium-plutonium oxide fuel. The typical composition for the fuel in the Prototype Fast Reactor (PFR) is $U_{0.7}Pu_{0.3}O_{1.98}$ which, in the form of dense pellets, is stacked as a column between upper and lower axial breeder regions of uranium dioxide pellets and packed within a stainless steel fuel pin. The reactor core contains many of these fuel pins. Liquid sodium coolant flows over the fuel pins at temperatures around 400-640°C and thus provides a highly corrosive environment within the reactor core. The chemical interaction of this sodium with the fuel oxide following a breach in the stainless steel cladding of a fuel pin (possibly caused by the formation of a low density caesium uranium oxide) could lead to the formation of low density compled sodium/uranium/plutonium oxides. This could, in turn, cause more fuel swelling and result in further clad failure and reaction. Sufficient interaction to cause interference of the sodium flow over adjacent fuel pins could lead to overheating and failure propagation. The enlargement of defects in the fuel pin cladding may lead to deposition of highly radioactive fission products in the cooler regions of the primary cooling circuit.

With respect to fuel pellet packing, as a contribution to the prevention of cladding failure and in particular, to determine how long a failed fuel pin can remain in the reactor core it is important to understand the thermodynamics and kinetics of these potential chemical interactions. A study into the reactions of sodium with urania and urania-plutonia solid

solutions has recently been carried out at Harwell[4].

However, from a purely scientific viewpoint the interesting range of properties exhibited by complex actinide oxides has stimulated research into the oxide systems of the actinide elements in general[5-12].

Owing to the availability and low radioactivity of thorium and uranium compared with the other actinides much early work involved studies with these elements and their compounds. Consequently, information for uranium-bearing materials in particular predominates. More recently with the increased availability of, and development of suitable handling techniques for the rarer and more radioactive actinides, the complex oxides of these elements are being investigated more fully. Several reviews are available dealing with complex thorium oxides[5,6], complex uranium oxides[6,7,8,9] and those of the transuranium elements[6,7,10]. A summary of the thermodynamic properties of several complex uranates[11] is available as part of a series of publications dealing with the chemical thermodynamics of actinide elements and compounds. Recent research on the structural, thermodynamic, magnetic and spectroscopic properties of ternary and other complex oxides containing actinide ions has also been reviewed[12].

1:3 BINARY OXIDES

Binary oxides are known for the elements actinium to einsteinium. Probably the most important actinide oxide system and certainly one of the most complex known is that of uranium. Dioxides, MO_2, are known for the elements thorium to californium and all have the fluorite structure. With the exception of ThO_2, these dioxides either lose or gain oxygen to form substoicheiometric oxides MO_{2-x} (for U, Pu, Am, Cm) or superstoicheiometric oxides MO_{2+x} (for Pa, U).

Although the actinide elements up to and including americium exist in a wide variety of oxidation states (Section 1:1) in solution and in complexes, it has been found that many accessible oxidation states (eg U^{3+}, Np^{6+}, Np^{7+}, Am^{5+}) are not exhibited by binary oxides. The well characterised binary oxides are tabulated in Table 1:3. Crystal structures of all these oxides are known and these are presented along with the enthalpies of formation, where these values are available, in Tables 1:4 to 1:8.

Table 1:3 - Well Characterised Binary Actinide Oxides

Oxidation State	Actinide Metal									
	Ac	Th	Pa	U	Np	Pu	Am	Cm	Bk	Cf
III	Ac_2O_3 ($AcO_{1.5}$)					Pu_2O_3 ($PuO_{1.5}$) $PuO_{1.61}$	Am_2O_3 ($AmO_{1.5}$)	Cm_2O_3 ($CmO_{1.5}$)	Bk_2O_3 ($BkO_{1.5}$)	Cf_2O_3 ($CfO_{1.5}$) Cf_7O_{12} ($CfO_{1.714}$)
IV		ThO_2	PaO_2	UO_2 U_4O_9 ($UO_{2.25}$) U_3O_7 ($UO_{2.33}$)	NpO_2	PuO_2	AmO_2	CmO_2	BkO_2	CfO_2
V			Pa_2O_5 ($PaO_{2.5}$)		Np_2O_5 ($NpO_{2.5}$)					
VI				U_3O_8 ($UO_{2.67}$) UO_3	Np_3O_8 ($NpO_{2.67}$)					

Table 1:4 - Actinium, Thorium and Protactinium Binary Oxides

Oxide	Lattice Type	Space Group	Lattice Parameters			Ref	Enthalpy of Formation ($kJ\ mol^{-1}$)	Ref
			a(Å)	c(Å)	α(°)			
Ac_2O_3	Hexagonal		4.07	6.29		13		
ThO_2	Cubic	Fm3m	5.5971			14	-1226.4 ± 3.5	15
PaO_2	Cubic					16,17		
Pa_2O_5	Cubic		5.446			16		
	Tetragonal		5.429	5.503		17		
	Hexagonal		3.817	13.220		17		
	Rhomohedral		5.424		89.76	17		

Table 1:5 - Uranium Binary Oxides

Oxide	Lattice Type	Space Group	Lattice Parameters						Ref	Enthalpy of Formation (kJ mol^{-1})	Ref
			a(Å)	b(Å)	c(Å)	α(°)	β(°)	γ(°)			
UO_2	Cubic	Fm3m	5.468						18	-1085.0 ± 1.0	15
α-U_4O_9	Pseudocubic		n5.4338						19	-1127.6 ± 1.2	20
β-U_4O_9	Cubic	$I\bar{4}3d$	n5.4338						19		
α-U_3O_7	Tetragonal		5.46		5.40				21		
β-U_3O_7	Tetragonal		5.388		5.561				22	-1142.4 ± 0.9	20
α-U_3O_8	Orthorhombic	C2mm	6.716	11.960	4.1469				23		
β-U_3O_8	Orthorhombic	Cmcm	7.069	11.445	8.303				23	-1191.6 ± 0.8	15
γ-UO_3	Orthorhombic	Fddd	9.813	19.93	9.711				24	-1223.8 ± 2.0	15
α-UO_3	Orthorhombic	C2mm	3.913	6.936	4.167				25*a*		
β-UO_3	Monoclinic	$P2_1$	10.34	14.33	3.910		99.03		26		
δ-UO_3	Cubic		4.146						27*b*		
ε-UO_3	Triclinic		4.002	3.841	4.165	98.10	90.20	120.17	28		
ξ-UO_3	Orthorhombic	$P2_12_12_1$	7.511	5.466					29		

a α-UO_3 is described as an imperfectly crystalline form of orthorhombic $UO_{2.9}$

b δ-UO_3 is also described as $UO_{2.82}$

Table 1:6 - Neptunium and Plutonium Binary Oxides

Oxide	Lattice Type	Space Group	Lattice Parameters				Ref	Enthalpy of Formation ($kJ\ mol^{-1}$)	Ref
			a(Å)	b(Å)	c(Å)	β(°)			
NpO_2	Cubic	Fm3m	5.434				30	-1074.0 ± 2.5	31
Np_2O_5	Monoclinic	$P2_1/a$	4.183	6.584	4.086	90.32	32		
Np_3O_8	Orthorhombic	C2mm	6.584	4.086	4.183		33		
β-Pu_2O_3 (A-Pu_2O_3)	Hexagonal	$P\bar{3}m1$	3.841		5.958		34	-842.5 ± ±0.4	35
C-Pu_2O_3	Cubic	Ia3	11.04				34		
$PuO_{1.62+x}$ (α- or C′-Pu_2O_3) ($PuO_{1.62-1.69}$)	Cubic	Ia3	11.00-11.03				36	-884.5 ± 16.7	35
PuO_2	Cubic	Fm3m	5.3960				37	-1056.2 ± 0.7	38

Table 1:7 - Americium and Curium Binary Oxides

Oxide	Lattice Type	Space Group	Lattice Parameters				Ref	Enthalpy of Formation ($kJ\ mol^{-1}$)	Ref
			a(Å)	b(Å)	c(Å)	β(°)			
$A\text{-}Am_2O_3$	Hexagonal	$P\bar{3}m1$	3.805		5.96		39		
$B\text{-}Am_2O_3$	Monoclinic	C2/m	14.38	3.52	8.92	100.4	39		
AmO_2	Cubic	Fm3m	5.376				40	-932.2 ± 2.7	41
$A\text{-}Cm_2O_3$	Hexagonal	$P\bar{3}m1$	3.845		6.092		42		
$B\text{-}Cm_2O_3$	Monoclinic	C2/m	14.276	3.656	8.913	100.39	42	-841.5 ± 6.0	43
$C\text{-}Cm_2O_3$	Cubic	Ia3	10.99				42,44		
CmO_2	Cubic	Fm3m	5.357				42	-911 ± 6	43

Table 1:8 - Berkelium and Californium Binary Oxides

Oxide	Lattice Type	Space Group	Lattice Parameters					Ref
			a(Å)	b(Å)	c(Å)	α(°)	β(°)	
$A\text{-}Bk_2O_3$	Hexagonal	$P\bar{3}m1$	3.754		5.958			45
$B\text{-}Bk_2O_3$	Monoclinic	C2/m	14.197	3.606	8.846		100.23	45
$C\text{-}Bk_2O_3$	Cubic	Ia3	10.880					46
BkO_2	Cubic	Fm3m	5.334					46
$A\text{-}Cf_2O_3$	Hexagonal	$P\bar{3}m1$	3.72		5.96			45
$B\text{-}Cf_2O_3$	Monoclinic	C2/m	14.124	3.591	8.809		100.31	47
$C\text{-}Cf_2O_3$	Cubic	Ia3	10.838					48
Cf_7O_{12}	Rhombohedral		6.596			99.40		49
CfO_2	Cubic	Fm3m	5.310					50

1:3:1 Actinium Oxide

The sesquioxide, Ac_2O_3, is the only known oxide of actinium. It has been prepared by thermal decomposition of the oxalate, $Ac_2(C_2O_4)_3 . aq.$, at 110°C [13].

1:3:2 Thorium Oxides

The dioxide of thorium, ThO_2, is commonly prepared by the thermal decomposition of the oxalate, $Th(C_2O_4)_2 . 6H_2O$, at 800-1200°C. The monoxide has been reported as a metastable product formed during the decomposition in vacuo at 800°C of the residue remaining after dissolution of thorium metal in HCl [51].

1:3:3 Protactinium Oxides

A monoxide, PaO, identified by X-ray crystallography has been reported to form as a film on protactinium metal [16]. However, this has not been obtained pure and its existence is still in doubt.

The dioxide, PaO_2, can be obtained by hydrogen reduction of Pa_2O_5 at 1550°C [16,17], by carbothermic reduction of Pa_2O_5 at 1100°C [52] and as one product of the vacuum thermal disproportionation of $PaOCl_2$ above 550°C [53, 54].

Four intermediate oxide phases in the PaO_2-Pa_2O_5 region have been identified by X-ray powder diffraction methods [17]. These phases, $PaO_{2.18}$-$PaO_{2.20}$, $PaO_{2.33}$, $PaO_{2.40}$-$PaO_{2.42}$ and $PaO_{2.42}$ - $PaO_{2.44}$ were prepared by hydrogen reduction of Pa_2O_5 and by oxidation of PaO_2.

The pentoxide, Pa_2O_5, is obtained by heating the hydrated oxide, $Pa_2O_5.aq.$, or a variety of other binary protactinium compounds, in air or oxygen to above 650°C, or by heating protactinium metal in oxygen at 300-500°C [55]. At least four different temperature dependent crystal modifications exist (Table 1:4). Cubic-Pa_2O_5 has been observed in the range 500-700°C [16], tetragonal-Pa_2O_5 in the range 700-1000°C, the hexagonal phase in the range 1075-1500°C and the rhombohedral form above 1240°C [17].

1:3:4 Uranium Oxides

The uranium-oxygen system is very complex and in addition to the well characterised binary oxides (Table 1:5) there are numerous intermediate phases.

The dioxide, UO_2, is obtained on reduction of the higher uranium oxides at around 1000°C. Under high vacuum at temperatures above 1800°C [56] this dioxide loses oxygen to form substoicheiometric UO_{2-x} phases which, on cooling, decompose to UO_2 and metallic uranium. These phases, which are best prepared by reactions between UO_2 and uranium metal, range in substoicheiometry from $UO_{1.994}$ at 1200°C through $UO_{1.7}$ at 2300°C to $UO_{1.65}$ at 2425°C.

A superstoicheiometric phase UO_{2+x}, with x ranging from zero at 300°C through 0.17 at 900°C to about 0.28 at 1600°C [57], exhibits a disordered fluorite structure which passes to the ordered U_4O_{9-y} phase at $UO_{2.23}$. Oxidation of single crystal films of UO_2 between 500°C and 750°C produces metastable $UO_{2.19}$, which is further oxidised at higher temperatures, up to 1123°C [58] where three oxides, UO_{2-x}, U_4O_{9-y} and $UO_{2.61}$, are in equilibrium.

Three modifications of U_4O_9 are known, α-U_4O_9 is formed at temperatures below 65°C, the beta phase forms between 65°C and 560°C [59] and at temperatures between 560°C and 1123 γ-U_4O_9 is produced

Below 550°C two intermediate phases exist in the $UO_{2.25}$-$UO_{2.6}$ region with structures which can be derived from the fluorite structure. The phase below 400°C has an oxygen to uranium ratio of 2.33-2.38 and decomposes above this temperature to a second phase with an oxygen to uranium ratio of $2.30 \leqq O:U \leqq 2.35$, (and $UO_{2.61}$) which in turn passes to U_4O_9 and $UO_{2.61}$ at 550°C.

The oxidation and thermal decomposition of all uranium oxides, in air or oxygen at normal pressure and at 800-900°C, yields U_3O_8 ($U^{V}_2U^{VI}O_8$), a phenomenon which allows this oxide to be used as the basis for the gravimetric determination of uranium (Section 2.11.1). Heating UO_2 in air or oxygen produces U_3O_8 via the intermediates UO_{2+x}, U_4O_9 and U_3O_7. There are two modifications of U_3O_8, the stoicheiometric α-form and the

slightly non-stoicheiometric high temperature β-U_3O_8, often designated $UO_{2.61}$.

At high pressures U_2O_5 has been detected [60]. This has three modifications, α-U_2O_5 at 500°C and 1.5 GPa, β-U_2O_5 at above 800°C and 4-5GPa and γ-U_2O_5 at 800°C above 6 GPa. The alpha or beta modifications form as U_3O_8 disproportionates at elevated pressures, and ξ-UO_3 is produced as the other product.

Six crystal modifications and one amorphous form are known for the trioxide, UO_3. The preparative methods are presented in Table 1.9. Gamma-UO_3 is the most stable modification of the trioxide and at 650°C and an oxygen pressure of 4.053 MPa *(40 atm)* all modifications are converted to this form. At normal pressure all crystalline modifications (with the exception of amorphous UO_3 which gives the intermediate $UO_{2.9}$ [61]) decompose to U_3O_8, γ-UO_3 decomposing at 650-690°C.

Table 1:9 - Preparative Conditions for the Uranium Trioxide Phases [61]

Form	Method	Temp (°C)
Amorphous	Thermal decomposition of $UO_4 . 2H_2O$, $UO_3.2H_2O$, $UO_2C_2O_4.3H_2O$ or $(NH_4)\ UO_2(CO_3)_3$	400
Alpha [a]	i) Amorphous UO_3 heated under an oxygen pressure of 4.053 MPa	470-500
	ii) Thermal decomposition of unwashed $UO_4.2H_2O$	525-575
Beta	i) U_3O_8 heated in 4.053MPa oxygen	500-550
	ii) Thermal decomposition of $(NH_4)_2\ U_7O_{22}$ in air	500
Gamma	i) Thermal decomposition of $UO_2(NO_3)_2.6H_2O$ in air	400-600
	ii) Heating α-, β-, δ-, ξ- and amorphous UO_3 under 4.053 MPa oxygen.	650
Delta	Thermal decomposition of β-$UO_3.H_2O$ in air above 24 hours	375
Epsilon [b]	Heating U_3O_8 in NO_2	250-375

a Reported to be an imperfectly crystalline form of orthorhombic $UO_{2.9}$ [25]

b ξ-UO_3 is a high pressure modification

1:3:5 Neptunium Oxides

The most stable oxide of neptunium is the dioxide, NpO_2, which is prepared by the thermal decomposition of various neptunium compounds, such as the hydroxide, oxalate and nitrate hydrates, at 600-1000°C. Owing to its stability, NpO_2 can be used as the basis for the gravimetric determination of neptunium.

The pentoxide, Np_2O_5, forms on thermal decomposition of $NpO_3.H_2O$ under a vacuum between 300 and 420°C [62]. It has also been prepared by bubbling ozone through molten $LiClO_4$ containing neptunium as the NpO_2^+ ion and by the reaction of neptunium metal with lithium perchlorate [32]. The precipitate formed on dissolution of the $LiClO_4$ melts in water, after drying at 100°C,

corresponds to the composition Np_2O_5.

Np_3O_8 and a probable single phase region in the $NpO_{2.50}$ - $NpO_{2.57}$ (Np_2O_5 - Np_3O_8) range have been reported [63]. Oxidation of neptunium (IV) or (V) hydroxide by air or NO_2 at 300-400°C or thermal decomposition of ammonium dineptunate (VI) hydrate in air at 275°C yields Np_3O_8.

Two trioxide hydrates of neptunium, $NpO_3.2H_2O$ and $NpO_3.H_2O$, have been reported [62]. These di- and mono-hydrates are prepared by ozone oxidation of aqueous suspensions of neptunium (V) hydroxide at 18 and 90°C respectively. Reddish-brown $NpO_3.H_2O$ is sufficiently stable to be dried in air at 100-105°C. The standard enthalpy of formation of the monohydrate has been determined and recalculated [11] to give the value, $\Delta H_f^{\ominus}$ ($NpO_3.H_2O$,s) = -1379.0 ± 4.6 kJ mol^{-1}.

1:3:6 Plutonium Oxides

The monoxide, PuO, possibly obtained as a surface layer on plutonium metal, has been shown to exist in the gaseous state by mass spectrometry [64].

The reduction of PuO_2 with carbon or metallic plutonium [65] produces the strictly stoicheiometric β-Pu_2O_3 (A-Pu_2O_3). The cubic sesquioxides C-Pu_2O_3 and C′-Pu_2O_3, which have actual compositions of $PuO_{1.52}$ and $PuO_{1.62}$ +x, respectively, are obtained by the reduction of PuO_2 with carbon or hydrogen at high temperatures. C′-Pu_2O_3 is only stable at temperatures above 300°C and its phase width increases with temperature from $PuO_{1.62-1.63}$ at 350°C to the constant $PuO_{1.62-1.69}$ above 600°C [66].

The stoicheiometric dioxide, PuO_2, is prepared by heating plutonium (IV) peroxide, oxalate, hydroxide or nitrate in a stream of oxygen at 800-1000°C. PuO can not be oxidised but, at temperatures above 1400°C, oxygen is lost and substoicheiometric oxides, PuO_2-x, are formed. The cubic, fluorite structured, substoicheiometric oxide $PuO_{1.98}$ has a lattice parameter of 5.3967 Å.

1:3:7 Americium Oxides

Black americium monoxide, AmO, forms on the surface of americium metal and is obtained in pure form by the reaction of the metal with the stoicheiometric quantity of oxygen, generated from Ag_2O, at 850°C over several days [67].

The sesquioxides C-$AmO_{1.5}$(+x) ($AmO_{1.50-1.59}$), A-Am_2O_3 and B-Am_2O_3 can be prepared by hydrogen reduction of the dioxide. Cubic C-$AmO_{1.5}$(+x) is formed

below 450°C, hexagonal A-Am_2O_3 at 850°C and the high temperature modification, monoclinic B-Am_2O_3, is obtained on rapid cooling from 800°C[39]. C-$AmO_{1.5}$ (+x) is stable at room temperature but, on heating to above 350°C, uptake of oxygen occurs with the formation of another cubic sesquioxide, C′-Am_2O_3 ($AmO_{1.62-1.68}$).

The dark brown dioxide AmO_2 is prepared by the thermal decomposition of americium oxalate or hydroxide at 700-800°C in oxygen. When AmO_2 is heated to temperatures above 1000°C the substoicheiometric phase AmO_2-x is observed[68].

1:3:8 Curium Oxides

Five modifications are known for curium sesquioxide. At 600-700°C, under high vacuum or by reduction with hydrogen, CmO_2 produces metastable, cubic C-Cm_2O_3, which can incorporate an excess of oxygen into the lattice to form the δ-phase, $CmO_{1.5}$ +x, which is of variable composition between $CmO_{1.54}$ and $CmO_{1.62}$, without a change in structure[70]. Decomposition at 900°C in air yields the monoclinic B-Cm_2O_3, having the composition $CmO_{1.498\pm0.005}$, which is thermodynamically stable at room temperature. At 1615°C C-Cm_2O_3 transforms reversibly into the hexagonal A-Cm_2O_3[71] and two additional, reversible, solid state transformations occur at 2000°C and 2110°C to yield the phases designated H-Cm_2O_3 and X-Cm_2O_3, respectively[72].

Owing to internal α-radiolysis, cubic C-Cm_2O_3 transforms spontaneously into hexagonal A-Cm_2O_5 within a few weeks[73]. A-Cm_2O_3 transforms to B-Cm_2O_3 at 800°C[74].

At temperatures between 320°C and 350°C, even under an oxygen pressure of 0.1MPa, CmO_2 loses oxygen, and passes through the α-phase, CmO_2-x, in its conversion to the δ-phase, $CmO_{1.82}$[69] ($CmO_{1.821}$-$CmO_{1.849}$). At still higher temperatures, around 500°C, the τ-phase is formed with the composition $CmO_{1.721}$; this is stable up to 1000°C. Since CmO_2 is not stable above 300°C, the preparation of curium dioxide by ignition of the hydroxide, oxalate or sesquioxide at 500-600°C must involve re-oxidation on cooling. The black oxide prepared in this way is, in fact, substoicheiometric, having a lattice parameter corresponding to a composition of $CmO_{1.98}$. The black stoicheiometric curium dioxide, CmO_2, is formed on oxidation of lower curium oxides at around 300°C in oxygen.

1:3:9 Berkelium Oxides

Hydrogen reduction of berkelium dioxide at 600°C for one hour yields the cubic sesquioxide, C-Bk_2O_3, which reverts to the dioxide on re-oxidation in air at 600°C. In addition to the cubic sesquioxide, hexagonal A-Bk_2O_3 and monoclinic B-Bk_2O_3 have been reported[45]. The hexagonal modification is obtained on rapid cooling of berkelium oxides from high temperatures whilst the monoclinic form results from the slow cooling of cubic C-Bk_2O_3 heated to about 1200°C.

The first structural data for a berkelium compound, prepared on a very small scale, were reported in 1962. These data were for the product obtained on heating Bk^{3+}, adsorbed on a single ion-exchange resin bead, in air at 1200°C. The compound was reported to be BkO_2[75] and the results were later confirmed[76, 46].

1:3:10 Californium Oxides

The yellow, monoclinic, sesquioxide, B-Cf_2O_3, was first prepared by igniting $^{249}Cf^{3+}$ adsorbed on a single ion-exchange bead in air, followed by heating in a stream of hydrogen to 600°C [47]. The cubic sesquioxide. C-Cf_2O_3, is the product of the hydrolysis of CfOF or CfOCl at 500-600°C [48]. Rapid cooling of californium oxides from high temperatures yields the hexagonal modification, A-Cf_2O_3 [77,45].

Under an oxygen pressure of 10.133 MPa (100 atm) and with heating to 300°C, Cf_2O_3 is converted to the dioxide, CfO_2. The dioxide is also the product of the reaction of the sesquioxide with atomic oxygen [50].

A study of the californium / oxygen system [49], using as a starting material C-Cf_2O_3, prepared by decomposition of oxalate precipitates in oxygen at 1000°C, showed the existence of the phases $CfO_{1.5+x}$ ($x < 0.05$) and Cf_7O_{12}. These oxides were prepared by heating the sesquioxide up to 1000°C in partial pressures of oxygen up to 0.1MPa (1 atm). $CfO_{1.5+x}$ was obtained from oxides quenched in air from 800°C or heated and cooled in a vacuum of about 0.133 Pa (10^{-3} Torr). Slow cooling in air or 0.1MPa (1 atm) of oxygen produced the stable oxide Cf_7O_{12}

1:3:11 Einsteinium Oxides

A cubic sesquioxide of einsteinium, C-Es_2O_3, has been identified [77]. It crystallises in the space group Ia3 with a lattice parameter of 10.766Å. The oxide was prepared by evaporation of an einsteinium solution in 0.05 mol dm^{-3} nitric acid with subsequent calcining at 600-1000°C in 4% hydrogen/argon. Electron diffraction evidence has been obtained for monoclinic and hexagonal sesquioxide modifications but the structures were formed by self-irradiation rather than high temperature treatment [78].

1:4 TERNARY ACTINIDE OXIDES

In contrast with the binary oxides, which tend to exhibit the lower actinide oxidation states, the ternary actinide oxides exist in the higher states. In the well-studied alkali metal/actinide metal/oxygen systems the +6 oxidation state predominates. Although complexes do exist with penta-, tetra- and trivalent actinides, most of the tetravalent and trivalent examples are with alkaline earth metals and transition metals.

The stabilities of these complex oxides can be considered in two ways. Structurally, the co-ordination number of oxygen is increased from two or three (MO_3) or four (M_2O_3, MO_2) in the binary oxides, to six in the complex oxides. This is due to the presence of the second lower-valent cation which, despite the unchanged co-ordination about the actinide ion (six or eight), stabilises the oxide anion in such highly oxidised compounds as Na_4AmO_5 and Li_5NpO_6. Chemically, the formation of complex oxides can be considered as acid-base reactions based on the Lux [79]-Flood [80] model in that an oxide ion is transferred from a basic oxide (eg Li_2O) to an acidic oxide (eg UO_3, PuO_2). This results in the replacement of bridged oxygen atoms by terminal oxygen atoms, which are co-ordinated to one or two highly charged (acidic) cations and, in addition, to several other cations.

As the main subjects of this work are alkali metal uranates (VI) and neptunates (VI) the following sections will concentrate on alkali metal actinide oxides. However, mention will be made of other known complex oxides of the actinide metals.

Table 1:10 to 1:20 present the well established alkali-metal actinide ternary oxides with their crystal structures and enthalpies of formation where these values are available.

Table 1:10 - Alkali Metal Thorates and Protactinates

Oxide	Lattice Type	Space Group	Lattice Parameters					Z	Ref
			a(Å)	b(Å)	c(Å)	α(°)	β(°)		
Na_2ThO_3	Monoclinic		6.16	10.23	6.07		112.4	4	81
K_2ThO_3	Monoclinic	C2/c	6.41	11.09	12.72		99.40	8	82
	Hexagonal		3.70		18.77			2	81
Rb_2ThO_3	Hexagonal		3.75		19.70			2	83
$LiPaO_3$	x-ray powder data not indexed								84
$NaPaO_3$	Orthorhombic	Pbnm	5.82	5.97	8.36			4	84
$KPaO_3$	Cubic	Pm3n	4.341					1	6
$RbPaO_3$	Cubic	Pm3n	4.368					1	6
$CsPaO_3$	x-ray powder data not indexed								85
Li_3PaO_4	Tetragonal		4.52		8.48			2	84
Na_3PaO_4	Tetragonal		6.865		9.598			2	84
Li_7PaO_6	Rhombohedral		6.18			53.40		3	84

Table 1:11 - Alkali Metal Uranates (V)

Oxide	Lattice Type	Space Group	Lattice Parameters				Z	Ref	Enthalpy of Formation ($kJ\ mol^{-1}$)	Ref
			a(Å)	b(Å)	c(Å)	α(°)				
$LiUO_3$	Rhombohedral	R3c	5.901			54.60	1	7	-1522.1 ± 1.7	86
$NaUO_3$	Orthorhombic	Pbnm	5.776	5.910	8.283		4	7	-1494.6 ± 1.6	86
KUO_3	Cubic	Pm3m	4.290				1	7	-1522.9 ± 1.6	86
$RbUO_3$	Cubic	Pm3m	4.323				1	7	-1520.9 ± 1.7	86
Li_3UO_4	Tetragonal		4.49		8.46		2	84		
Na_3UO_4	Cubic	Fd3m	9.574				4	87	-2027 ± 4	11
$0.5Li_2O.U_2O_5$	Cubic		10.70					88		
Li_7UO_6	Rhombohedral		6.61			53.27	3	84		

Table 1:12 - Alkali Metal Uranates (VI) : $M^{I}{}_2UO_4$ and $M^{I}{}_2U_2O_7$

Oxide	Lattice Type	Space Group	Lattice Parameters				Z	Ref	Enthalpy of Formation ($kJ\ mol^{-1}$)	Ref
			a(Å)	b(Å)	c(Å)	β(°)				
$LiUO_4$	Orthorhombic	Pnma	10.547	6.065	5.134		4	89	-1971.9 ± 1.7	20
α-Na_2UO_4	Orthorhombic	Cmmm	9.769	5.734	3.498		2	7	-1897 ± 1	90
β-Na_2UO_4	Orthorhombic	Pccn Fmmm	5.979	5.807	11.724		4	7	-1886 ± 1	90
K_2UO_4	Tetragonal	I4/mmm	4.333		13.17		2	91	-1921.3 ± 1.7	20
Rb_2UO_4	Tetragonal	I4/mmm	4.354		13.86		2	91	-1923.0 ± 1.7	20,11
Cs_2UO_4	Tetragonal	I4/mmm	4.392		14.803		2	91	-1929	20
$Na_2U_2O_7$	Monoclinic	C2/m	12.796	7.822	6.896	111.42	4	92,93	-3194.7 ± 1.4	86
$K_2U_2O_7$	Monoclinic	$P2_1/m$	6.925	7.973	6.992	109.62	2	94	-3250.4 ± 4.5	*a*
$Rb_2U_2O_7$	Monoclinic	$P2_1/m$	6.947	8.018	7.328	108.64	2	94	-3231.4 ± 4.3	*a*
α-$Cs_2U_2O_7$	Monoclinic	C2/m	14.528	4.264	7.605	112.93	2	95		
β-$Cs_2U_2O_7$	Monoclinic	C2/m	14.516	4.320	7.465	113.78	2	95	(-3220.2 ± 1.8 (-3226.3 ± 4.8	96 *a*
γ-$Cs_2U_2O_7$	Hexagonal	P6/mmc	4.108		14.646		4	95		

a Section 3.4.3

Table 1:13 - Alkali Metal Uranates (VI) : $M^{I}_2U_4O_{13}$, $M^{I}_2U_7O_{22}$, and $M^{I}_4UO_5$

Oxide	Lattice Type	Space Group	Lattice Parameters			Z	Ref	Enthalpy of Formation ($kJ\ mol^{-1}$)	Ref
			a(Å)	b(Å)	c(Å)				
$K_2U_4O_{13}$	Hexagonal	$P6_3/m$	14.307		13.998	8	94		
$Rb_2U_4O_{13}$	Hexagonal	$P6_3/m$	14.307		14.298	8	97		
$Cs_2U_4O_{13}$	Orthorhombic	Cmmm(?)	13.494	15.476	7.911	5	98		
$K_2U_7O_{22}$	Orthorhombic	Pbam	6.950	19.525	7.212	2	94		
$Rb_2U_7O_{22}$	Orthorhombic	Pbam	6.958	19.590	7.279	2	97		
$Cs_2U_7O_{22}$	Orthorhombic	Pbam	6.949	19.711	7.396	2	98		
Li_4UO_5	Tetragonal	I4/m	6.721		4.451	2	7	-2641	20
α-Na_4UO_5	Cubic(?)	Fm3m(?)	4.766			1	93	-2451	11,90
β-Na_4UO_5	Tetragonal	I4/m	7.536		4.630	2	7	-2310 ± 10	90

Table 1:14 - Miscellaneous Alkali Metal Uranates (VI)

Oxide	Lattice Type	Space Group	Lattice Parameters						Z	Ref	Enthalpy of Formation ($kJ\ mol^{-1}$)	Ref
			a(Å)	b(Å)	c(Å)	α(°)	β(°)	γ(°)				
$Li_2U_3O_{10}$	Monoclinic	$P2_1/c$	6.821	18.91	7.300		121.56		4	99		
α-Li_6UO_6	Hexagonal	$R\bar{3}$	8.338		7.352				3	100		
β-Li_6UO_6	Triclinic	$P\bar{1}$	5.203	5.520	5.536	114.7	120.7	75.5	1	101		
$Li_2O.1.75UO_3$			X-ray powder data not indexed							102		
$Li_2O.1.60UO_3$	Orthorhombic		20.382	11.511	11.417					102		
$Na_6U_7O_{24}$	Triclinic		6.933	3.911	6.311	89.91	110.09	90.25		93	-11355	11
$Cs_4U_5O_{17}$	Orthorhombic	Pbcn	18.776	7.070	14.958				4	103		

Table 1:15 - Alkali Metal Neptunates (V) and (VII)

Oxide	Lattice Type	Space Group	Lattice Parameters				Z	Ref
			a(Å)	b(Å)	c(Å)	α(°)		
Li_3NpO_4	Tetragonal		4.485		8.390		2	84
Na_3NpO_4	— Unknown : but same structure as Na_3PuO_4 (?) —							10
Li_7NpO_6	Rhombohedral		6.16			53.40	3	84
K_3NpO_5								
Rb_3NpO_5	— No crystallographic data available —							104
Cs_3NpO_5								
Li_5NpO_6	Hexagonal	$R\bar{3}$	5.21		14.61			105

Table 1:16 - Alkali Metal Neptunates (VI) : $M^{I}_2NpO_4$ and $M^{I}_2Np_2O_7$

Oxide	Lattice Type	Space Group	Lattice Parameters				Z	Ref	Enthalpy of Formation (kJ mol^{-1})	Ref
			a(Å)	b(Å)	c(Å)	β(°)				
Li_2NpO_4	Orthorhombic	Pnma	10.48	6.018	5.121		4	91		
αNa_2NpO_4	Orthorhombic	Cmmm	9.685	5.705	3.455		2	10		
β-Na_2NpO_4	Orthorhombic	Fmmm	5.936	5.785	11.652		4	10		
K_2NpO_4	Tetragonal	I4/mmm	4.299		13.15		2	91		
Rb_2NpO_4	Tetragonal	I4/mmm	4.325		13.85		2	91		
Cs_2NpO_4	Tetragonal	I4/mmm	4.367		14.78		2	91		
$Na_2Np_2O_7$	Monoclinic	C2/m	12.779	7.822	6.902	111.46	4	106 *a*	-2893.8 ± 9.9	106 *b*
$K_2Np_2O_7$	Monoclinic	$P2_1/m$	6.908	7.977	6.998	109.67	2	*a*	-2932.4 ± 9.9	*b*
$Rb_2Np_2O_7$	Monoclinic	$P2_1/m$	7.027	8.046	7.430	109.53	2	*a*	-2913.9 ± 10.0	*b*
$Cs_2Np_2O_7$	Monoclinic	C2/m	14.30	4.330	7.400	113.58	2	91	-2897.6 ± 10.0	*b*

a This work, see Section 3:3:2

b This work, see Section 3:4:3

Table 1.7 - Alkali Metal Neptunates (VI) : Miscellaneous Compounds

Oxide	Lattice Type	Space Group	Lattice Parameters			Z	Ref	Enthalpy of Formation ($kJ\ mol^{-1}$)	Ref
			a(Å)	b(Å)	c(Å)				
Li_4NpO_5	Tetragonal	I4/m	6.698		4.432	2	12		
α-Na_4NpO_5	Cubic	Fm3m(?)	4.739			1	10		
β-Na_4NpO_5	Tetragonal	I4/m	7.515		4.597	2	10	-2310 ± 10	106
Li_6NpO_6	Hexagonal	$R\bar{3}$ (?)	5.217		14.70	3	10		
Na_6NpO_6	Hexagonal	$R\bar{3}$ (?)	5.78		16.0	3	10		
$Cs_2Np_3O_{10}$	Orthorhombic		15.77	7.600	14.34		91		
$Cs_4Np_5O_{17}$	Orthorhombic	Pbcn	18.64	7.023	14.86		91		

Table 1:18 - Alkali Metal Plutonates (IV), (V) and (VII)

Oxide	Lattice Type	Space Group	Lattice Parameters			Z	Ref
			a(Å)	c(Å)	α(°)		
$Li_3Pu^{IV}O_6$	Hexagonal		5.64	15.95			84
$Li_3Pu^{V}O_4$	Tetragonal		4.464	8.367		2	84
$Na_3Pu^{V}O_4$	Unknown: but same structure as Na_3NpO_4 (?)						10
$Li_7Pu^{V}O_6$							
$Rb_3Pu^{VII}O_5$	No crystallographic data available						10
$Cs_3Pu^{VII}O_5$							
$Li_5Pu^{VII}O_6$	Hexagonal	$R\bar{3}$(?)	5.19	14.48		3	107

Table 1:19 - Alkali Metal Plutonates (VI): $M^{I}_{2}PuO_4$ $M^{I}_{4}PuO_5$ and $M^{I}_{6}PuO_6$

Oxide	Lattice Type	Space Group	Lattice Parameters		Z	Ref
			a(Å)	c(Å)		
K_2PuO_4	Tetragonal	I4/mmm	4.298	13.07	2	91
Rb_2PuO_4	Tetragonal	I4/mmm	4.323	13.74	2	91
Cs_2PuO_4	Tetragonal	I4/mmm	4.368	14.71	2	91
Li_4PuO_5	Tetragonal	I4/m	6.677	4.421	2	108
α-Na_4PuO_5	Cubic	Fm3m(?)	4.718		1	108
β-Na_4PuO_5	Tetragonal	I4/m	7.449	4.590	2	108
Li_6PuO_6	Hexagonal	$R\bar{3}$ (?)	5.184	14.59	3	108
Na_6PuO_6	Hexagonal	$R\bar{3}$ (?)	5.76	15.9	3	108

Table 1:20 - Alkali Metal Americates

O.S	Oxide	Lattice Type	Space Group	Lattice Parameters					Z	Ref
				a(Å)	b(Å)	c(Å)	α(°)	β(°)		
III	$LiAmO_2$	Monoclinic	$P2_1/c$	—— Unknown Parameters ——					4	12
IV	Li_2AmO_3	—— No crystallographic data available ——								10
	Na_2AmO_3	Monoclinic	C2/c	5.9	10.26	11.23		100.12	8	10
	Li_8AmO_6	Hexagonal		5.62		15.96				10
V	Li_3AmO_4	Tetragonal		4.459		8.355			2	84
	Na_3AmO_4	Cubic		4.757					1	10
	Li_7AmO_6	Rhombohedral		6.12			53.5		3	84
VI	Li_4AmO_5	Tetragonal	I4/m	6.666		4.415			2	10
	Na_4AmO_5	Cubic	Fm3m	4.70					1	10
	Li_6AmO_6	Hexagonal		5.174		14.59			3	10
	Na_6AmO_6	Hexagonal		5.76		16.10			3	10
	K_2AmO_4	Tetragonal	I4/mmm	4.286		13.05			2	109
	Rb_2AmO_4	Tetragonal	I4/mmm	4.316		13.71			2	109
	Cs_2AmO_4	Tetragonal	I4/mmm	4.364		14.65			2	109

1:4:1 Alkali Metal Thorates (Table 1:10)

The three complexes identified have been prepared by direct combination of stoichieometric quantities of thorium dioxide and the required alkali metal oxide by heating under an argon atmosphere which was free from water, oxygen and carbon dioxide.

Sodium metathorate is formed at temperatures between 550°C[82] and 750°C and decomposes at 770°C in a stream of nitrogen, liberating Na_2O with the regeneration of ThO_2[82].

$$Na_2O + ThO_2 \xrightarrow[\text{argon}]{550\text{-}750^\circ} Na_2ThO_3 \xrightarrow[N_2]{770^\circ C} ThO_2 + Na_2O \uparrow .$$

The analogous potassium oxide is produced at 530°C[82] or according to the reaction,

$$KO_{0.55} + ThO_2 \xrightarrow[48\text{hrs}]{550^\circ C} K_2ThO_3 .$$

Decomposition of the potassium metathorate occurs at 650°C under nitrogen.

Rubidium metathorate (Rb_2ThO_3) is formed in the reaction between the two dioxides[83].

1:4:2 Alkali Metal Protactinates[110] (Table 1:10)

The lithium protactinium(V) oxides which have been reported; $Li_2O.xPa_2O_5$, $LiPaO_3$, Li_3PaO_4 and Li_7PaO_6, have all been prepared in direct combination reactions between finely powdered mixtures of Pa_2O_5 and Li_2CO_3. Specifically for Li_7PaO_6, the reaction conditions are 700 to 1000°C for 24 hours. This oxide has also been prepared using lithium oxide as the source of the alkali-metal,

$$Pa_2O_5 + 7Li_2O \xrightarrow[24\text{hrs}]{600\text{-}700^\circ C} 2Li_7PaO_6$$

The complex not included in Table 1:10, $Li_2O.xPa_2O_5$ with x>1, is reported to have a cubic crystal structure with a = 5.358Å[111]. However, it is not known whether this exists as a solution of Li_2O in Pa_2O_5, in its pure form or only as a mixture with $LiPaO_3$.

Preparation of the oxides in the Na_2O-Pa_2O_5 system has been achieved in a similar manner by the thermal reaction of Pa_2O_5 with Na_2CO_3. The following compounds have been described: $Na_2O.xPa_2O_5 (x>2)$, $NaPa_3O_8$, $NaPaO_3$ and Na_3PaO_4.

The compound $Na_2O.xPa_2O_5$ (x>2) is reported to form when $NaPaO_3$ is heated at 950°C for 48 hours. This decomposition product, which can also be prepared by the direct combination of Na_2CO_3 and Pa_2O_5, has a fluorite structure with the lattice parameter a = 5.399Å, and can be considered to be a solution of Na_2O in Pa_2O_5. In a high temperature X-ray powder diagram recorded at 700°C, a hexagonal lattice with the parameters a = 6.282, c = 8.243A has been identified and attributed to the compound $NaPa_3O_8$ [111].

$NaPaO_3$ is said to exist in two modifications. When Na_2CO_3 and Pa_2O_5 are heated together in the ratio 1:1 at 500°C an orthorhombic structure is assumed. However, when heated to 850°C $NaPaO_3$ adopts a rhombohedral Perovskite structure [111] with a lattice parameter a = 2x4.182Å and α = 90.8°.

The reaction of finely-powdered mixtures of K_2CO_3 and Pa_2O_5 at temperatures between 600 and 800°C has yielded the single complex, $KPaO_3$, which, like its uranium analogue, has a cubic Perovskite structure. Similarly, the only reported rubidium and caesium protactinates are, respectively, $RbPaO_3$ and $CsPaO_3$, which are formed between 600 and 800°C in the reactions between Pa_2O_5 and the respective alkali-metal carbonate.

1:4:3 Alkali Metal Uranates [7]

Over thirty well-characterised alkali-metal uranates are known (Tables 1:11 to 1:14). These are probably best considered in the groups M^IUO_3, $M^I{}_3UO_4$, $M^I{}_2UO_4$, $M^I{}_2U_2O_7$, $M^I{}_2U_4O_{13}$, $M^I{}_2U_7O_{22}$ and $M^I{}_4UO_5$, plus the miscellaneous compounds not fitting into these categories.

1:4:3:1 M^IUO_3 (M^I=Li, Na, K, Rb; U(V)) (Table 1:11)

All these uranates (V) can be prepared by the symproportionation reaction of uranium (IV) and uranium (VI) in an evacuated ampoule,

$$M^I{}_2UO_4 + UO_2 \longrightarrow M^IUO_3 .$$

The temperatures at which this reaction takes place differ for each alkali-metal, being between 650 and 700°C for the lithium and sodium complexes and 400 to 500°C for the potassium and rubidium analogues.

Additionally, pure $NaUO_3$ is obtained by the reactions of UO_2 with Na_2O_2 in an evacuated ampoule at 650-750°C and of Na_2CO_3 with UO_2 in a stream of argon at 700°C for 160 hours or 1000°C for 16 hours[112]. Pure KUO_3 is also reported to be the product of the reduction of potassium diuranate ($K_2U_2O_7$) with hydrogen at 450°C[113] and of the reaction of UO_3 with potassium oxide at 800°C under a pressure of 6.5 GPa[114].

1:4:3:2 <u>$M^I{}_3UO_4$ (M^I = Li, Na; U(V)) (Table 1:11)</u>

Both the lithium and sodium complexes can be prepared by the symproportionation reaction,

$$M^I{}_2UO_4 + UO_2 + 2M^I{}_2O \longrightarrow 2M^I{}_3UO_4,$$

in evacuated quartz ampoules at 750°C for Li_3UO_4, and at temperatures between 500 and 600°C for Na_3UO_4.

Reaction of M^IUO_3 (M^I = Li, Na) with alkali metal monoxide also yields the product $M^I{}_3UO_4$ according to the equation,

$$M^IUO_3 + M^I{}_2O \longrightarrow M^I{}_3UO_4.$$

The reaction is carried out in an evacuated ampoule at 500°C for 20 hours to produce Li_3UO_4. For the sodium analogue the use of sodium metal accelerates the reaction at 700°C in argon to produce purer, better-crystallised Na_3UO_4[93]. However, there is controversy as to the exact formulation of this phase and the alternative, $Na_{11}U_5O_{16}$[112], has been suggested, which, it has been reported, could be better represented as $Na_{11}U_2{}^{IV}U_3{}^{VI}O_{18.5}$ or $Na_{11}U^V{}_4U^{VI}O_{18.5}$[93]. It is suggested that some oxidation of uranium in $NaUO_3$ by Na_2O occurs, a fact supported by the equally possible reaction,

$$Na_2O + UO_2 \longrightarrow \text{'}Na_3UO_4\text{'} + Na\ (g).$$

Na_3UO_4 oxidises extremely readily, ultimately yielding $Na_2U_2O_7$.

Additionally, Li_3UO_4 has been prepared by the hydrogen reduction of a mixture of Li_2UO_4 and Li_2CO_3 at 750 to 900°C according to the reaction,

$$2Li_2UO_4 + Li_2CO_3 \xrightarrow[\Delta]{H_2} 2Li_3UO_4 + CO_2 + H_2O\ .$$

1:4:3:3 <u>$M^I{}_2UO_4$ (M^I = Li, Na, K, Rb, Cs; U(VI)) (Table 1:12)</u>

All five complexes have been prepared by the reaction in air of U_3O_8 or

UO_3 with the respective alkali metal carbonate at high temperatures (600°C (Cs)[97], 700°C (Rb and K)[115], 700-800°C (Li)[7] and 700-1000°C (Na)[93]).

Na_2UO_4 exists in two modifications, β-Na_2UO_4 being the high temperature form. The α→β transition is reportedto occur at 900°C[116].

Na_2UO_4 has been reported to be the product of the decomposition of $Na_4UO_2(CO_3)_3$ at 600-800°C via the intermediate $Na_2U_2O_7$[117]. Also, the interaction of equimolar amounts of Na_2O_2 and UO_2 at temperatures between 600 and 760°C yields α-Na_2UO_4 contaminated with $Na_2U_2O_7$.

Recent research[90] has failed to yield pure Na_2UO_4 by heating together UO_3 and Na_2CO_3 in dry air. Even after periods of longer than 120 hours at 760 to 800°C, the product was contaminated with $Na_2U_2O_7$ and Na_2CO_3. An alternative reaction involving 1:1 molar ratios of β-Na_4UO_5 and UO_2 at 700°C in oxygen produced almost pure α-Na_2UO_4 after 63 hours. X-ray powder diffraction analysis indicated only traces of unreacted β-Na_4UO_5. The reaction at 800°C yielded β-Na_2UO_4 of similar purity. The lower α to β transition temperature than that previously reported was attributed to the prolonged heating periods, during which the α→β conversion at about 800°C was found to be complete only after greater than 40 hours.

1:4:3:4 <u>$M^I{}_2U_2O_7$ (M^I = Li, Na, K, Rb, Cs; U(VI)) (Table 1:12)</u>

The reaction of U_3O_8 with alkali metal chloride (M^ICl) in air at 500°C has been described as a preparative route for $Na_2U_2O_7$ and $K_2U_2O_7$[118] and at 600°C for $Rb_2U_2O_7$[94]. However, $Na_2U_2O_7$ is formed together with $Na_2U_2O_7$. $NaUO_3Cl$, and in a similar reaction between U_3O_8 and NaF at 700°C, sodium diuranate is produced with $NaUO_3F$. The preparation of $Cs_2U_2O_7$ from U_3O_8 and CsCl proceeds via the intermediate compound $CsUO_3Cl$[119].

Caesium diuranate has been prepared by the reaction of caesium carbonate with UO_3. Heating at 300°C for periods of several days produced the α-phase and β-$Cs_2U_2O_7$ was obtained at 600°C as was another phase γ- $Cs_2U_2O_7$[95]. This method has also been used for the preparation of $Rb_2U_2O_7$ at 600°C[119] and $Na_2U_2O_7$ at 600 to 800°C.

The reaction of U_3O_8 with alkali metal sulphates in air has been described for the preparation of both sodium and potassium diuranates[120] above 500°C

and at 800°C, respectively. In the case of the sodium complex, the double sulphate, $Na_2SO_4.2UO_2SO_4$, appears to be formed as an intermediate product[121].

The decomposition of Rb_2UO_4 at 1200°C yields $Rb_2U_2O_7$[122].

The complex oxalates $Na_2(UO_2)_2(C_2O_4)_3.5H_2O$, $K_2(UO_2)_2(C_2O_4)_3.4H_2O$, $Rb_2(UO_2)_2(C_2O_4)_3.3H_2O$ and $Cs_2(UO_2)_2(C_2O_4)_3.nH_2O$ decompose in air above 320°C to yield $Na_2U_2O_7$, $K_2U_2O_7$, $Rb_2U_2O_7$ and $Cs_2U_2O_7$, respectively. The final products were obtained at 900°C[123]. The preparation of $Li_2U_2O_7$ from $Li_2(UO_2)_2(C_2O_4)_3.7H_2O$ has also been reported[123].

Although X-ray powder diffraction data for $Li_2U_2O_7$ have been published [123,124] recent work on the lithium uranium(VI) oxygen system[125] has corroborated the results of earlier findings[126,127,128] in failing to isolate $Li_2U_2O_7$. The product in the system Li_2O-UO_3 with Li/U = 1 was found to be a mixture of $Li_2U_3O_{10}$ and $Li_2O.\ 1.75\ UO_3$. Many of the X-ray powder diffraction lines for the product from the thermal decomposition of $Li_2(UO_2)_2(C_2O_4)_3.7H_2O$ can be indexed as $Li_2O.1.75\ UO_3$[127].

Sodium diuranate has been observed as the product of the thermal decomposition of sodium uranyl (VI) triacetate ($NaUO_2(CH_3COO)_3$) above 365°C[129].

1:4:3:5 <u>$M^I{}_2U_4O_{13}$, $M^I{}_2U_7O_{22}$ (M^I= K, Rb, Cs; U(VI) (Table 1:13)</u>

The preparation of all six complexes has been achieved by heating carefully ground mixtures of alkali metal carbonate and amorphous uranium trioxide. The reaction temperatures were 700°C for the potassium and rubidium complexes ($K_2U_4O_{13}$, $K_2U_7O_{22}$, $Rb_2U_4O_{13}$ and $Rb_2U_7O_{22}$)[94] and 600°C for the caesium compounds ($Cs_2U_4O_{13}$ and $Cs_2U_7O_{22}$)[98].

1:4:3:6 <u>$M^I{}_4UO_5$ (M^I = Li, Na, K, Rb; U(VI)) (Table 1:13)</u>

The preparation of Li_4UO_5 has been shown to occur in a three stage reaction of lithium carbonate with uranium trioxide at 1000°C,

$$2UO_3 + Li_2CO_3 \longrightarrow Li_2U_2O_7\ (?) + CO_2$$
$$Li_2U_2O_7\ (?) + Li_2CO_3 \longrightarrow Li_2UO_4 + CO_2$$
$$Li_2UO_4 + Li_2CO_3 \longrightarrow Li_4UO_5 + CO_2\ .$$

The same preparative route has been described for the sodium complex, β-Na_4UO_5 being formed at 700°C[93].

Reaction of sodium oxide with uranium trioxide at 400-450°C is said to give the low temperature α-modification of Na_4UO_5 which transforms to the high temperature β-phase at 500°C[7]. These results have been brought into question by later work[93] which failed to achieve isolation of the α-phase by this route. Only β-Na_4UO_5 was found. This was also prepared by the UO_3/Na_2CO_3 reaction described above. More recent work[90] has confirmed the existence of α-Na_4UO_5, formed by the reaction of sodium dioxide (Na_2O_2) with uranium dioxide below 400°C. The same reaction produced the β-phase at higher temperatures, but, in both cases the products were contaminated with other sodium uranates.

1:4:3:7 Miscellaneous Compounds

i) 0.5 $Li_2O.U_2O_5$ (U(V); Table 1:11)

This complex has been prepared by direct synthesis using Li_2O and U_2O_5 and also by heating $LiUO_3$ at 800°C in air with the evaporation of Li_2O[7]. This may also be the complex described as the fluorite phase, $(Li, U)O_{2-x}$, in the thermal decomposition of Li_2UO_4[130].

ii) Li_7UO_6 (U(V); Table 1:11)

The following have been described as preparative routes for Li_7UO_6[7].

(a) Heating $LiUO_3$ with Li_2O in an evacuated quartz ampoule for 20 hours at 500°C.

(b) Heating together Li_2UO_4, UO_2 and Li_2O in an evacuated quartz ampoule at 750°C,

$$Li_2UO_4 + UO_2 + 6Li_2O \longrightarrow 2Li_7UO_6 .$$

(c) Hydrogen reduction of a Li_2UO_4/Li_2O mixture at 750°C,

$$2Li_2UO_4 + 5Li_2O \xrightarrow[750°C]{H_2} 2Li_7UO_6 .$$

iii) $Li_2U_3O_{10}$ (U(VI); Table 1:14)

This complex has been prepared by sintering together stoicheiometric amounts of lithium carbonate and U_3O_8 in air at 750°C[99].

iv) Li_6UO_6 (U(VI); Table 1:14)

The two modifications of Li_6UO_6 have been obtained by heating together Li_4UO_5 and lithium oxide (Li_2O). The α-phase forms below 680°C, above

which temperature the reversible phase change to β-Li_6UO_6 occurs[100]. More recent work, using amorphous UO_3 and Li_2O as reactants, has suggested that 'Li_6UO_6' has a true composition of $Li_{6.43}$ $UO_{6.215}$ (or $Li_2O.0.311UO_3$).[125]

v) $Li_2O.1.75UO_3$, $Li_2O.1.60UO_3$ (U(VI); Table 1:14)

These complexes have been formed by the direct reaction between Li_2O and amorphous UO_3 above 700°C[125].

vi) $Na_6U_7O_{24}$ (U(VI); Table 1:14)

This complex has been prepared by heating amorphous UO_3 and sodium carbonate (Na/U = 0.857 ± 0.010) in air between 700 and 1000°C[93].

vii) $Cs_4U_5O_{17}$ (U(VI); Table 1:14)

The complex $Cs_4U_5O_{17}$, of which single crystals have been produced, has been obtained by heating together carefully ground mixtures of amorphous UO_3 and caesium carbonate in the required Cs/U atomic ratio at 600°C for periods of up to 1 week[98].

1:4:3:8 Additional Complexes

A number of other alkali metal uranates have been described but which are not unambiguously characterised. Some, indeed, have not been isolated in subsequent studies. The following are complexes in this category which do not appear in the foregoing tables:

i) Lithium Uranates

0.15 $Li_2O.U_2O_5$[88]
$Li_2U_6O_{19}$[127]
$Li_2O.(2.67-2.75)$ $UO_{2.95}$[127]
$Li_2O.(1.60-1.64)$ UO_3 or Li_{22} U_{18} O_{65}[127] *a*
$Li_2O.1.67UO_3$ or $LiU_{0.83}O_3$ *b*
β-Li_2UO_4[131]
$Li_2U_2O_7$ *c*

a Subsequently reported[128] to be a mixture of $Li_2O.$ $1.60UO_3$ and $Li_2O.$ $1.75UO_3$.

b Described in α- and β- phases as the compounds $Li_2O.(1.60-1.64)$ UO_3 and Li_2O $1.75UO_3$ respectively, but recently reported to be $Li_2O.1.60UO_3$[125].

c Discussed in Section 1:4:3:4.

ii) Sodium Uranates

$Na_{11}U_5O_{16}$[112] *a*

$Na_2O \approx 13UO_3$[7]

$Na_2O.2.5\ UO_3$[7]

a Discussed in Section 1:4:3:2

Additionally, a sodium uranium bronze, Na_xUO_3, with x<0.14 has been described[132] where the inclusion of sodium in the hexagonal α-UO_3 lattice produces a slight change in the parameters[7].

iii) Potassium Uranates

$K_2U_6O_{19}$[8]

$K_2U_3O_{10}$[153]

β-K_2UO_4 *a*

K_4UO_5[134]

a The reported high-temperature phase transition of K_2UO_4 into a cubic form is probably the decomposition to KUO_3[94].

iv) Rubidium Uranates

Rb_4UO_5[135]

v) Caesium Uranates

α-, β- and γ- $Cs_2U_4O_{12}$[136]

$Cs_2U_6O_{18}$[98]

$Cs_2U_9O_{27}$[98]

$Cs_2U_3O_{10}$[115] *a*

$Cs_2U_5O_{16}$[98]

$Cs_2U_6O_{19}$[115]

$Cs_2U_{16}O_{49}$[98]

a This complex was not observed in a more recent study[98] in which $Cs_4U_5O_{17}$ was isolated instead.

1:4:4 Alkali Metal Neptunates

1:4:4:1 Neptunates (V) (Table 1:15)

i) $M^I{}_3NpO_4$ (M^I = Li, Na)[84]

The best method for the preparation of Li_3NpO_4 and Na_3NpO_4 is reported

to be the symproportionation reaction of alkali metal neptunates (VI) and neptunium dioxide, for example

$$Na_6NpO_6 + NpO_2 \xrightarrow[500^\circ C\ 8\ hours]{vacuum} 2Na_3NpO_4 .$$

However, even in this 'best' method, the sodium complex could not be prepared pure. An alternative method, the thermal decomposition of the neptunium (VI) ternary oxide, is reported to yield Li_3NpO_4,

$$4Li_6NpO_6 \xrightarrow[900-1000^\circ C\ 4\ hours]{argon} 4Li_3NpO_4 + 6Li_2O + O_2 .$$

The oxidation of a mixture of Na_2O_2 and NpO_2 has also been used to prepare the sodium complex,

$$Na_2O_2 + 2NpO_2 + 2Na_2O \xrightarrow[500^\circ C\ 8\ hours]{vacuum} 2Na_3NpO_4 .$$

ii) Li_7NpO_6 [84]

The oxidation of a mixture of Li_2O and NpO_4 in a stream of oxygen is described as the best preparative route to this complex,

$$7Li_2O + 2NpO_2 \xrightarrow[600^\circ C\ 8\ hours]{O} 2Li_7NpO_6 .$$

1:4:4:2 Neptunates (VI) (Tables 1:16 and 1:17)

i) $M^I{}_2NpO_4$ (M^I = Li-Cs) and $M^I{}_2Np_2O_7$ (M^I = Na-Cs)

The alkali metal mononeptunates, $M^I{}_2NpO_4$, and dineptunates, $M^I{}_2Np_2O_7$ (M^I = K, Rb and Cs), have been prepared by the following two methods[91].

a) Thermal decomposition of co-deposited (by evaporation) alkali-metal-actinide nitrates.

b) Reaction of alkali-metal hydroxides with Np_2O_5.

In each of the two preparative methods temperatures of at least 450°C were necessary to achieve complete reaction within 8 hours.

Lithium mononeptunate has been prepared by the nitrate method in (a) above in which it is reported to be the initial ternary oxide formed, regardless of the Li/Np molar ratio employed.

Sodium mononeptunate, Na_2NpO_4, exists in two modifications which have been prepared by the thermal reaction of 1:1 mixture of NpO_2 and Na_2O[108],

$$NpO_2 + Na_2O \xrightarrow[>500°C]{O_2} \alpha\text{-}Na_2NpO_4 \xrightarrow{800°C} \beta\text{-}Na_2NpO_4 .$$

Sodium dineptunate is reported as the product of the reaction of NpO_2 and Na_2O (ratio 2:1) in oxygen below 400°C[108].

ii) $M^I{}_4NpO_5$ and $M^I{}_6NpO_6$ (M^I = Li, Na)[108]

Thermal reaction of NpO_2 and $M^I{}_2O$ (M^I = Li, Na) in the ratio 1:2 yields $M^I{}_4NpO_5$ and in the ratio 1:3 yields $M^I{}_6NpO_6$. A temperature in the range 400-500°C is required for both reactions. Na_4NpO_5 exists in two modifications, the α-form is the product at 400°C and the transition to the β-phase occurs at around 500°C.

iii) $Cs_2Np_3O_{10}$ and $Cs_4Np_5O_{17}$

These two complexes have been identified in the nitrate and hydroxide reactions previously described (1:4:4:2 (i))[91]. However, it is not clear whether pure phases or only mixtures (Cs_2NpO_4-$Cs_4Np_5O_{17}$; Cs_2NpO_4-$Cs_2Np_3O_{13}$; $Cs_2Np_2O_7$-$Cs_2Np_3O_{10}$) were obtained.

1:4:4:3 Neptunates (VII) (Table 1:15)

i) $M^I{}_3NpO_5$ (M^I = K, Rb, Cs)[104]

These complexes have been reported as the products of the reaction between NpO_2 and alkali metal superoxide M^IO_2,

$$NpO_2 + 3M^IO_2 \longrightarrow M^I{}_3NpO_5 + {}^3/_2O_2\uparrow .$$

The reaction conditions are 24 hours at 355°C for the potassium complex, 20 hours at 320°C for the rubidium neptunate(VII) and 24 hours at 320°C for Cs_3NpO_5.

ii) Li_5NpO_6

Heating Li_2O and NpO_2 in the molar ratio 2.7:1 in oxygen at 400°C is reported to yield Li_5NpO_6. The slight excess of Li_2O over the theoretical molar ratio of 2.5:1 aids the reaction.

The existence of the analogous sodium complex, Na_5NpO_6, has been suggested, following observation of Np^{VII} in a 1 Mol dm^{-3} NaOH solution of the product from the reaction of Na_2O_2 and NpO_2 in the ration 2.7:1 at 400°C in oxygen.

1:4:5 Alkali Metal Plutonates (Table 1:18)

1:4:5:1 Plutonates (IV) and (V) [10]

i) Li_8PuO_6 (Pu(IV))

The reaction of Li_2O with PuO_2 (molar ratio of about 4.2:1) in a vacuum at 600°C is reported to yield Li_8PuO_6, which is isostructural with Li_8SnO_6.

ii) $M^I{}_3PuO_4$ (M^I = Li, Na; Pu(V))

These complexes are reported to form on the thermal decomposition of complexes of plutonium (VI) and also in the direct reaction of alkali metal oxide/PuO_2 mixtures (ratio 2:1) in oxygen at 700 to 900°C.

iii) Li_7PuO_6 (Pu(V))

The purest Li_7PuO_6 is obtained by the reaction of Li_3PuO_4 with Li_2O at 700°C. An excess of about 0.5 mole Li_2O is reported to be necessary for a product free from Li_3PuO_4.

1:4:5:2 Plutonates (VI) (Table 1:19)

i) $M^I{}_2PuO_4$ (M^I = K, Rb, Cs) [91]

These complexes have been formed by the reaction of alkali metal hydroxide with PuO_2 in oxygen at temperatures above 450°C.

ii) $M^I{}_4PuO_5$ and $M^I{}_6PuO_6$ (M^I = Li, Na) [108]

All these complexes have been prepared by the thermal reaction of alkali metal oxide with PuO_2 in oxygen. Heating a mixture of Li_2O and PuO_2 (ratio 2:1) at 450-500°C yields Li_4PuO_5, and in the ratio 3:1 yields Li_6PuO_6. The sodium salt, Na_4PuO_5 exists as α- and β-phases which are formed at 400°C and 500°C, respectively, when a 2:1 mixture of Na_2O and PuO_2 is heated in oxygen. Formation of Na_6PuO_6 takes place at 500°C when Na_2O and PuO_2 are heated together in the ratio 3:1 in oxygen.

1:4:5:3 Plutonates (VII) (Table 1:18)

i) $M^{I}{}_{3}PuO_5$ (M^{I} = Rb, Cs) [10]

These complexes, which are formed by the reaction of RbO_2 or CsO_2 with PuO_2 at 250°c, are isostructural with the analogous Np(VII) and Re(VII) complexes. They are thermally very unstable and decompose at 320°C to $M^{I}{}_{2}PuO_4$.

ii) Li_5PuO_6 [10]

The preparation of Li_5PuO_6 by heating Li_2O and PuO_2 (ratio 3:1) in oxygen at 430°C is reported to require a slight excess of Li_2O for the oxidation to Pu(VII). The existence of Na_5PuO_6 has been suggested.

1:4:6 Alkali Metal Americates (Table 1:20)

1:4:6:1 Lithium and Sodium Americates

The lithium and sodium americium oxides have been prepared by heating finely powdered mixtures of AmO_2 and Li_2O or Na_2O (or Na_2O_2) under oxygen, nitrogen or hydrogen or in a vacuum [10,84,108]. The reaction conditions and thermal stabilities are presented in the following schemes:

Figure 1.1 - Preparations and Thermal Stabilities of Lithium Americates

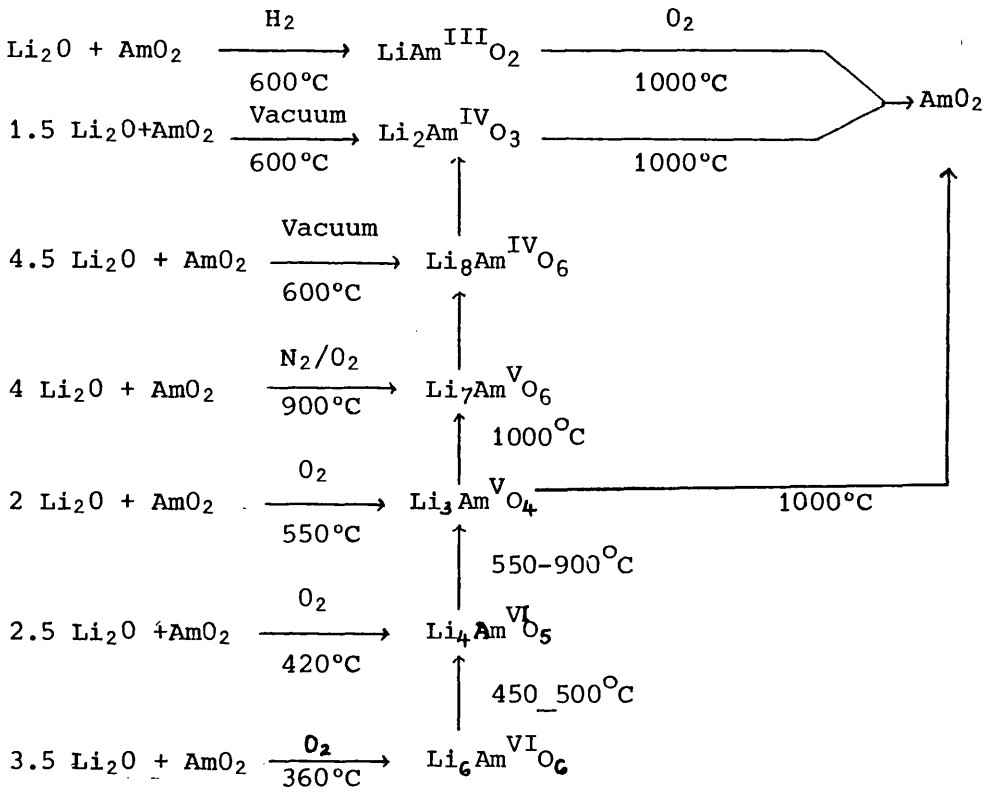

Figure 1:2 - Preparations and Thermal Stabilities of Sodium Americates

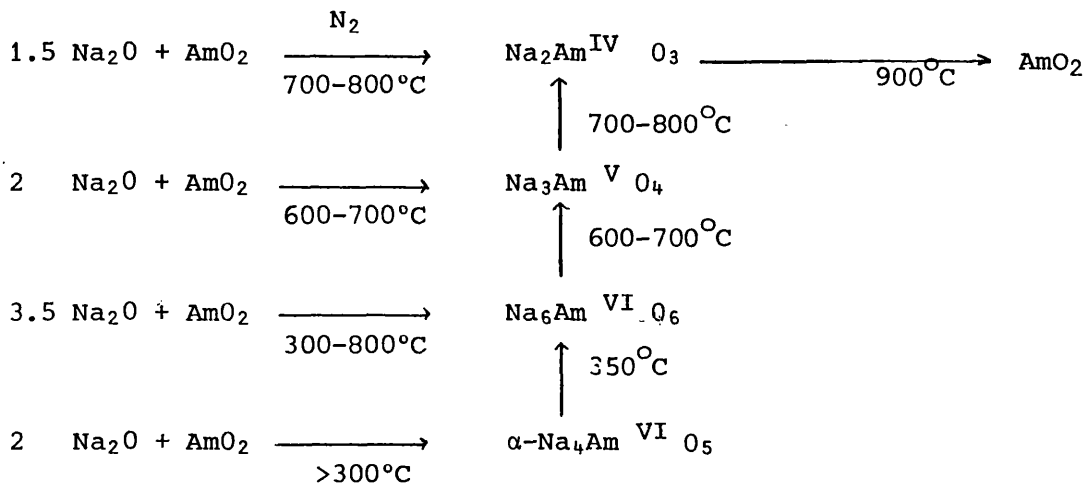

Additionally, the following decomposition reaction is reported to generate lithium and sodium americates (V) from americates (VI),

$$M^{I}{}_{6}AmO_{6} \xrightarrow[550°C,\ 6\ hrs]{O_2} M^{I}{}_{3}AmO_{4} + 1.5\ M^{I}{}_{2}O.$$

1:4:6:2 Potassium, Rubidium and Caesium Americates[109]

Only one alkali metal americium(VI) oxide, $M^{I}{}_{2}AmO_4$ has been identified for M^{I} = potassium, rubidium and caesium. The preparative route is the reaction of AmO_2 (freshly prepared by evaporating an americium nitrate solution and heating in oxygen at 450°C for 16 hours) with a 0.5mol dm^{-3} alkali metal hydroxide solution added to the AmO_2, evaporated and then heated gradually to 250°C over a 4 hour period. The temperature of 250°C is maintained for at least 16 hours,

$$2AmO_2 + 4M^{I}OH + O_2 \longrightarrow 2M^{I}{}_{2}AmO_4 + 2H_2O.$$

A 50% excess of the alkali metal hydroxide was found to be necessary to achieve complete conversion of AmO_2 to the americate (VI) below 300°C.

1:4:7 Ternary Oxides with Other Elements

A large number of ternary oxides of the actinides with Group II, III and IV, transition, lanthanide and other actinide elements are known. Complexes with the actinide metals protactinium to curium have been prepared. As stated before, most of the thermodynamic data available are for compounds of uranium although enthalpy of formation values have been determined for the

neptunium complexes Sr_3NpO_6, Ba_3NpO_6 and Ba_2MgNpO_6. Compounds for which such data are known are presented in Table 1:21.

The preparation of these complexes, like those of the alkali metal oxides, has usually involved direct combination of the required binary oxides with heating or decomposition of higher ternary oxides. The following are examples of these types of preparation[6,10],

$$Pa_2O_5 + In_2O \xrightarrow[1000°C]{air} InPaO_4$$

$$UO_3 + FeO \xrightarrow[1050°C]{2\ weeks} FeUO_4$$

$$2NpO_3.H_2O + 4BaO_2 + Li_2O_2 \xrightarrow{450°C} 2Ba_2LiNpO_6$$

$$Sr_3PuO_6 \xrightarrow[1200-1300°C]{H_2} SrPuO_3$$

$$AmO_2 + V_2O_5 \xrightarrow[\substack{600°C,\ 10\ hrs \\ +1000°C,\ 10\ hrs}]{air} AmVO_4$$

$$CmO_2 + Pa_2O_5 \xrightarrow{1200°C} CmPaO_4\ .$$

Table 1:21 - Enthalpies of Formation for Actinide Ternary Oxides with Elements Other than Alkali-Metals[12]

Compound	$\Delta Hf^{\ominus}$ (kJ mol^{-1})
Hexavalent Actinides	
CaU_2O_7	- 3335
$Sr_2U_3O_{11}$	- 5239
$MgUO_4$	- 1856.9
$CaUO_4$	- 2001.6 ± 2.1
α-$SrUO_4$	- 1987
β-$SrUO_4$	- 1988
$BaUO_4$	- 1997.1 ± 2.1
Sr_2UO_5	- 2630
Ca_3UO_6	- 3302 ± 3
Sr_3UO_6	- 3260 ± 4
Sr_3NpO_6	- 3123 ± 6
Ba_3UO_6	- 3210.6 ± 4.1
Ba_3NpO_6	- 3085 ± 6
Ba_2MgUO_6	- 3245.3 ± 4.8
Ba_2MgNpO_6	- 3096.4 ± 6.5
Ba_2CaUO_6	- 3294 ± 5
$Ba_2Dy\ ^2/_3\ UO_6$	- 3198 ± 6
NiU_3O_8	- 3942
Pentavalent Actinides	
CaU_2O_6	- 3210

Other preparative routes which have been employed include heating aqueous americium(IV) hydroxide and aqueous germanium oxide at 230°C over 7 days to from $AmGeO_4$ and the use of binary hydroxides as reactants as in the reaction to form americium(III) aluminate,

$$Am(OH)_3 + Al(OH)_3 \xrightarrow[1250 \rightarrow 1400°C]{H_2} AmAlO_3$$

More recently[137], reactants such as $Ba(NO_3)_2$ and $Mg(CH_3COO)_2.4H_2O$ have been used together with U_3O_8, $UO_2(NO_3)_2.6H_2O$ or NpO_2. These are useful reagents because of their reproducable chemical analyses, moderate decomposition temperatures and ease of weighing in air. The preparations of Ba_2MgUO_6 and Ba_2MgNpO_6 from these starting materials require protracted heating periods, in which the temperature is raised gradually in 100°C increments from 300°C to between 1045 and 1095°C.

1:5 OBJECTIVES

As discussed in the previous sections, preparations of the alkali metal actinide oxides have historically involved the direct combination, with heating, of an alkali metal oxide or carbonate and an actinide metal oxide in the correct stoicheiometry for the required product. An extension of this has been to use materials prepared in the above manner for further reaction to provide other complex oxides.

There are several reasons why the direct combination method is not entirely satisfactory:

i) the possible occurrence of weighing errors
ii) difficulty in effecting complete mixing of the oxides
iii) unreactivity of the actinide oxide
iv) difficulty in obtaining pure alkali metal oxide
v) volatility of the alkali metal oxide
vi) necessarily lengthy heating periods and the need for frequent regrinding.

Additionally, in the sodium uranium(VI) oxygen system, the relative ease with which $Na_2U_2O_7$ is formed is also a problem, particularly in view of the side reactions which it can undergo. For these reasons it has been found

difficult to prepare phases of the high purity required for thermodynamic studies by this type of reaction[90].

An alternative preparative route[90] has now been examined in more detail with a view to preparing pure phases containing all the alkali metals and either neptunium or uranium, for thermodynamic studies. This alternative method involves the preparation of salts containing the alkali metal and actinide metal in the correct stoicheiometry for the required ternary oxide and their subsequent decomposition to those oxides. Suitable complexes for thermal decomposition include acetates and oxalates and the aim of this work has been to prepare the oxides $M^{I}{}_2M^{VI}{}_2O_7$ (M^{I} = Li, Na, K, Rb, Cs; M^{VI} = U, Np) by decomposition of the acetates $M^{I}M^{VI}O_2(CH_3COO)_3$. In only a few cases have materials been prepared by these decomposition methods and usually the intention has been to identify the decomposition products[123,129] rather than to use the route to provide phases for further investigation. However, an initial study into the preparation of pure oxide phases by the decomposition of complex acetates and oxalates has provided thermodynamic data for several uranates and neptunates[90,106].

Initially the alkali metal uranium system was studied since the enthalpies of formation of $Na_2U_2O_7$ and $Cs_2U_2O_7$ were well established and could be used as an additional check of the purity of the products. Additionally, it was advantageous to commence the research with uranium because of its availability and easier handling and its stable oxidation state of +6 in aqueous solution, required for the acetate preparations.

This acetate decomposition method has been used to further investigate the oxide system with lithium and uranium(VI) in the ratio 1:1 and also the analogous neptunium(VI) system. As discussed previously (Section 1.4.3.4) the oxide $Li_2U_2O_7$ has been reported[123,124] but there is evidence to suggest that such an oxide does not exist[125,126,127,128]. The existence of the neptunium oxide $Li_2Np_2O_7$ is therefore also in doubt.

Although all these oxides, with the exception of $Li_2Np_2O_7$, have been reported no thermodynamic data have been previously published for $K_2U_2O_7$, $Rb_2U_2O_7$, $K_2Np_2O_7$, $Rb_2Np_2O_7$ and $Cs_2Np_2O_7$. The first thermodynamic data for

sodium neptunates(VI), $Na_2Np_2O_7$ and β-Na_4NpO_5, prepared by thermal decomposition of $NaNpO_2(CH_3COO)_3$ and $Na_4Np(C_2O_4)_4.nH_2O$, respectively, were reported at a conference in 1981[106].

During the course of this work the previously uncharacterised acetate complexes, $LiUO_2(CH_3COO)_3.nH_2O$, $LiNpO_2(CH_3COO)_3$, $KNpO_2(CH_3COO)_3$ and $RbNpO_2(CH_2COO)_3$ were prepared.

2. EXPERIMENTAL

2:1 HANDLING OF RADIOACTIVE CHEMICALS

All the isotopes of the actinide elements are radioactive and special precautions are necessary, therefore, when handling most of these elements. The nuclides handled during this work are predominantly α-emitters; they are listed in Table 2:1 with their half-lives and specific activities.

Table 2:1 Half-Life and Specific Activity of Various Nuclides

Nuclide	Half Life ($T_{\frac{1}{2}}$, years)[138]	Specific Activity [a] (dpm μg^{-1})
^{238}U	4.468×10^{9}	7.4618×10^{-1}
^{237}Np	2.145×10^{6}	1.5645×10^{3}
^{238}Pu	8.774×10^{1}	3.7998×10^{7}
^{239}Pu	2.411×10^{4}	1.3770×10^{5}

[a] $$\text{Specific Activity} = \frac{\text{Avogadro's Number} \times \ln 2}{T_{\frac{1}{2}} \times \text{Atomic Weight}}$$

The particular hazard of α-emitters results from their inhalation or ingestion. Solutions of low activity can be handled in well ventilated fume cupboards, but, in view of the high radioactivity of the transuranium elements, all operations with dry solid compounds of these elements must be performed in special enclosures. The base of these 'glove boxes'[139] then forms an enclosed laboratory bench. The boxes are maintained at a lower pressure than the laboratory atmosphere by an extract system provided with absolute filters; this prevents the discharge of radioactive material into the laboratory in the event of a leak in the gloves, welds or ports of the box.

The atmosphere maintained within a glove box is dependent on the nature of the operations to be performed. Four different atmospheres were main-

tained in boxes used during this work as summarised in Table 2:2.

The glove box containing a tube furnace for the neptunium complex decompositions, illustrated in Figure 2:1, is typical of the type in use at Harwell.

The nitrogen and argon filled boxes are flushed continuously with dry gas at the rate of about 10 litres per minute; where a negative pressure is required the extract is augmented by a compressed air ejector. For the dry boxes, type 5A molecular sieves are used as a secondary dehydrating agent. A motorised fan circulates the box atmosphere through the degassed sieves contained in a gauze based brass bowl.

During the work, small items of equipment and materials were 'posted' into the boxes as required via a tunnel which was flushed with dry nitrogen for about 20 minutes before being opened to the box atmosphere. Material was removed in radio-frequency welded polyethylene bags attached to the box via a circular, bunged port.

High active solution and preparative work was carried out in a nitrogen atmosphere box equipped with a centrifuge, heating mantle and infra-red lamp and having a direct connection to a vacuum line. Active materials were weighed on a balance in an air filled box. An air atmosphere box containing a vacuum line and an oxygen-gas torch was used when sealing ampoules containing radioactive compounds. A purposely designed chain of three nitrogen flushed boxes was used for loading and weighing calorimetric samples and loading the microcalorimeter.

Table 2:2 Glove Box Atmospheres and Operations

Atmosphere	Pressure	Operations
Nitrogen	-ve	High activity or high concentration radioactive solid and solution work
Dry Nitrogen	-ve	(i) Decomposition work and handling of solid neptunium compounds (ii) Handling and weighing of calorimetric samples (iii) Alkali metal uranates(VI), handling
Air	-ve	Radiochemical balance work, sample tube sealing
Dry Argon	+ve	Alkali metal uranates(VI), handling and weighing

Fig. 2:1

Example of Glove Box Used at A.E.R.E. Harwell

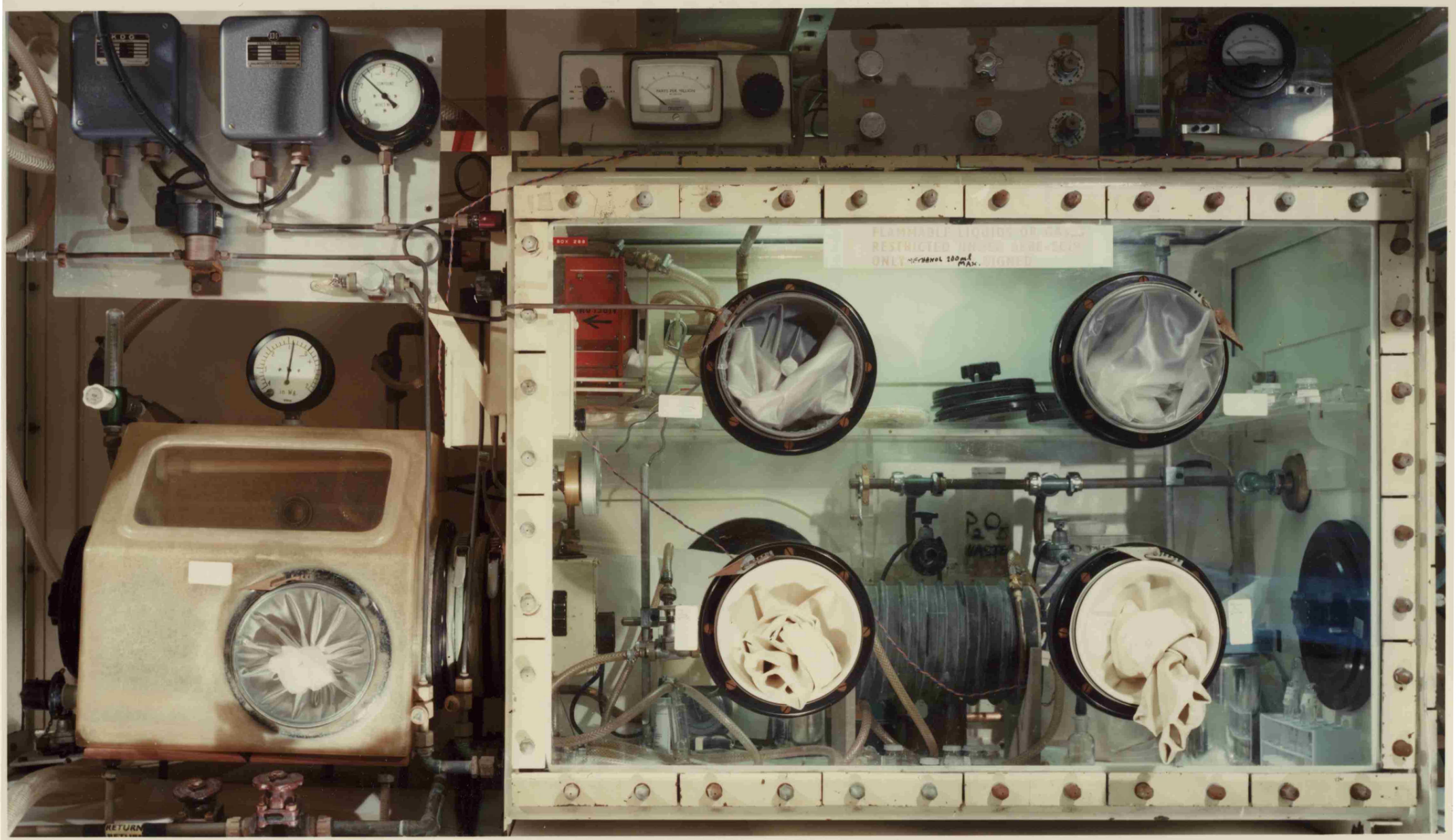
PARTS PER MILLION
BOX 289
RETURN

2:2 FURNACE FACILITIES

A tube furnace, as illustrated diagrammatically in Figure 2:2, contained within a dry nitrogen atmosphere box (Figure 2:1) was used for the neptunium complex decomposition work.

Power was supplied to the furnace via a Eurotherm 070 unit, having a temperature range of 0 to 1200°C. The power input was thermostatically controlled to maintain a required, pre-set temperature measured inside the furnace by a Pt/13% Rh-Pt thermocouple.

Water from an external heat exchanger circuit was used to cool the furnace jacket. The furnace cooling circuit included a 'Rotameter' water flow switch which would cut the power supply to the furnace in the event of a break down of the water supply.

Oxygen fed into the alumina reaction tube was kept isolated from the box atmosphere and the exhaust passed through an 'Arnold' bulb containing silicon oil and then through a filter to a fume cupboard extract. A magnetic inlet valve could only be operated with the box pressure below -1 inches w g (the normal operating pressure being -1.4 inches w g) so that a pressure increase due to a leak of oxygen into the box atmosphere automatically shut off the supply.

A similar arrangement, not contained in a box, was used for the uranium complex decompositions. In all the decomposition work crucibles constructed with 0.125mm thickness 99.96% gold foil were used to contain the material being fired.

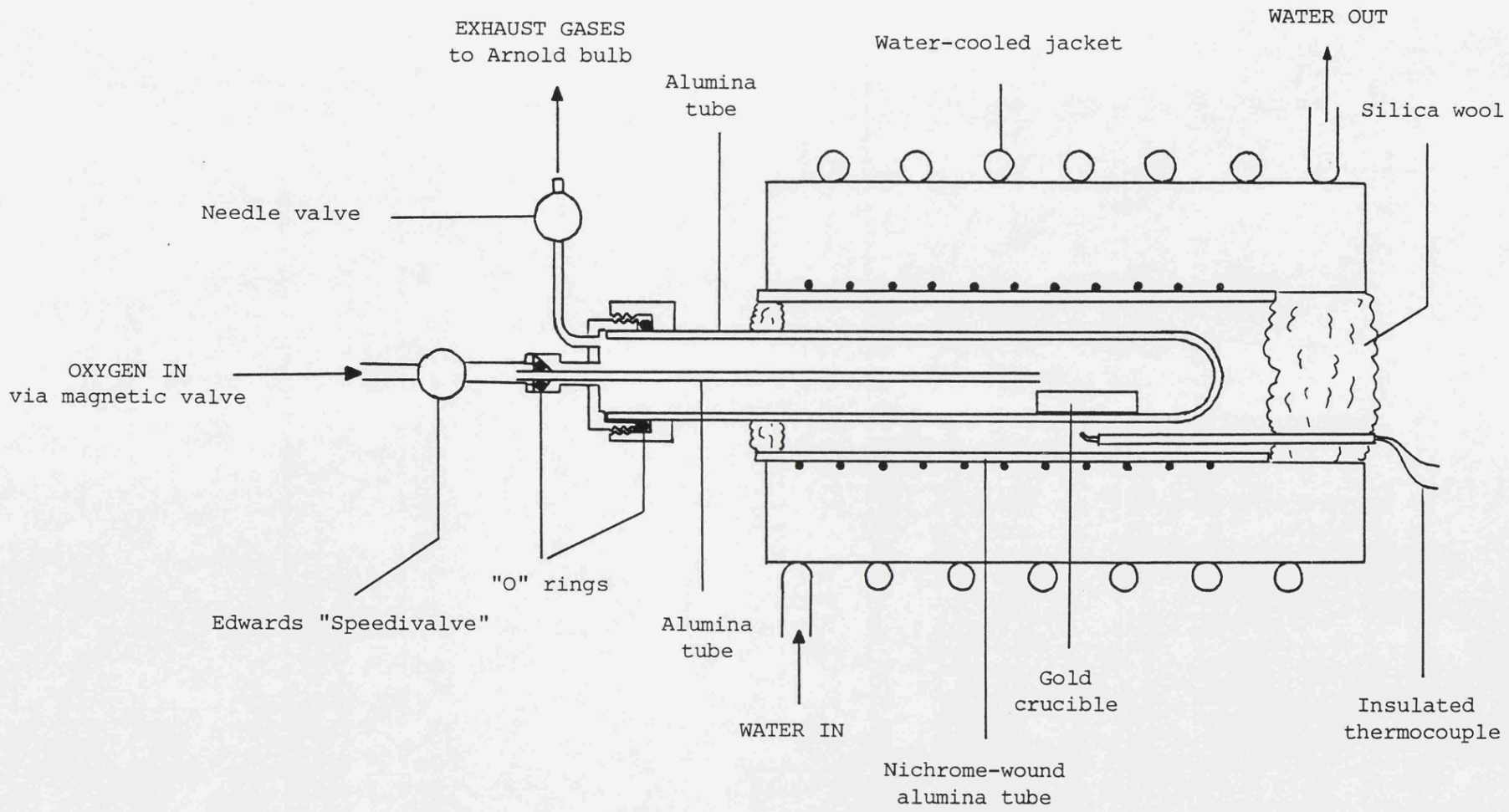

Fig. 2:2. Furnace Arrangement for Decomposition of Neptunium Complexes

2:3 CRYSTALLOGRAPHIC STUDIES

2:3:1 Equipment and Experimental Procedure

X-ray powder diffraction data were collected using nickel-filtered Cu-K_α radiation (λ_m = 1.54179Å) with either a 19cm diameter Debye-Scherrer camera, in which two strips of film were mounted according to the Bradley-Bragg method[140], or a 10cm Guinier-Hägg focusing camera. Samples were finely ground and, for the Debye-Scherrer method, loaded into 0.3mm diameter, Lindemann capillaries which were then flame sealed, or, for the Guinier camera, sandwiched between 'Sellotape' on a sample holder. For radioactive samples, the sealed capillary was coated with 'Bostikote'[141] to contain surface α-activity and to afford protection against accidental breakage. An extra piece of 'Sellotape' was applied to the top face of the Guinier mounting ring prior to coating it with 'Bostikote'.

2:3:2 Unit Cell Determination

The positions of the diffraction lines were measured in centimetres with a micrometric ruler to a precision of 0.005cm. The procedures for converting the measurements into reflection angles, θ, differed for the methods employed.

2:3:2:1 Debye-Scherrer

Each line was measured from the low angle knife-edge image and converted to θ in degrees, by the following expression,

$$4\theta = \frac{(\Delta_1 + \Delta_2)}{(\Delta_1' + \Delta_2')} f + c \quad .$$

Δ_1 and Δ_2 are the positions of the lines on the two strips of film, in centimetres, $(\Delta_1' + \Delta_2')$ is the total length of the two strips of film between the knife-edge images and c is the camera constant in degrees. The film constant, f, represents the number of degrees of θ on the film and is given by $[360 - (c + \phi)]^\circ$ where c and ϕ are the angles subtended

by the low and high angle knife-edges, respectively.

The constants for the two Debye-Scherrer cameras used are given in Table 2:3.

Table 2:3 Debye-Scherrer Camera Constants

Camera	c	ϕ	(f)
A	20.000	19.744	(320.256)
B	19.972	19.876	(320.152)

2:3:2:2 Guinier-Hägg

Each line was measured from the focal line in centimetres and converted to θ in degrees by multiplying by the constant for the camera used, in this case 2.8762.

Miller indices were assigned to each $\sin^2\theta$ value by comparison either with values quoted in the literature or with values generated by the computer programme GENSTRUCK[142]. This programme calculated all values of $\sin^2\theta$ and hkl allowed for a particular space group and cell size from known or approximate cell dimensions.

Unit cell dimensions were refined using the computer programme COHEN[142] which calculated the best least-squares fit between observed and calculated $\sin^2\theta$ values, using the Nelson-Riley extrapolation[143]

$$\tfrac{1}{2}\left(\frac{\cos^2\theta}{\sin\theta} + \frac{\cos^2\theta}{\theta}\right)$$

2:3:3 Errors

Errors were minimised by using precision made cameras, by making sure that the sample was accurately centred and by taking care during film processing. These systematic errors are described in the following paragraphs.

(i) Film Shrinkage

With the Bradley-Bragg method of film mounting in a camera, accurately

measured angles subtended by the knife-edge shadows were printed on the film by scattered radiation during the exposure. If care was taken during processing, film shrinkage should have been uniform and did not, therefore, present a problem.

The Guinier camera constant accounted for any film shrinkage provided that the standard film processing procedure was followed.

(ii) Mounting of the Specimen

If the sample was displaced towards the entrance or the exit slit of the beam the values of θ would be either increased or decreased, respectively. In the Debye-Scherrer camera it was important to align the sample exactly at the centre of the camera and ensure that on rotation there was no discernible eccentricity. With the Guinier sample the retaining Sellotape disc had to sit flush with the backing tape to maintain the sample in one plane.

(iii) Absorption of the Beam in the Specimen

The thickness of a perfectly transparent specimen would only broaden the diffraction lines. However, if the specimen was very absorbent the diffracted lines would arise only at its surface and at different places according to the angle of diffraction. This error decreased as θ increased and was zero for $\theta = 180^{o}$ [144].

(iv) Refractive Index of the Crystal for X-Rays

This error arose from the variation of the wavelength of X-rays in the sample. The magnitude of the effect was small (0.003%) [145] and was neglected for this work.

(v) Sample Radiation Effects

Fogging of the film due to the radioactivity of daughter products in the neptunium samples did not present a problem for the length of exposure employed.

2:4 SPECTROPHOTOMETRIC STUDIES

Solution uv/visible spectra of neptunium(VI) complexes in 1M HCl were recorded on a Cary 14 or Cary 14H spectrophotometer to check for a neptunium(V) contaminant. Two methods were used to determine the approximate percentage of neptunium(V) in the materials and the methods were checked against each other.

2:4:1 Sodium Nitrite Reduction

A spectrum was recorded between 12000 and 4000Å to include the neptunium (V) peak at 9800Å. Solid $NaNO_2$ was then added to both the neptunium solution and the blank and after complete reduction of the neptunium(VI) a second spectrum was recorded. The percentage of neptunium(VI) in the starting material was then determined by a ratio of the heights of the two neptunium(V) peaks.

2:4:2 Beer Lambert Law

A spectrum was recorded between 13500 and 9000Å to include both the neptunium(VI) and neptunium(V) peaks at 12230 and 9800Å, respectively. The percentage of neptunium(V) was determined by employing the Beer Lambert law modified to:

$$\frac{[Np(V)]}{[Np(VI)]} = \frac{OD(V)}{OD(VI)} \times \frac{\varepsilon(VI)}{\varepsilon(V)} .$$

Where OD is the optical density which was measured directly from the spectra and $\varepsilon(VI)$ and $\varepsilon(V)$ are the molar extinction coefficients in 1 mol dm^{-3} HCl for the neptunium(VI) and neptunium(V) peaks, respectively. Comparison of literature values for neptunium(IV) molar extinction coefficients in both 2 mol dm^{-3} $HClO_4$ and 1 mol dm^{-3} HCl[146] (127 and 126, respectively, for the 7230Å peak and 162 and 160, respectively, for the 9600Å peak) indicated that the values for the neptunium (VI), 12230Å peak (ε = 45) and the neptunium(V), 9800Å peak (ε = 395) in 2 mol dm^{-3} $HClO_4$[147] were acceptable for solutions in 1 mol dm^{-3} HCl.

2:5 THERMOGRAVIMETRIC STUDIES

The decompositions of the alkali metal uranyl(VI) triacetates $M^{I}UO_2(CH_3COO)_3$ (M^{I} = NH_4, Li, Na, K, Rb and Cs) were followed on a Stanton Redcroft 'Massflow' vacuum and gas atmosphere thermobalance.

Samples of each of the acetates were heated in platinum buckets from room temperature to 1000°C at a rate of 10°C per minute under an atmosphere of dry oxygen. The temperature of 1000°C was maintained for one hour.

Thermogravimetric analysis and differential thermal analysis traces were obtained to determine the decomposition conditions for the preparation of the alkali metal diuranates(VI). X-ray powder diffraction data were collected for the products.

2:6 ALPHA ANALYSIS TECHNIQUES[148]

2:6:1 Quantitative

Analysis of neptunium complexes was achieved by gross α-counting of prepared sources (see Section 2:11:2) using a Simpson counter. This is illustrated diagramatically in Figure 2:3.

The Simpson counter is a gas multiplication counter or proportional counter, consisting of a metallic cylinder, the earthed negative electrode, and a thin wire along the cylinder axis as the positive electrode. The cylinder is continuously flushed with a slow flow of argon. The argon atoms form ion-pairs on bombardment with α-particles, each α-particle forming many ion pairs as it dissipates its energy. The electrons thus produced are accelerated towards the anode until they gain sufficient kinetic energy to cause further ionisation on collision with neutral argon atoms. This process, known as gas multiplication, continues as an avalanche which terminates when all free electrons are collected at the anode. By this method each incident α-particle induces an amplified pulse of charge at the anode which is proportional to its initial energy.

The Simpson counter is also known as a 2π counter as this is the solid angle from which it accepts radiation. Errors produced by inaccuracies such as alpha self-absorption and scattering in the source itself were corrected for by using a standard of precisely known disintegration rate to determine the geometry factor accurately.

2:6:2 Qualitative

Thin sources were also used for qualitative analysis by alpha-spectrometry. This makes use of the fact that nuclides emit alpha-particles of known, characteristic energies. A surface barrier detector is used to detect the α-emissions and the pulses are accumulated in channels,

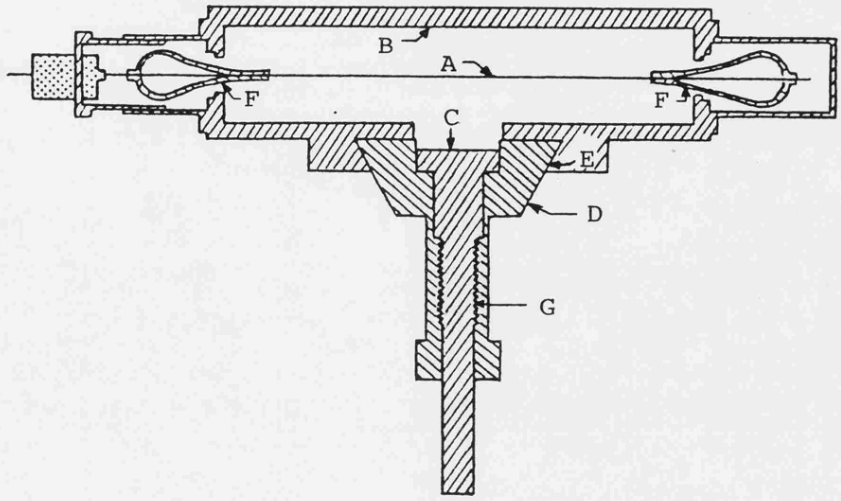

Fig. 2:3. The Simpson Counter A, centre wire (0.002" diameter); high-voltage positive electrode. B, outer cylinder; earthed negative electrode. C, sample holder (height adjustable). D, forward and backward movable slide. E, sliding surface. F, glass insulator. G, screw for raising sample.

dependent on their energies, by a multi-channel analyser.

An alpha-spectrum shows the number of particles of each energy emitted but due to coincidences in α-energies it is sometimes impossible to determine the emitting nuclide unambiguously. An example of this is the case of ^{238}Pu and ^{241}Am which have principal α-energies of 5.4992 and 5.4857 MeV[149], respectively. Further information is usually elucidated from the fine structure or daughter product chains which produce characteristic α-spectra.

A high resolution α-spectrum of ^{237}Np is illustrated in Figure 2:4 showing the different α-energies, in MeV, and the percentage α-particle abundancies.

Fig. 2:4. Alpha Spectrum of Neptunium-237[a]

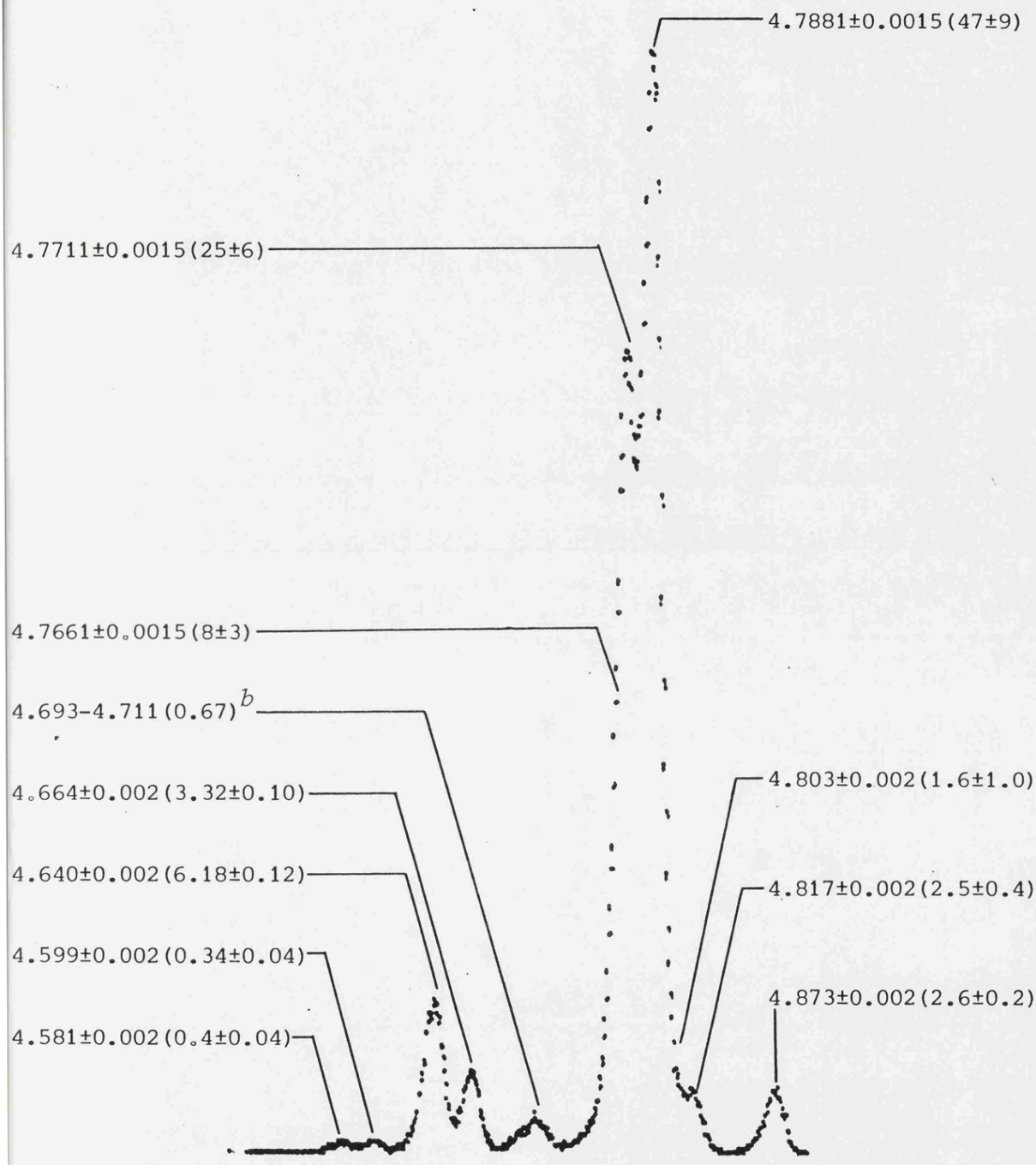

Alpha-energies (E_α) are given in MeV
Alpha-abundancies (I_α), as percentages, are shown in parentheses

[a] Numerical data from Ref.138 except [b] (Ref. 150)

2:7 THERMODYNAMIC STUDIES

Enthalpies of solution in Merck-titrated 1.000 mol dm^{-3} HCl were measured at 298.15 ± 0.10K for alkali metal uranates(VI), $M^{I}_{2}U_2O_7$ and for alkali metal neptunates(VI), $M^{I}_{2}Np_2O_7$ (M^{I} = Na, K, Rb, Cs). In addition the enthalpy of solution of US NBS Standard Reference Material 999:KCl[151] in 1 mol dm^{-3} HCl was measured to add to the available auxiliary thermodynamic data.

2:7:1 The Microcalorimeter

Enthalpies of solution for the alkali metal neptunates(VI) were determined using the isoperbolic microcalorimeter built at the Radiochemistry Laboratory of the University of Liège[152]. The main details of the microcalorimeter are described briefly in the following paragraphs.

(i) The Thermostatted Bath

This consisted of a tank of about 25 litres which was refrigerated with water from a preliminary thermostat (regulated to ±0.05K) by means of a proportional controller feeding a 250 Watt heating resistance. The overall stability of the bath was $\pm 0.5 \times 10^{-3}$K for 24 hours in a room thermostated to within ±0.7°C.

(ii) The Standard Circuit

The determination of the heat capacity depended on the temperature increase observed when an accurately known quantity of energy was dissipated by the Joule effect. For this purpose a stabiliser which generated a current with constant voltage (0.005% within 1 hour) was used to supply a heating resistance and accurate timing was provided by a quartz crystal chronometer.

By using a digital voltmeter (Solatron LM 1440) to measure the potential drop across the terminals of the heating resistance and a standard resistance placed in series an accurate measurement of the Joule effect was

obtained. The circuit had been constructed to produce about 0.01 calories per second in the calorimeter chamber and, by means of a resistance set, this input energy could be reduced by factors of 2, 5, 10 ... 100 as required.

(iii) Temperature Measurement Circuit

This was a modified Wheatstone Bridge shown diagramatically in Figure 2:5. R_1 - R_3 and R_5 - R_7 were high precision resistors with very low temperature coefficients, R_8 and R_9 formed the balancing resistance of the bridge and were mounted as a potentiometer with a total resistance of 3kΩ. R_4 was the thermistor.

The thermistor, positioned in one of the calorimeter chamber wells, was isolated by Mylar film and covered in low vapour pressure oil. The other resistors were immersed in oil and contained in a water-tight copper box in contact with the water in the thermostatted bath.

(iv) The Calorimeter Chamber

This was a tantalum chamber, illustrated diagramatically in Figure 2:6, designed to hold 8.5ml of solution. The two wells contained the thermistor and the heating resistance.

The solution within the chamber was stirred by means of a platinum propeller attached to a 1mm diameter silica rod. The sample, enclosed in a thin walled Pyrex bulb, was attached to the end of the silica rod with 'Apiezon' sealing wax and was released into the solution by breaking the bottom of the bulb against the stud in the base of the chamber. This was achieved by depression of the stirring mechanism.

(v) The Calorimeter Assembly (Figure 2:7)

To reduce the thermal exchange between the thermostat and the calorimeter the latter was placed within an enclosure which was evacuated to less than 13.33×10^{-3}Pa and the assembled apparatus was immersed in the thermo-

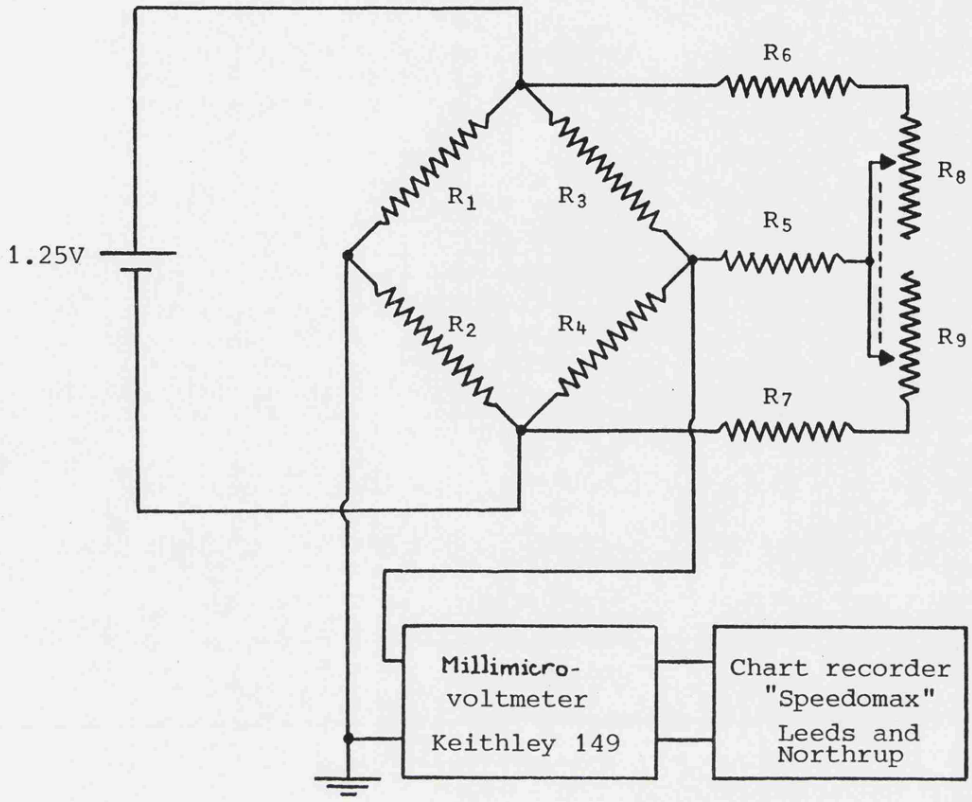

Fig. 2:5. Diagram of the Modified Wheatstone Bridge

R_1 = 100 Ω		Metal film resistors "Elettronica" (5×10^{-3} %/K)
R_2 5 Ω		
R_3 500 Ω		
R_5 10kΩ		
R_6 2kΩ		
R_7 500 Ω		
R_8 0-3kΩ		2 decade type resistors 0-3kΩ "John Fluke 65A/c" mounted as a potentiometer of 3kΩ resistance
R_9 3-0kΩ		
R_4 25 Ω		"Philips B832020" Thermistor (3%/K)

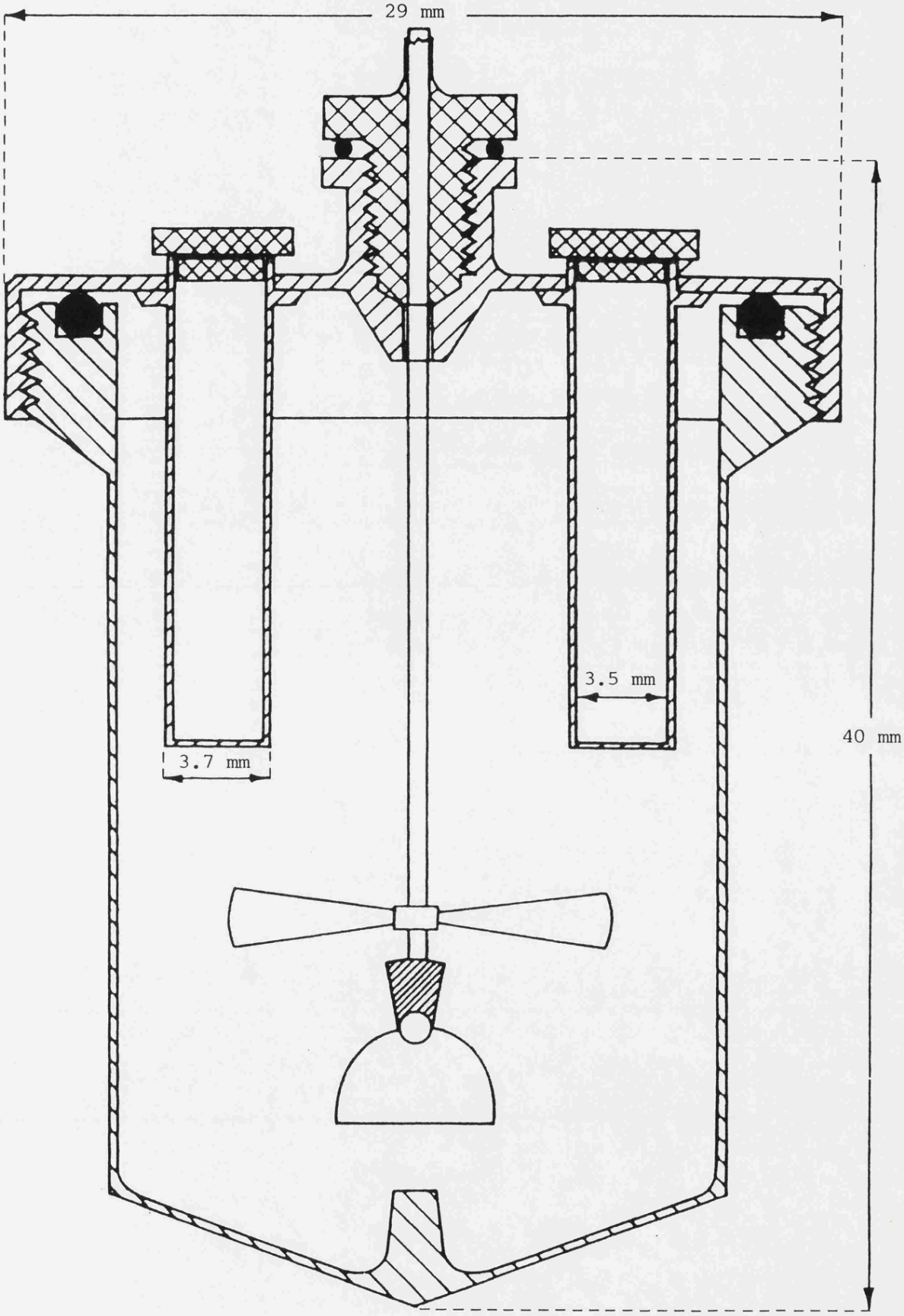

Fig. 2:6. The Microcalorimeter Chamber

statted bath.

The vacuum was produced by a mercury diffusion pump backed by a rotary vein pump.

The thermal characteristics of the microcalorimeter are summarised in Table 2:4.

Table 2:4 Thermal Characteristics of the Microcalorimeter

Heat Capacity	about 45 JK^{-1} (with 8.5ml H_2O)
Temperature of Operation	298K
Sensitivity	$5 \times 10^{-6}K$
Thermal Leakage Modulus	4.5×10^{-3} min^{-1}
Homogenisation Time (to 0.1%) after a Thermal Effect	2.5 min
Stability of the Bath	better than $10^{-3}K$ per 24 hours
Heat of Breakage of Sample Holder	$(3 \pm 1.5) \times 10^{-4}J$, but taking into account a 5 sec stopping of the stirrer $\pm 2 \times 10^{-4}J$

2:7:2 The LKB Calorimeter

The commercially available LKB 8700-1 Precision Calorimetry System[153] was used to determine enthalpies of solution of the alkali metal uranates (VI) and of KCl. The uranium complex measurements were recorded for the dissolution of the sample in 100ml 1 mol dm^{-3} HCl under an atmosphere of dry nitrogen. The KCl samples were dissolved in 25ml aliquots of 1 mol dm^{-3} HCl under an air atmosphere of 50% humidity.

A block diagram of the calorimetry system is illustrated in Figure 2:8. Apart from a few minor differences the system and its operation were essentially the same as the microcalorimeter.

(i) The Thermostatted Bath

The tank containing about 18 litres of water was cooled by circulating water at 1-2°C below the bath temperature. The temperature of the bath

Fig. 2:7

The Microcalorimeter Assembly


VÉGÉ

was regulated by a resistance heater of 70Ω and the overall stability was better than ±0.3K for 48 hours provided the mean room termperature did not vary by more than ±0.5°C.

(ii) The Standard Circuit

Heating in the calorimeter chamber was achieved by a stabilised supply feeding a 50Ω heater which was immersed in paraffin oil in one of the chamber wells. A stepwise selector could be set to provide 20, 50, 100, 200 or 500mW to the heater and a quartz crystal controlled oscillator provided accurate timing.

A precision DC potentioneter, standardised with a Weston standard cell, was used to measure the potential drop across the heater.

(iii) Temperature Measurement Circuit

This was a precision Wheatstone Bridge, illustrated diagramatically in Figure 2:9, which had a resistance range of 0-6000Ω in six decades,

5 x	1000	Ω ± 0.01%
10 x	100	Ω ± 0.02%
10 x	10	Ω ± 0.02%
10 x	1	Ω ± 0.05%
10 x	0.1	Ω ± 0.10%
10 x	0.01	Ω ± 0.20% .

The thermistor was positioned in one of the calorimeter chamber wells and was covered with paraffin oil.

(iv) The Calorimeter Chamber

Two chambers were used with capacities of 25ml and 100ml, respectively. Both vessels were Pyrex glass but the wells in the 25ml chamber were made of platinum.

The solution within the chamber was stirred by a pure-gold plated, 18 carat gold bulb holder/propeller attached to a metal rod. The thin walled Pyrex bulb which contained the sample was fastened to the holder/propeller with wax and was broken against a sapphire tipped stud by depression of

Fig. 2:8. Block Diagram of the LKB Calorimetry System

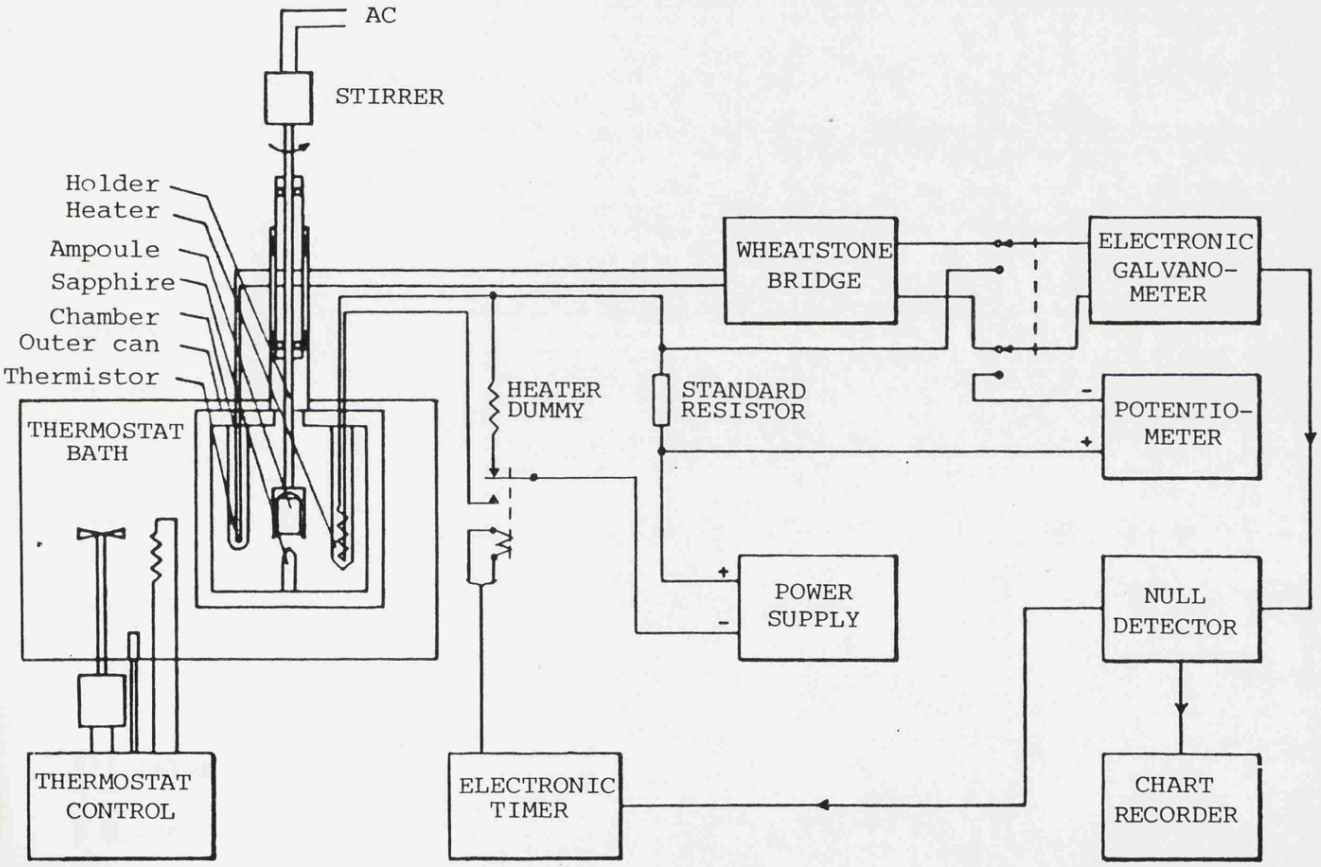

the stirring mechanism.

(v) The Calorimeter Assembly

For immersion into the thermostatted bath, the calorimeter chamber was enclosed in a chromium-plated brass can.

The performance of both calorimeters had been checked by measuring the enthalpy of solution of tris hydroxymethyl aminomethane (NBS Standard Reference Material 724) in 0.1 mol dm^{-3} HCl under conditions recommended by the US Bureau of Standards[154]. The results obtained[155,156] were in good agreement (within 0.1%) with the literature data[157,158, 159,160].

2:7:3 Units and Limits of Errors

Throughout this work the Joule (J) has been used as the unit of energy in order to comply with the International System of Units (SI Units). Where auxiliary data quoted in calories have been used these were recalculated using the conversion factor 1 cal (thermochemical) = 4.184J.

The ^{12}C scale of atomic weights[161] was used to calculate relative molecular masses.

All calorimetric measurements are reported for a temperature of 298.15 ± 0.05K.

Uncertainty limits on the mean of several identical measurements are based on the 95% confidence level. These were calculated by the standard statistical method[162] as the product of the standard error and the 5% Student t value for the number of degrees of freedom of the data. In calculating enthalpies of formation the errors on the individual terms in the thermodynamic cycle have been combined as the square-root of the sum of the squares to obtain the overall uncertainty limits[163]. Where data from other sources have been used the error has been taken as that

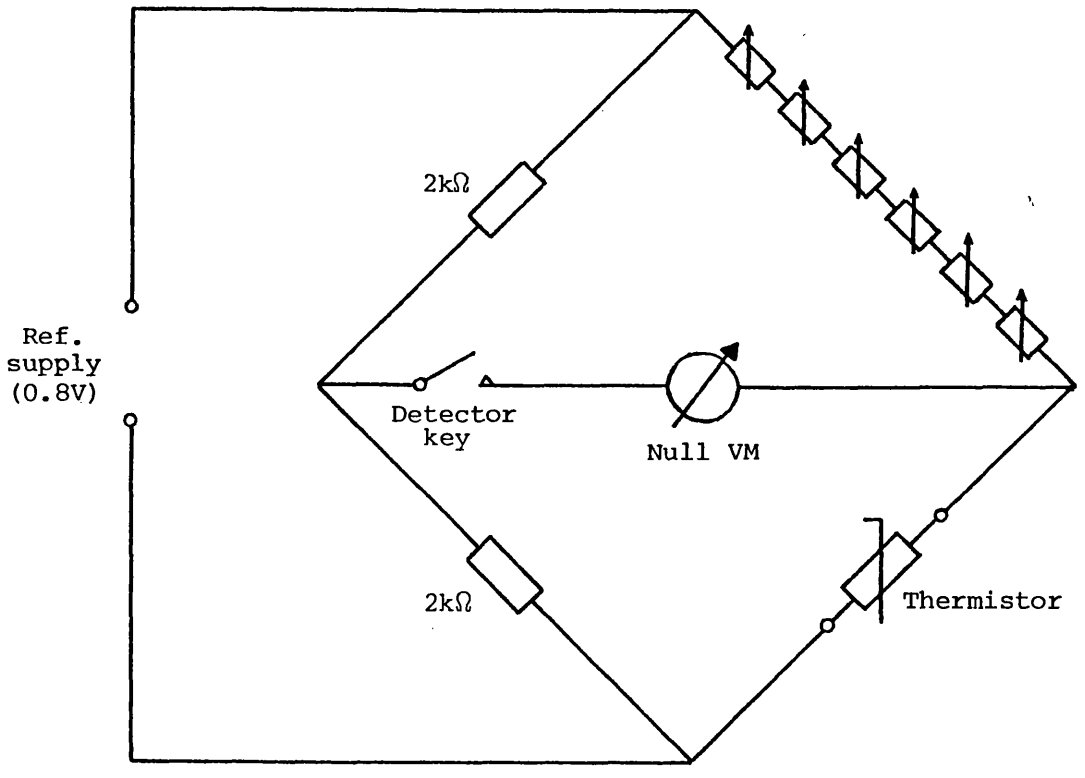

Fig. 2:9. LKB Precision Wheatstone Bridge

stated by the authors.

Where available, auxiliary thermodynamic data have been preferentially taken from the selected CODATA values[164], the selected thermochemical data compatible with the CODATA recommendations[165] or from US NBS Technical Notes, in order to be consistent with recent and current assessments of thermodynamic data on actinide elements and compounds[11,166-175].

2:7:4 Enthalpies of Solution

The uranium and neptunium calorimetric samples were weighed and sealed in thin-walled Pyrex bulbs in glove boxes filled with dry nitrogen. All samples were weighed on a Cahn gram electric microbalance with an ultimate sensitivity of 0.1μg.

Following the measurement of the enthalpy of solution of a neptunyl(VI) oxide, the spectrum between 12000 and 9000Å was recorded to monitor for reduction to neptunium(V) occurring during the calorimetry.

Several small corrections needed to be applied in the calculation of the enthalpies of solution[176] from the experimental data.

(i) The resistance of the thin wires connecting the heating resistance in the calorimeter chamber to the point where the potential was measured caused extra heat to be dissipated in the system when a current was passed. Thus, when calibrating the system, the temperature rise measured in the chamber was higher than that caused by the dissipation of the known quantity of input energy. To correct for this the calibration values were reduced by 0.07% in the microcalorimeter and by 0.013Ω in the LKB calorimeter. These values have been calculated from the measured resistance of the wires for the length involved based on the assumption that 50% of the induced heat was lost and 50% was transferred into the calorimeter chamber.

(ii) An amount of heat was produced by the breaking of the Pyrex ampoule. In the microcalorimeter this heat production was balanced by the endothermic effect introduced for a 5 second interruption of the stirring. These effects produced an uncertainty of about 2×10^{-4} but any subsequent stopping of the stirrer caused a heat loss of 8×10^{-5}J per second. Breaking of the LKB calorimeter bulbs produced 0.005J in the system.

(iii) When the sample bulb was broken the gas enclosed became saturated to the amount of the vapour pressure of the solvent constituents. At 25°C in 1 mol dm^{-3} HCl this effect caused a heat absorption of 5.8×10^{-5}J per µl of dry gas. This value was due to the vapourisation of H_2O from 1 mol dm^{-3} HCl as the vapour pressure of HCl over 1 mol dm^{-3} HCl at 25°C is negligible[177].

2.8 REAGENTS

High purity salts of the alkali metals, as shown in Table 2:5, were used in order to minimise cross-contamination between these elements.

Table 2:5 Purity of Alkali Metal Salts

Salt	Source	Purity
$LiOH.H_2O$	Koch-Light	'Puriss' > 99%
Li_2CO_3	Koch-Light	99.995%
$NaCH_3COO$	BDH	'Aristar' 99.999%
KOH	Koch-Light	'AR' > 85%[a]
KCH_3COO	Koch-Light	'Puriss' > 99%
$K_2CO_3.\frac{1}{2}H_2O$	BDH	'Aristar' 99.999%
RbOH	Koch-Light	> 99.8%
Rb_2CO_3	Koch-Light	> 99.8%
CsOH	Koch-Light	99%
Cs_2CO_3	Koch-Light	99%

[a] K_2CO_3 as the main impurity

Two sources of uranium were used: uranyl(VI) diacetate dihydrate as supplied by BDH and amorphous uranium trioxide available at AERE Harwell.

Neptunium, supplied as the dioxide or in recovered solutions, was purified and then used from a calibrated stock solution in 4 mol dm^{-3} hydrochloric acid.

Deionised water was passed through a mixed bed resin prior to use as low sodium content water for alkali metal analyses. All other chemicals and solvents used were reagent grade.

2:9 PURIFICATION OF NEPTUNIUM

The neptunium available was contaminated with plutonium-238 and possibly americium (see Section 2:6:2) and was purified by anion exchange[178].

A four-times excess of 50-100 mesh, 1.2 meq ml^{-1} anion exchange resin (Bio-Rad AG 1-X4, chloride form) was used to prepare a column. This was conditioned by washing it successively with 2, 4, 6, 8,10 mol dm^{-3} and concentrated hydrochloric acid immediately before use.

Neptunium dioxide was dissolved in boiling nitric acid. Addition of a single crystal of ammonium fluoride was necessary to complete the dissolution. The resulting solution was diluted and treated with ammonium hydroxide solution to precipitate neptunium hydroxide. Neptunium was precipitated as the hydroxide from recovered solutions by the same process. The precipitate was collected by centrifugation.

Freshly precipitated neptunium hydroxide was washed well with water and dissolved in concentrated hydrochloric acid. The precipitation and washing was repeated and the hydroxide redissolved in concentrated hydrochloric acid saturated with ammonium iodide as a reducing agent. Further reductant was added and the solution was heated at 60°C for 30 minutes. This ensured that neptunium was in the quadrivalent state and that plutonium was in the trivalent state. When the solution had cooled, further concentrated hydrochloric acid was added to ensure a high acid concentration. This solution was passed through the resin at a rate of 1ml min^{-1}, when the neptunium was absorbed. The column was then washed with six column volumes of concentrated hydrochloric acid to remove the trivalent plutonium and americium. Neptunium was then eluted with 1 mol dm^{-3} HCl.

The purified neptunium solution was used to prepare a 50ml stock solution which was analysed qualitatively by α-spectrometry (Section 2:6:2) and quantitatively by gross α-counting (Section 2:6:1).

2:10 PREPARATIVE METHODS

2:10:1 Acetate Complexes

The preparation of the complex acetates of the form $M^{I}M^{VI}O_2(CH_3COO)_3$ (M^{I} = Li, Na, K, Rb, Cs; M^{VI} = U, Np) can be described by the general equation,

$$M^{VI}O_2{}^{2+}(aq) + M^{I+}(aq) \xrightarrow{CH_3COOH} M^{I}M^{VI}O_2(CH_3COO)_3(s).$$

2:10:1:1 Alkali Metal Uranyl(VI) Triacetates

Usually, the preparations of these complexes were carried out in aqueous solutions of acetic acid. In preparations involving uranyl(VI) diacetate dihydrate, the dihydrate was brought into solution in hot dilute acetic acid by the addition of a sufficient volume of aqueous ammonium acetate. Uranium trioxide was dissolved by heating in a moderate or concentrated acetic acid solution.

The alkali metal was added to the hot uranyl(VI) solution as a saturated aqueous solution of the acetate or as a solution of the carbonate dissolved and neutralised in 9 mol dm^{-3} acetic acid. The resulting mixture was filtered whilst hot and then reduced in volume to initiate crystallisation.

Where products were recrystallised, this was from 0.4 mol dm^{-3} acetic acid. The products were washed with glacial acetic acid at about 16°C, and ether at room temperature.

This general route was not used for two of the preparations of sodium uranyl(VI) triacetate. These are described in the following pages.

(i) Preparation 1

$NaUO_2(CH_3COO)_3$

Sodium uranyl(VI) triacetate was prepared by adding solid uranyl(VI) nitrate hexahydrate (6.35 mmoles) to a saturated aqueous solution of sodium

acetate (31.4 mmoles), with stirring. Dissolution of the uranyl nitrate resulted in the precipitation of the product. The precipitate was recrystallised from 0.2 mol dm^{-3} acetic acid and, after washing, dried at 130°C. The yield was 54%.

The preparations of the analogous potassium, rubidium and caesium salts are summarised in Table 2:6.

Table 2:6 Preparation 1

Product	Concentration of Acetic Acid (mol dm^{-3})	Uranium Salt	Alkali Metal Salt	Yield[a]
$KUO_2(CH_3COO)_3$	2	$UO_2(CH_3COO)_2.2H_2O$ 9.3 mmoles	KCH_3COO 9.3 mmoles	28%
$RbUO_2(CH_3COO)_3$	2	$UO_2(CH_3COO)_2.2H_2O$ 8.7 mmoles	Rb_2CO_3 4.4 mmoles	22%
$CsUO_2(CH_3COO)_3$	2.5	$UO_2(CH_3COO)_2.2H_2O$ 5.8 mmoles	Cs_2CO_3 2.8 mmoles	28%

[a] After recrystallisation

(ii) Preparation 2

$NaUO_2(CH_3COO)_3$

Sodium uranyl(VI) triacetate was crystallised from a 0.6 mol dm^{-3} HNO_3/ 4 mol dm^{-3} CH_3COOH aqueous solution containing stoicheiometric amounts of uranyl(VI) diacetate dihydrate and sodium acetate. The product was recrystallised from 0.4 mol dm^{-3} acetic acid and, after washing, was dried at 130°C.

The preparations of the lithium, potassium, rubidium and caesium analogues are summarised in Table 2:7.

Table 2:7 Preparation 2

Product	Concentration of Acetic Acid (mol dm^{-3})	Uranium Salt	Alkali Metal Salt	Yield[a]
$LiUO_2(CH_3COO)_3.nH_2O$	17	UO_3 4.9 mmoles	Li_2CO_3 2.5 mmoles	28%[b]
$KUO_2(CH_3COO)_3$	17	UO_3 6.1 mmoles	KCH_3COO 6.6 mmoles	64%[c]
$RbUO_2(CH_3COO)_3$	17	UO_3 6.3 mmoles	Rb_2CO_3 3.6 mmoles	57%
$CsUO_2(CH_3COO)_3$	14	UO_3 6.1 mmoles	Cs_2CO_3 3.3 mmoles	45%

a After recrystallisation and vacuum drying

b Based on the trihydrate[179]

c Not recrystallised

(iii) Preparation 3

The preparative details are summarised in Table 2:8.

Table 2:8 Preparation 3

Product	Concentration of Acetic Acid (mol dm^{-3})	Uranium Salt	Alkali Metal Salt	Yield[a]
$LiUO_2(CH_3COO)_3.nH_2O$	9	UO_3 13.0 mmoles	Li_2CO_3 6.4 mmoles	76%[b]
$NaUO_2(CH_3COO)_3$	9	UO_3 12.9 mmoles	$NaCH_3COO$ 13.2 mmoles	85%
$KUO_2(CH_3COO)_3$	9	UO_3 12.4 mmoles	$K_2CO_3.1\frac{1}{2}H_2O$ 6.6 mmoles	75%
$RbUO_2(CH_3COO)_3$	9	UO_3 11.3 mmoles	Rb_2CO_3 5.7 mmoles	30%
$CsUO_2(CH_3COO)_3$	9	UO_3 10.3 mmoles	Cs_2CO_3 5.2 mmoles	58%

a Products were not recrystallised

b Based on a hydration number of 1.8 as the result of a uranium analysis

2:10:1:2 Alkali Metal Neptunyl(VI) Triacetates[180,181]

These complexes were all precipitated from concentrated acetic acid solutions using the following general preparative route.

A small volume (1-2ml) of a neptunium(IV) stock solution in 4 mol dm^{-3} HCl was oxidised to neptunium(VI) by ozone at 80-90°C. After cooling, neptunium(VI) hydroxide was precipitated by dropwise addition of '880' NH_3 solution for the sodium preparations or alkali metal hydroxide solutions (3-6 mol dm^{-3}) for the other alkali metal complexes. The resulting precipitate was washed twice with 2ml aliquots of water and dissolved in a minimum volume of hot glacial acetic acid. This solution was diluted two fold with water and the ozonisation, precipitation, washing and dissolution sequence was repeated.

The required alkali metal was added to the hot acetic acid neptunyl(VI) solution as a saturated solution of the acetate in glacial acetic acid or as the carbonate dissolved in and neutralised by glacial acetic acid.

Where necessary, precipitation was induced by volume reduction and cooling in ice. The products were washed with glacial acetic acid at about 16°C, a cold solution of equal parts glacial acetic acid and diethyl ether and finally with diethyl ether.

With the exception of one sample of sodium neptunyl(VI) triacetate crystallised from 0.2 mol dm^{-3} acetic acid for single crystal X-ray diffraction[182], the products were not recrystallised. All the products were ground to fine powders and vacuum dried.

Although the following tabulated summaries of the preparations (Tables 2:9 and 2:10) indicate the use of approximately stoicheiometric amounts of alkali metal and neptunium, there was always a small excess of alkali metal in the neptunyl(VI) solutions arising from the use of alkali metal hydroxides. For this reason all yields are based on the neptunium content.

The yields are calculated from weighings taken after grinding and vacuum drying.

Table 2:9 Preparation 4

Product	Precipitating Solution	Quantity of Neptunium	Alkali Metal Salt	Yield
$LiNpO_2(CH_3COO)_3$	4 mol dm^{-3} LiOH	0.438 mmoles	Li_2CO_3 0.212 mmoles	59%[a]
$NaNpO_2(CH_3COO)_3$	'880' NH_3	0.655 mmoles	$NaCH_3COO$ 0.711 mmoles	88%
$KNpO_2(CH_3COO)_3$	3.5 mol dm^{-3} KOH	0.655 mmoles	KCH_3COO 0.660 mmoles	81%
$RbNpO_2(CO_3COO)_3$	5 mol dm^{-3} RbOH	0.655 mmoles	$RbCH_3COO$[b] 0.645 mmoles	54%
$CsNpO_2(CH_3COO)_3$	6 mol dm^{-3} CsOH	0.655 mmoles	Cs_2CO_3 0.333 mmoles	59%

a Based on the non-hydrated salt

b Precipitated from a solution of Rb_2CO_3 in glacial acetic acid (183)

Table 2:10 Preparation 5

Product	Precipitating Solution	Quantity of Neptunium	Alkali Metal Salt	Yield
$NaNpO_2(CH_3COO)_3$	'880' NH_3	0.655 mmoles	$NaCH_3COO$ 0.712 mmoles	92%
$KNpO_2(CH_3COO)_3$	6 mol dm^{-3} KOH	0.655 mmoles	$K_2CO_3.1\frac{1}{2}H_2O$ 0.326 mmoles	81%
$RbNpO_2(CH_3COO)_3$	5 mol dm^{-3} RbOH	0.655 mmoles	Rb_2CO_3 0.331 mmoles	53%
$CsNpO_2(CH_3COO)_3$	6 mol dm^{-3} CsOH	0.655 mmoles	Cs_2CO_3 0.281 mmoles	44%

Preparation 6

A sample of caesium neptunyl(VI) triacetate, $CsNpO_2(CH_3COO)_3$, was prepared with 0.327 mmoles of neptunium(VI) as the hydroxide dissolved in glacial acetic acid by addition of Cs_2CO_3 (0.163 mmoles) in acetic acid.

The product was not vacuum dried. After preparation the material was kept in the dark.

2:10:2 Oxides

Alkali metal diuranates(VI) and dineptunates(VI) were prepared by controlled decomposition of the acetate complexes previously described. Finely powdered samples of the alkali metal actinyl(VI) acetates were fired in gold crucibles at temperatures between 400 and 750°C, under oxygen, in a tube furnace (Section 2:2).

This decomposition can be described as follows:

$$2M^{I}M^{VI}O_2(CH_3COO)_3 + 12O_2 \xrightarrow{\Delta} M^{I}_2M^{VI}_2O_7 + 12CO_2 + 9H_2O.$$

2:10:2:1 Alkali Metal Diuranates(VI)

(i) Preparation 7

The alkali metal uranyl(VI) triacetates from 'Preparation 1' were decomposed to the corresponding alkali metal diuranates(VI), $M^{I}_2U_2O_7$, as summarised in Table 2:11.

Table 2:11 Preparation 7

Starting Material[a] (from 'Preparation 1')	Temp (°C)	Duration of Heating (hrs)	Re-fire temp (°C)	Duration of Re-firing (hrs)	Final Colour	Product
$NaUO_2(CH_3COO)_3$ 0.503 mmoles	750	16			Saffron	$Na_2U_2O_7$
$KUO_2(CH_3COO)_3$ 0.443 mmoles	750	16	650	2	Saffron	$K_2U_2O_7$[b]
$RbUO_2(CH_3COO)_3$ 0.311 mmoles	750	16	650	2	Saffron	$Rb_2U_2O_7$[b]
$CsUO_2(CH_3COO)_3$ 0.215 mmoles	750	16	650	2	Orange	$Cs_2U_2O_7$[b]

a All starting materials were pale yellow in colour

b The potassium, rubidium and caesium materials were ground prior to re-firing

(ii) Preparation 8

The alkali metal uranyl(VI) triacetates from 'Preparation 2' were decomposed as summarised in Table 2:12.

Table 2:12 Preparation 8

Starting Material[a] (from 'Preparation 2')	Temp (°C)	Duration of Heating (hrs)	Re-fire temp (°C)	Duration of Re-firing (hrs)	Final Colour	Product
$LiUO_2(CH_3COO)_3 . nH_2O$	400	2			Yellow ochre	Mixture predominantly $Li_2U_3O_{10}$
$LiUO_2(CH_3COO)_3 . nH_2O$	750	2			Yellow	$Li_2U_3O_{10}$/ $Li_2O.1.75UO_3$
$NaUO_2(CH_3COO)_3$ 0.518 mmoles	750	2			Saffron	$Na_2U_2O_7$
$KUO_2(CH_3COO)_3$ 0.674 mmoles	750	2	650	2	Saffron	$K_2U_2O_7$[b]
$RbUO_2(CH_3COO)_3$ 0.764 mmoles	750	2	650	2	Saffron	$Rb_2U_2O_7$[b]
$CsUO_2(CH_3COO)_3$ 0.513 mmoles	750	2	650	2	Orange	$Cs_2U_2O_7$[b]

a All starting materials were pale yellow in colour

b The potassium, rubidium and caesium materials were ground prior to re-firing

(iii) Preparation 9

The acetate complexes from 'Preparation 3' were fired at 650°C as summarised in Table 2:13.

Table 2:13 Preparation 9

Starting Material from 'Preparation 3'	Temp (°C)	Duration of Heating (hrs)	Re-fire temp (°C)	Duration of Re-firing (hrs)	Final Colour	Product
$LiUO_2(CH_3COO)_3 . nH_2O$	650	2.5	650	2	Yellow	$Li_2U_3O_{10}$/ $Li_2O.1.75UO_3$
$NaUO_2(CH_3COO)_3$ 1.68 mmoles	650	2.5			Saffron	$Na_2U_2O_7$
$KUO_2(CH_3COO)_3$ 1.58 mmoles	650	2.5	650	2	Saffron	$K_2U_2O_7$
$RbUO_2(CH_3COO)_3$ 1.32 mmoles	650	2.5	650	2	Saffron	$Rb_2U_2O_7$
$CsUO_2(CH_3COO)_3$ 1.22 mmoles	650	2.5	650	2	Orange	$Cs_2U_2O_7$

2:10:2:2 Stability of Alkali Metal Diuranates(VI) in Air

The decomposition of the alkali metal uranyl(VI) triacetates in air was investigated by firing the complexes from 'Preparation 2', contained in silica crucibles, on an electric Bunsen. Weight losses for the decompositions were determined. A summary of the results is presented in Table 2:14.

No change in weight, colour or X-ray diffraction pattern was observed after samples of the alkali metal diuranates(VI) from 'Preparation 7' were exposed to the laboratory atmosphere for 21 days.

Table 2:14 Decomposition of Alkali Metal Uranyl(VI) Triacetates in Air

Starting Material from 'Preparation 7'	Temp (°C)	Duration of Heating (hrs)	Exptl Wt Loss (%)	Theor Wt Loss[a] (%)	Final Colour	Product[b]
$LiUO_2(CH_3COO)_3.nH_2O$	430	6	37.86	(33.72)	Yellow and v dk green mixture	No Identification
$NaUO_2(CH_3COO)_3$ 0.134 mmoles	490	2.5	32.23	32.57	Saffron	$Na_2U_2O_7$
$KUO_2(CH_3COO)_3$ 0.174 mmoles	430	5.5	31.23	31.49	Saffron	$K_2U_2O_7$
$RbUO_2(CH_3COO)_3$ 0.174 mmoles	530	2.5	28.73	28.75	Saffron	$Rb_2U_2O_7$
$CsUO_2(CH_3COO)_3$ 0.107 mmoles	640	5	26.54	26.40	Orange/ Saffron mixture	$Cs_2U_2O_7$

Table 2:14 *a* Based on the reaction $M^{I}UO_2(CH_3COO)_3 \rightarrow \frac{1}{2}M^{I}_2U_2O_7$

b Based on X-ray powder diffraction data, weight loss and colour

2:10:2:3 Alkali Metal Dineptunates(VI)

These preparations were carried out in pre-fired, pre-weighed gold crucibles and weight losses for the decompositions were determined.

In the following tables summarising the preparations of the alkali metal dineptunates(VI):

(a) The theoretical percentage weight loss is for the reaction, $M^{I}NpO_2(CH_3COO)_3 \rightarrow \frac{1}{2}M^{I}_2Np_2O_7$;

(b) The products are as indicated by X-ray powder diffraction, weight loss and analysis. All the products were black.

(i) Preparation 10

Table 2:15 shows the decomposition of the alkali metal neptunyl(VI) triacetates from 'Preparation 4'.

Table 2:15 Preparation 10

Starting Material[a] from 'Preparation 4'	Temp (°C)	Duration of Heating (hrs)	Exptl Wt Loss (%)	Theor Wt Loss (%)	Product
$LiNpO_2(CH_3COO)_3$ 0.072 mmoles	400	2	37.90		NpO_2[b]
$LiNpO_2(CH_3COO)_3$ 0.144 mmoles	650	2	39.02		NpO_2/ Li_2NpO_4
$NaNpO_2(CH_3COO)_3$ 0.269 mmoles	700	1.5	32.96	32.64	$Na_2Np_2O_7$
$KNpO_2(CH_3COO)_3$ 0.244 mmoles	600	2	31.45	31.56	$K_2Np_2O_7$
$RbNpO_2(CH_3COO)_3$ 0.189 mmoles	600	2	29.01	28.81	$Rb_2Np_2O_7$
$CsNpO_2(CH_3COO)_3$ 0.176 mmoles	600	2	26.91	26.45	$Cs_2Np_2O_7$

a Starting materials were pale green or grey-green in colour

b Only lines due to NpO_2 were visible on an X-ray powder film

(ii) Preparation 11

A second decomposition of 'Preparation 4' alkali metal neptunyl(VI) triacetates is summarised in Table 2:16.

Table 2:16 Preparation 11

Starting Material from 'Preparation 4'	Temp (°C)	Duration of Heating (hrs)	Exptl Wt Loss (%)	Theor Wt Loss (%)	Product
$NaNpO_2(CH_3COO)_3$ 0.106 mmoles	650	1.5	32.80	32.64	$Na_2Np_2O_7$
$KNpO_2(CH_3COO)_3$ 0.119 mmoles	600	2.25	31.66	31.56	$K_2Np_2O_7$
$RbNpO_2(CH_3COO)_3$ 0.087 mmoles	600	2	29.03	28.81	$Rb_2Np_2O_7$
$CsNpO_2(CH_3COO)_3$ 0.097 mmoles	600	2	26.88	26.45	$Cs_2Np_2O_7$

(iii) Preparation 12

Table 2:17 summarises the decomposition of the alkali metal neptunyl(VI) triacetates from 'Preparation 5'.

Table 2:17 Preparation 12

Starting Material from 'Preparation 5'	Temp (°C)	Duration of Heating (hrs)	Exptl Wt Loss (%)	Theor Wt Loss (%)	Product
$NaNpO_2(CH_3COO)_3$ 0.306 mmoles	650	2	32.63	32.64	$Na_2Np_2O_7$
$KNpO_2(CH_3COO)_3$ 0.254 mmoles	600	2	31.61	31.56	$K_2Np_2O_7$
$RbNpO_2(CH_3COO)_3$ 0.257 mmoles	600	2	28.95	28.81	$Rb_2Np_2O_7$
$CsNpO_2(CH_3COO)_3$ 0.250 mmoles	600	2	26.83	26.45	$Cs_2Np_2O_7$

(iv) Preparation 13

'Preparation 6' caesium neptunyl(VI) triacetate (0.052 mmoles) was fired at 600°C for 2 hours under a circulating oxygen atmosphere to yield caesium dineptunate(VI), $Cs_2Np_2O_7$.

2:11 ANALYTICAL TECHNIQUES

2:11:1 Determination of Uranium

Weighed samples of the compounds were dissolved in 8 mol dm^{-3} HNO_3 (1ml) and the solution diluted three fold with water. Uranium(VI) hydroxide was precipitated with a 1:1:1 solution of '880' NH_3, water and acetone. After washing thoroughly with the ammoniacal solution and a 10% acetone solution in water, the hydroxide was collected in a pre-fired, pre-weighed, grade 4 silica filter crucible. The solid was fired in air at 800°C and, when cool, weighed as U_3O_8.

2:11:2 Determination of Neptunium

Quantitative analysis of neptunium was achieved by gross α-counting of known aliquots of 5ml acid solutions containing a weighed amount of compound.

Stainless steel discs were treated as follows. The discs were boiled in concentrated nitric acid and washed with water and then acetone. The clean, degreased discs were fired to dull red heat in air to produce a thin oxide film. A band of 'Zapon' lacquer was applied to the rim of each disc to limit the active area.
5 or 10μl aliquots of the prepared solutions in 2 mol dm^{-3} nitric acid were pipetted onto the discs from mercury calibrated pipettes, along with at least three aqueous washings of the pipette. One or two drops of tetraethylene glycol were added as a spreading agent (to produce a uniform source) and the solution was evaporated under an infra-red lamp. The dry discs were then fired to red heat in air to fix the activity.

The prepared discs were counted in a gas flow (argon) proportional counter (Section 2:6:1). The final α-count was corrected for background and geometry factor and the amount of neptunium determined by dividing the number of disintegrations by the specific activity of neptunium-237 (1.5645×10^3 dpm μg^{-1}).

The same method was used to prepare sources for the quantitative and qualitative analysis (Section 2:6:2) of the neptunium stock solution (Section 2:9) except that tantalum discs were used to be compatible with the hydrochloric acid solution.

2:11:3 Determination of Alkali Metal

(i) Alkali Metal Diuranates(VI)

The precipitating and washing solutions from the appropriate gravimetric uranium analysis were transferred to a calibrated volumetric flask (25ml) and the solution diluted to the required volume with specially purified water (Section 2:8). Samples of the resulting solution were analysed by atomic absorption or emission spectrophotometry.

(ii) Alkali Metal Dineptunates(VI)

Samples of the solutions prepared for neptunium analysis were analysed for alkali metal content by atomic absorption or emission spectrophotometry after removal of the neptunium by anion exchange.

2:11:4 Analytical Results

Chemical analysis results are presented in the following tables.

Table 2:18 Typical Analytical Data for the Alkali Metal Uranyl(VI) Triacetates

Compound	Colour[a]	% of U	
		Exptl	Theor
$NaUO_2(CH_3COO)_3$	Pale Yellow	50.63	50.63
$KUO_2(CH_3COO)_3$	Pale Yellow	48.87	48.95
$RbUO_2(CH_3COO)_3$	Pale Yellow	44.96	44.69
$CsUO_2(CH_3COO)_3$	Pale Yellow	40.68	41.03

[a] Finely powdered material

Table 2:19 Typical Analytical Data for the Alkali Metal Neptunyl(VI) Triacetates

Compound	Colour[a]	% of Np		% of M^I	
		Exptl	Theor	Exptl	Theor
$LiNpO_2(CH_3COO)_3$	Pale Green	52.44	52.31	1.28	1.53
$NaNpO_2(CH_3COO)_3$	Grey Green	50.39	50.52	5.11	4.90
$KNpO_2(CH_3COO)_3$	Pale Green	48.81	48.84	7.70	8.06
$RbNpO_2(CH_3COO)_3$	Pale Green	44.87	44.58	16.44	16.08
$CsNpO_2(CH_3COO)_3$	Pale Bright Green	40.75	40.93	23.46	22.95

[a] Finely powdered material

Table 2:20 Analytical Data for the Alkali Metal Diuranates(VI)

Compound	% of M^I		% of U		M^I:U Ratio[a]
	Exptl	Theor	Exptl	Theor	
$Na_2U_2O_7$ 'Prep 8'	7.26	7.25	74.08	75.08	1.03
$Na_2U_2O_7$ 'Prep 9'	7.40		74.56		1.01
$K_2U_2O_7$ 'Prep 9'	11.80	11.74	71.47	71.45	1.00
$Rb_2U_2O_7$ 'Prep 8'	22.03	22.52	62.49	62.72	1.02
$Rb_2U_2O_7$ 'Prep 9'	22.17		62.70		1.02
$Cs_2U_2O_7$ 'Prep 8'	31.33	31.13	55.76	55.75	0.99
$Cs_2U_2O_7$ 'Prep 9'	30.92		55.56		1.00

a $$\frac{M^I(\text{found}) \times U^{VI}(\text{theoretical})}{M^I(\text{theoretical}) \times U^{VI}(\text{found})}$$

Table 2:21 Analytical Data for the Alkali Metal Dineptunates(VI)

Compound[a]	% of M^I		% of Np		M^I:Np Ratio[b]
	Exptl	Theor	Exptl	Theor	
$Na_2Np_2O_7$ 'Prep 10'	7.85	7.28	76.41	75.00	1.06
$Na_2Np_2O_7$ 'Prep 12'	7.03		75.87		0.95
$K_2Np_2O_7$ 'Prep 10'	12.12	11.77	72.54	71.36	1.01
$K_2Np_2O_7$ 'Prep 12'	11.83		72.83		0.98
$Rb_2Np_2O_7$ 'Prep 10'	22.64	22.52	63.05	62.46	1.00
$Rb_2Np_2O_7$ 'Prep 12'	22.47		63.66		0.98
$Cs_2Np_2O_7$ 'Prep 10'	30.43	31.21	54.69	55.65	0.99
$Cs_2Np_2O_7$ 'Prep 12'	31.03		56.44		0.98

a All materials were black

b $$\frac{M^I(\text{found}) \times Np^{VI}(\text{theoretical})}{M^I(\text{theoretical}) \times Np^{VI}(\text{found})}$$

3. RESULTS AND DISCUSSION

3:1 ACETATE COMPLEXES

3:1:1 Preparative Methods

The preparations of various alkali metal actinyl(VI) triacetates have been described previously[129, 179-181]. Using the reported methods as a guide, adaptations were made to provide preparative routes to the uranyl salts, and ultimately to the uranates, and in the case of the neptunyl salts, to maximise the yields of pure products. These acetate complexes were analysed by chemical methods (Tables 2:18 and 2:19) and by X-ray powder diffraction (see Section 3:1:2).

3:1:1:1 Alkali-Metal Uranyl(VI) Triacetates

In experiments to test the efficacy of the proposed methods for the preparation of the series of pure alkali-metal uranyl(VI) triacetates, the following results were obtained.

Uranium trioxide dissolved fairly readily in glacial acetic acid, with heating, and uranyl(VI) acetate crystallised from the resulting solution. Dissolution of uranyl(VI) diacetate dihydrate in aqueous acetic acid was achieved only by the addition of ammonium acetate with heating. However, prolonged heating of the resulting solution containing an excess of ammonium ions produced acetamide. Addition of ether to a saturated uranyl(VI) acetate solution containing ammonium ions resulted in the precipitation of ammonium uranyl(VI) triacetate, but addition of a saturated solution of alkali metal (with the exception of lithium) in acetic acid to a similar solution, precipitated the alkali metal uranyl(VI) triacetate. It was not possible to precipitate lithium uranyl(VI) triacetate by this method as ammonium uranyl(VI) triacetate crystallised preferentially from uranyl acetate solutions containing ammonium and lithium ions. This was detected by thermal decomposition of the product which produced a green-black solid shown to be U_3O_8 by X-ray powder diffraction. Preparations of

caesium uranyl(VI) triacetate required extensive vacuum drying.

As a consequence of these results precautions were taken to ensure the best possible purity of the products. In particular, the absolute minimum of ammonium acetate was added to dissolve uranyl(VI) diacetate dihydrate. The resulting triacetate salts were washed with glacial acetic acid to remove any acetamide and were recrystallised from dilute aqueous acetic acid. In general, it was preferable to use uranium trioxide as a starting material since this eliminated the introduction of unwanted ions into the reaction solutions.

Low yields were often obtained in the preparations due to the use of large volumes of solvent or to the necessity for the products to be recrystallised.

3:1:1:2 Alkali Metal Neptunyl(VI) Triacetates

The limited availability and high radioactivity of neptunium compared with uranium called for the use of much smaller quantities for preparative work so that it was important to maximise the yields. This was achieved by using minimum volumes of solvent, cooling precipitating solutions in ice, washing with pre-cooled solutions and by not recrystallising the products. Additionally, because the stable oxidation state of neptunium in aqueous solution is +5(NpO_2^+) the preparations required the use of the vigorous oxidising conditions of bubbling ozone through the heated (90°C) reaction solution (Section 2:10:1) to promote neptunium to the +6 oxidation state (NpO_2^{2+}).

The preparative route to sodium neptunyl(VI) triacetate had been used satisfactorily, previously[90], and the route used for the preparation of the caesium salt was based on the reported method[181]. Because ammonium uranyl(VI) triacetate was the product from uranyl(VI) acetate solutions containing lithium and ammonium ions, lithium hydroxide was used as the

precipitating agent for the preparation of lithium neptunyl(VI) triacetate.

On the basis of X-ray powder diffraction patterns, apparently pure samples of potassium and rubidium neptunyl(VI) triacetates were obtained by using ammonium hydroxide as the precipitating agent in the preparations. However, when these materials were decomposed thermally under oxygen, X-ray powder diffraction data showed the products contained neptunium dioxide as well as the alkali metal dineptunate(VI). This indicated the presence of ammonium neptunyl(VI) triacetate in the alkali metal neptunyl (VI) triacetate products which was not detected by X-ray powder diffraction. This may have been due to the similarities of the cell parameters. However, it should be noted that with this technique it is difficult to detect impurities at less than the 5-10% level. The route employed in the preparation of lithium and caesium neptunyl(VI) triacetates using alkali metal hydroxide as the precipitating agent was therefore used.

The precipitation of neptunium(VI) by alkali metal hydroxide solutions had to be performed with great care as addition of an excess caused dissolution of the precipitate. For this reason the alkali metal hydroxide solution was added dropwise, diluting it as necessary towards the end of the precipitation, to the point where the neptunium was still in slight excess. In this way almost 100% precipitation of the neptunium was achieved without redissolution.

3:1:2 Crystallographic Properties

Single crystal X-ray diffraction data have been reported for sodium[184], potassium[185], rubidium[186] and ammonium[185] uranyl(VI) triacetates and for sodium neptunyl(VI) triacetate[182].

The two sodium actinyl(VI) triacetates are isostructural and crystallise in the cubic space group $P2_13$. Unit cell parameters were calculated directly from the X-ray powder diffraction data. Dividing the $\sin^2\theta$ values

by a common factor produced the integer values, N,[187] where N = $(h^2 + k^2 + l^2)$. In both sets of data there were the characteristic primitive cubic absences and all the lines were indexed by their N values from the tabulated data[188].

Using the equations,

$$(1) \qquad \sin^2\theta_{hkl} \doteq A(h^2 + k^2 + l^2) = AN$$

$$(2) \qquad a = \frac{\lambda}{2\sqrt{A}}$$

each $\sin^2\theta$ value was divided by its integer value, N, to obtain the factor A_n for each reflection. The average of the individual A_n values was taken to give a more accurate common factor, A, from which the unit cell parameter was calculated. Because of the decrease in systematic errors as θ approached 180° (Section 2:3:3), high angle reflections were used preferentially in the calculations as these provide the most accurate unit cell parameter. The results were in good agreement with the published single crystal data which are given in Table 3:1.

The powder diffraction data for potassium and rubidium uranyl(VI) triacetates were in good agreement with the data generated (Section 2:3:2) from the published values and all reflections were indexed according to the reported $I4_12$ cells. These two materials and the ammonium uranyl(VI) triacetate are all isostructural. Two phases of the potassium salt have been reported but only the α-phase was observed during the present work.

Potassium and rubidium neptunyl(VI) triacetates were found to be isostructural with the uranium analogues. Approximate unit cell parameters were determined directly from the X-ray powder diffraction data by using the $\sin^2\theta$ values for two reflections from each of the neptunium data sets indexed as 200 and 114 in accordance with the equivalent uranium data. These reflections were chosen since they were strong and readily identifiable on all the films and allowed calculation of the two cell parameters

for both potassium neptunyl(VI) triacetate and rubidium neptunyl(VI) triacetate from the following equations.

(1) $$\sin^2\theta_{hkl} = A(h^2 + k^2) + Cl^2$$

(2) $$a = \frac{\lambda}{2\sqrt{A}}$$

(3) $$c = \frac{\lambda}{2\sqrt{C}}$$

The calculated cell parameters were used to generate diffraction data with which the experimental reflections were indexed. The data were refined (Section 2:3:2) twice to yield the results presented in Table 3:1. Unlike the uranium analogue, two phases of potassium neptunium(VI) triacetate were observed with the β-phase being the more prevalent, the α-phase was found only once.

The caesium neptunyl(VI) triacetate X-ray diffraction data were treated in the same manner as this complex is isostructural with the potassium and rubidium salts. The equivalent two reflections, 200 and 114, were used to determine approximate cell parameters. The reflections were indexed on the basis of these calculated parameters and the data refined twice to provide the results presented in Table 3:1.

The X-ray powder diffraction results for caesium uranyl(VI) triacetate, lithium uranyl(VI) triacetate and lithium neptunyl(VI) triacetate have not been fully interpreted. The data for caesium uranyl(VI) triacetate, obtained from several different preparations, were identical but showed little similarity to the neptunium analogue. It was possible, however, to index most of the reflections based on a tetragonal unit cell of space group $I4_12$ with the parameters a = 12.34Å and c = 26.13Å. It is possible that all the reflections could be indexed on such a tetragonal cell but without the limiting conditions imposed by the $I4_12$ space group. The diffraction data are presented in Table 3:2.

Table 3:1 Crystallographic Data for Alkali Metal Actinyl(VI) Triacetates

Compound	Symmetry	Space Group	Lattice Parameters (Å)[a]		Ref
			a	c	
$NaUO_2(CH_3COO)_3$	Cubic	$P2_13$	10.67 (10.688)		184
$NaNpO_2(CH_3COO)_3$	Cubic	$P2_13$	10.64 (10.638)		182
$NH_4UO_2(CH_3COO)_3$	Tetragonal	$I4_12$	(13.82)	(27.66)	185
α-$KUO_2(CH_3COO)_3$	Tetragonal	$I4_12$	14.39 (14.41)	25.73 (25.85)	185
β-$KUO_2(CH_3COO)_3$	Tetragonal	$I4_12$	(14.02)	(27.76)	185
α-$KNpO_2(CH_3COO)_3$	Tetragonal	$I4_12$	14.30	25.95	
β-$KNpO_2(CH_3COO)_3$	Tetragonal	$I4_12$	13.82	26.12	
$RbUO_2(CH_3COO)_3$	Tetragonal	$I4_12$	13.88 (13.84)	27.56 (27.57)	186
$RbNpO_2(CH_3COO)_3$	Tetragonal	$I4_12$	13.70	27.66	
$CsNpO_2(CH_3COO)_3$	Tetragonal	$I4_12$	14.05	29.14	

[a] published values are given in parentheses

Table 3:2 Experimental X-ray Powder Diffraction Data for $CsUO_2(CH_3COO)_3$

$Sin^2\theta_{obs}$	I_{est}	Possible index for $I4_12$ cell
0.0156	S	200
0.0217	M	114
0.0250	W	105
0.0314	W	220
0.0445	S	224
0.0488	M	-
0.0497	W	-
0.0526	W	314
0.0560	W	008
0.0604	W	-
0.0625	W	400 226
0.0732	M	332
0.0893	W	415 219
0.0930	W	327
0.0985	M	431 501
0.1043	S	512
0.1074	M	-
0.1155	S	514
0.1418	M	2012
0.1556	W	527
0.1599	M	622
0.1712	M	4111
0.1779	M	-

The results for lithium uranyl(VI) triacetate and lithium neptunyl(VI) triacetate which indicated that the two complexes are isostructural are listed in Table 3:3. It was not possible to obtain good quality photographs and only a few diffraction lines are visible. The neptunium complex provided the clearest X-ray diffraction patterns.

3:1:3 Spectroscopic Properties of the Alkali Metal Neptunyl(VI) Triacetates

As previously mentioned, samples of alkali metal neptunyl(VI) triacetates were precipitated from solutions in which the stable oxidation state of neptunium in aqueous solution of +5(NpO_2^+) had been promoted, by vigorous oxidising conditions, to the +6 state (NpO_2^{2+}). It was thought that subsequent precipitation would stabilise the +6 oxidation state in the resulting solid complexes. However, all the alkali metal neptunyl(VI) triacetate samples analysed by electronic absorption spectroscopy showed an increasing neptunium(V) content with time.

This rate of increase was monitored for a sample of the potassium complex from Preparation 5 (Section 2:10:1) by the following method:

(i) a spectrum was recorded (83 days after the preparation)

(ii) a second spectrum was recorded after a further 58 days

(iii) a third spectrum was recorded after keeping the sample enclosed in a darkened container for a further 39 days.

The results are presented in Table 3:4. The fact that the rate of increase of neptunium(V) content is not significantly retarded by the total exclusion of light suggests that the reaction is not photochemically dependent and may in fact be the result of self irradiation. It is not clear why the +6 oxidation state is not fully stabilised by the solid complexation.

Table 3:3 Experimental X-Ray Powder Diffraction Data for $LiUO_2(CH_3COO)_3$ and $LiNpO_2(CH_3COO)_3$

$LiUO_2(CH_3COO)_3$		$LiNpO_2(CH_3COO)_3$	
$\sin^2\theta_{obs}$	I_{est}	$\sin^2\theta_{obs}$	I_{est}
0.01016	W *d*	0.01047	W
0.01249	M *d*	0.01285	S *d*
0.01572	M	0.01618	M
0.01645	S	0.01712	S
0.01726	M	0.01812	W
		0.02415	W
0.02683	W	0.02709	M
0.03169	W	0.03304	W
0.03976	M	0.04090	M
0.04284	W	0.04322	M
		0.05123	M
0.05516	W	0.05458	W

d Diffuse line

Table 3:4 Neptunium(V) Content in Potassium Neptunyl(VI) Triacetate from Preparation 5

Spectrum	Conditions of Storage	Np(V) Content(%)	Increase in Np(V) Content(%)	Time Elapsed (Days)	Rate of Increase (% per day)	Overall Rate of Increase (% per day)
1	Normal	2.2	2.2[a]	83[b]	0.027	0.027
2	Normal	4.1	1.9	58	0.033	0.029
3	Total Darkness	5.3	1.2	39	0.031	0.029

a assuming no Np(V) content when first prepared

b from date of preparation

The rate of increase of neptunium(V) content in the other triacetates from Preparation 5 was also monitored by recording two spectra for each sample as indicated in Table 3:5.

It can be seen from Tables 3:4 and 3:5 that there is a decreasing trend in the rate of increase in neptunium(V) content in the complexes on going from sodium through potassium and rubidium to caesium. It may be significant that this is in line with a decreasing percentage by weight of neptunium in the complexes.

Table 3:5 Neptunium(V) Content in Sodium, Rubidium and Caesium Neptunyl (VI) Triacetates from Preparation 5

Sample	Np(V) Content from 1st Spectrum (%)	Np(V) Content from 2nd Spectrum (%)	Increase in Np(V) Content (%)	Time Between Spectra (days)	Rate of Np(V) Increase (% per day)
$NaNpO_2(CH_3COO)_3$	2.1	4.0	1.9	50	0.038
$RbNpO_2(CH_3COO)_3$	2.3	10.2	7.9	302	0.026
$CsNpO_2(CH_3COO)_3$	5.2	10.5	5.3	308	0.017

Similar data obtained for the alkali metal neptunyl(VI) triacetates from other preparations are presented in Table 3:6.

Table 3:6 Neptunium(V) Content in Alkali Metal Neptunyl(VI) Triacetates from Preparations 4 and 6

Sample	Preparation	Np(V) Content (%)	Age from Preparation (days)
$NaNpO_2(CH_3COO)_3$	4	4.3	197
$KNpO_2(CH_3COO)_3$	4	4.5	183
$RbNpO_2(CH_3COO)_3$	4	4.9	180
$CsNpO_2(CH_3COO)_3$	4	4.3	118
	6	2.7	1

It was apparent from the spectra recorded that in the case of the neptunyl(VI) triacetate preparations there could be a presence of neptunium (V) immediately after the preparation. The contamination in the other complexes at this early age is unknown. However, since the oxide obtained from the decomposition of 1 day old, Preparation 4 $NaNpO_2(CH_3COO)_3$ showed no neptunium(V) contamination, it can be inferred that this triacetate had no such contamination immediately after its preparation.

3:2 THERMOGRAVIMETRIC RESULTS

Analysis of the data from the differential thermal analyses of the alkali metal uranyl(VI) triacetates was limited to the measurement of the decomposition temperatures, the weight loss occurring in the decomposition (Table 3:7) and the identification, by X-ray powder diffraction, of the products. The twin peak traces obtained suggested a two-stage reaction for the decomposition of alkali metal uranyl(VI) triacetates to alkali metal diuranates(VI). It is possible that these stages are a decomposition to uranium and alkali metal oxides followed by a recombination although it

Table 3:7 Results of Thermogravimetric Studies of Alkali Metal Uranyl(VI) Triacetates

Sample	Experimental Mass (g)	Experimental Wt Loss (g)	Expected Product	Overall Recorded Wt Loss (%)	Expected Wt Loss (%)	Initiation Temp (°C)	1st Peak Max (°C)	2nd Peak Max (°C)	Reaction End Temp (°C)
$NH_4UO_2(CH_3COO)_3$	0.12913	0.0515	U_3O_8	39.88	39.66	(275 NH_3) 277	368	385	417
$LiUO_2(CH_3COO)_3 . nH_2O$	0.12950	0.0485	$Li_2U_2O_7$?	37.45	?	(175 H_2O) 298	338	363	398
$NaUO_2(CH_3COO)_3$	0.11316	0.0370	$Na_2U_2O_7$	32.70	32.57	298	380	403	424
$KUO_2(CH_3COO)_3$	0.12920	0.0400	$K_2U_2O_7$	30.96	31.49	272	366	382	410
$RbUO_2(CH_3COO)_3$	0.11315	0.0347	$Rb_2U_2O_7$	30.67	28.75	303	?	388	515
$CsUO_2(CH_3COO)_3$	0.11271	0.0300	$Cs_2U_2O_7$	26.62	26.40	312	?	378	416

is not clear what the intermediates would be. Such a reaction scheme may explain why the X-ray powder diffraction data obtained for the products of the decompositions of the potassium and rubidium complexes differed from those obtained in the furnace preparations 7, 8 and 9. It is possible that a lack of oxygen or surface poisoning by carbon dioxide in the small, densely packed platinum reaction crucibles could result in the formation of lower or substoicheiometric oxides.

In the case of the product of the differential thermal analysis of potassium uranyl(VI) triacetate there were four extra lines visible on the X-ray powder photograph. Three of these could be indexed as β-UO_3 and the fourth could be indexed based on the reported $P2_1/m$ cell[94] for $K_2U_2O_7$ (Table 3:8) although it is not clear why this line does not feature on other photographs.

The data in the analogous rubidium case differed totally from the data obtained for the products of the furnace preparations and could not be indexed. Like the films from the furnace preparations, the X-ray data for the dta product could be indexed based on the reported orthorhombic cell[133] with a = 24.00 Å, b = 13.86 Å and c = 20.57 Å. However, unlike the films of the furnace preparation products this dta product data could not be indexed based on the preferred monoclinic $P2_1/m$ cell[12]. The X-ray powder diffraction data for the product of the differential thermal analysis of rubidium uranyl(VI) triacetate are listed in Table 3:9.

The data obtained for the sodium and caesium materials were in agreement with the results from the respective furnace preparations. The product from the decomposition of the ammonium uranyl(VI) triacetate was indexed as U_3O_8 and the data for the lithium product were consistent with those from a mixture of $Li_2U_3O_{10}$ and $Li_2O.1.75UO_3$.

Apart from the black U_3O_8 and the ochre $Li_2U_3O_{10}/Li_2O.1.75UO_3$ the products

Table 3:8 X-Ray Powder Diffraction Data for the Product of the Differential Thermal Analysis of Potassium Uranyl(VI) Triacetate

Line No	$\sin^2\theta$	I_{est}	Index for $P2_1/m$ Cell	Extra Lines to Furnace Preparations	Index for β-UO_3
1	0.01392	M	001		
2	0.04896	VW		*	230
3	0.05160	M	120		
4	0.05532	M	002, $12\bar{1}$		
5	0.05629	S	200		
6	0.06319	M		*	320
7	0.07482	M	121		
8	0.08847	W	201, $22\bar{1}$		
9	0.09942	VW		*	$24\bar{1}$
10	0.12394	W	$20\bar{3}$		
11	0.14738	W	$12\bar{3}$, 202		
12	0.14971	M	040		
13	0.16016	VVW	023, $22\bar{3}$	*	
14	0.16383	M	140		
15	0.20089	M	$40\bar{1}$, $24\bar{1}$, $20\bar{4}$		
16	0.20342	M	$40\bar{2}$		
17	0.20522	S	042, 321, $11\bar{4}$, 240		
18	0.21993	M	004		
19	0.22364	M	$24\bar{2}$, 400		
20	0.23478	W	203		
21	0.27385	M	$24\bar{3}$, 322, 401, $34\bar{2}$		

from the decompositions of the sodium, potassium, rubidium and caesium uranyl(VI) triacetates were saffron yellow (Na, Rb), dark yellow (K), and orange (Cs) in colour. These colours are consistent with alkali metal uranate formation.

Table 3:9 X-Ray Powder Diffraction Data for the Product of the Differential Thermal Analysis of Rubidium Uranyl(VI) Triacetate

n	$\sin^2\theta$
1	0.01204
2	0.01385
3	0.04980
4	0.05147
5	0.05476
6	0.05785
7	0.06013
8	0.06208
9	0.06691
10	0.07505
11	0.08589
12	0.08751
13	0.12141
14	0.12348
15	0.13518
16	0.13851
17	0.14741
18	0.15106
19	0.15379
20	0.15740
21	0.16201
22	0.17041
23	0.17797
24	0.18321
25	0.19067
26	0.19523
27	0.19856
28	0.21041
29	0.21761
30	0.22196

3:3 OXIDE COMPLEXES

3:3:1 Preparation and Analysis

The alkali metal diuranates(VI) and dineptunates(VI) were prepared by the decomposition method previously described (Section 2:10:2). The well characterised alkali metal actinyl(VI) triacetates (Section 3:1) were used as starting materials as these contained both alkali metal and actinide metal in the correct ratio for the required products.

X-ray powder diffraction data were collected for all the oxides in each of the preparations, this being a convenient method of analysing the decomposition products. The results are discussed in Section 3:3:2. Chemical analyses for both alkali metal and actinide metal were performed. These showed that the oxides prepared contained alkali metal and actinide metal in a ratio consistent with the required products, $M_2^{I}M_2^{VI}O_7$ (Tables 2:20 and 2:21). Additionally, as shown in Tables 2:15, 2:16 and 2:17, the weight losses for the neptunium complex decompositions were monitored and the results were consistent with the required reaction,

$$M^{I}NpO_2(CH_3COO)_3 \rightarrow \tfrac{1}{2}M_2^{I}Np_2O_7.$$

As a further check on the purity of two of the diuranates(VI), $Na_2U_2O_7$ and $Cs_2U_2O_7$, and as a way of determining the potential of the decomposition method as a route to pure oxide phases, the enthalpies of formation were compared with the well-established, published data (see Section 3:4:3).

3:3:2 X-Ray Powder Diffraction Results

As shown in Tables 1:12 and 1:16 crystallographic data have been determined for alkali metal diuranates(VI) and dineptunates(VI). The experimental data obtained for materials prepared in this work were compared with GENSTRUCK (Section 2:3:2) listings generated from the published crystallographic data. These published data are tabulated in Table 3:10. Also included in this table are the unit cell parameters which had pre-

viously been determined[106] for $Na_2Np_2O_7$ based on the data for $Na_2U_2O_7$.

Table 3:10 Published Crystallographic Data for Alkali Metal Diuranates (VI) and Dineptunates(VI)

Complex	Space Group	Cell Parameters				Ref
		a(Å)	b(Å)	c(Å)	β(°)	
$Na_2U_2O_7$	C2/m	12.796	7.822	6.896	111.42	92
$K_2U_2O_7$	$P2_1/m$	6.925	7.973	6.992	109.62	94
$Rb_2U_2O_7$	$P2_1/m$	6.947	8.018	7.328	108.64	94
β-$Cs_2U_2O_7$	C2/m	14.516	4.320	7.465	113.78	95
$Na_2Np_2O_7$	C2/m	12.779	7.822	6.902	111.46	106
$Cs_2Np_2O_7$	C2/m	14.30	4.330	7.400	113.58	91

The experimental results obtained for $K_2Np_2O_7$ and $Rb_2Np_2O_7$ indicated that these complexes are isostructural with their uranium analogues. They therefore exhibited monoclinic rather than the reported[91] hexagonal cells.

The X-ray powder diffraction data obtained for the alkali metal diuranates(VI) and dineptunates(VI) are listed in Tables 3:11 to 3:19. In these tables the estimated intensity (I_{est}) of each line is based on the Guinier data as these films were of better definition and were consequently easier to interpret than the Debye-Scherrer films.

Where there appear to be fairly large discrepancies between the $\sin^2\theta$ values from each set of data (up to 0.00200) this is due to inaccuracies in the measurement of weak or diffuse lines on the Debye-Scherrer films. Comparison of the films permitted the correlation of the individual lines between the two types of data set as tabulated in Tables 3:11 to 3:19.

In these tables the Debye-Scherrer (D/S) and Guinier (G) data are tabulated with the GENSTRUCK generated data for the published cells (identified by space group) for comparison.

3:3:2:1 $Na_2U_2O_7$

The data obtained from the Debye-Scherrer films were indexed according to the GENSTRUCK generated $\sin^2\theta$ values for the published C2/m cell parameters. These data were refined to an accuracy of 0.00083 $\sin^2\theta$ to yield the experimental parameters,

$$a = 12.800\text{Å};\quad b = 7.837\text{Å};\quad c = 6.897\text{Å} \text{ and } \beta = 111.42^{\circ}.$$

Some weak lines which could not be so indexed were observed on 16 hour exposure Guinier films. However, these reflections have also been observed by other researchers.[93]

The experimental Debye-Scherrer data for $Na_2U_2O_7$ from Preparations 7, 8 and 9 were identical. Additionally, matching X-ray powder diffraction data were obtained by the Guinier method for the products from Preparations 7 and 8. Both sets of data included the lines which could not be indexed according to the reported cell.

The X-ray powder diffraction data for sodium diuranate(VI) are summarised in Table 3:11.

Table 3:11 X-Ray Powder Diffraction Data for $Na_2U_2O_7$ (Preparation 7)

n	$\sin^2\theta$ C2/m cell	$\sin^2\theta$ D/S	$\sin^2\theta$ G	I est		n	$\sin^2\theta$ C2/m cell	$\sin^2\theta$ D/S	$\sin^2\theta$ G	I est
1	0.01390					34	0.11247			
2	0.01442					35	0.11441		0.11488	VW
3	0.01675	0.01708	0.01677	VS		36	0.11533			
4	0.01982					37	0.11813		0.11745	VW
5	0.02264		0.02259	W		38	0.12250		0.12298	W
			0.02403	VW		39	0.12511			
			0.02977	VVW		40	0.12610			
6	0.03400		0.03398	W		41	0.12665	0.12695	0.12728	M
7	0.03885					42	0.12867			
8	0.04252					43	0.12978			
9	0.04480					44	0.13113			
10	0.04740		0.04760	VVW		45	0.13599			
11	0.05173	0.05220	0.05195	S		46	0.13793		0.13815	VW
12	0.05327	0.05361	0.05329	VS		47	0.13914		0.13953	VW
13	0.05560					48	0.14034		0.14092	VVW
14	0.05768	0.05806	0.05787	S		49	0.14298		0.14214	VW
15	0.05867								0.14389	M
16	0.05872	0.05917	0.05881	VS		50	0.14873			
17	0.06023		0.06047	VW		51	0.15077			
			0.06179	VVW		52	0.15133	0.15210	0.15189	VS
18	0.06701	0.06721	0.06745	S		53	0.15541	0.15542	0.15532	M
19	0.07103		0.07126	VVW		54	0.15656		0.15641	VW
20	0.07885					55	0.15721			
21	0.07928	0.08008	0.07965	M		56	0.15905			
22	0.08138	0.08151	0.08177	S		57	0.16064			
23	0.08293		0.08314	VVW		58	0.16071	0.16164	0.16171	W
24	0.09058					59	0.16753			
25	0.09160					60	0.16863	0.16905	0.16915	S
26	0.09653					61	0.16983			
27	0.09714					62	0.16998			
28	0.09758	0.09815	0.09807	S		63	0.17010	0.17122	0.17103	S
29	0.10035		0.10046	VW		64	0.17216		0.17254	M
30	0.10045		0.10197	VVW		65	0.17523			
31	0.10413					66	0.17816			
32	0.10586		0.10764	VW		67	0.17838			
33	0.11170		0.11187	VVW		68	0.17919			

Table 3:11 Continued

n	$\sin^2\theta$ C2/m cell	$\sin^2\theta$ D/S	$\sin^2\theta$ G	I est	n	$\sin^2\theta$ C2/m cell	$\sin^2\theta$ D/S	$\sin^2\theta$ G	I est
69	0.18059				105	0.24526			
70	0.18961				106	0.24576			
71	0.18962		0.19028	VVVW	107	0.24701		0.24727	VW
72	0.19212				108	0.25254		0.25268	W
73	0.19304				109	0.25576			
74	0.19314				110	0.25954			
75	0.19793				111	0.26159			
76	0.19924		0.20059	VVW	112	0.26490			
77	0.20206				113	0.26711			
78	0.20380		0.20341	M	114	0.26732			
79	0.20436		0.20502	VW	115	0.26732			
80	0.20691				116	0.26788			
81	0.20714	0.20778	0.20786	S	117	0.26803			
82	0.20895		0.20867	M	118	0.26908	0.26893	0.26961	MW
83	0.21001		0.21132	VVW	119	0.26957			
84	0.21309	0.21356	0.21337	MS	120	0.27084			
85	0.21413				121	0.27375			
86	0.21493				122	0.27590			
87	0.21684				123	0.27656)	0.27687	0.27786	M
88	0.32723		0.21831	W	124	0.27791)			
89	0.21944	0.21900	0.21913	M	125	0.28052			
90	0.22191				126	0.28408			
91	0.22242	0.22310	0.22308	MS	127	0.28411			
92	0.22551				128	0.28519			
93	0.22827				129	0.28654			
94	0.22885		0.22936	VW	130	0.28671			
95	0.23072				131	0.28771		0.28891	VVW
96	0.23161		0.23189	W	132	0.29263			
97	0.23469				133	0.29288			
98	0.23490				134	0.29334		0.29414	VW
99	0.23492	0.23545	0.23549	MS	135	0.29574)	0.29632	0.29734	MW
100	0.23676				136	0.29962)			
101	0.23704)	0.23846	0.23762	W	137	0.30044		0.30124	VW
102	0.23810)				138	0.30321	0.30300	0.30354	W
103	0.23841		0.23932	M	139	0.30375			
104	0.24091				140	0.30414			

n	$\sin^2\theta$ C2/m cell	$\sin^2\theta$ D/S	$\sin^2\theta$ G	I est
141	0.30445		0.30492	VW
142	0.30597			
143	0.30618			
144	0.30656			
145	0.30688	0.30680	0.30745	MW
146	0.30931			
147	0.31197			
148	0.31228			
149	0.31398			
150	0.31541			
151	0.31604			
152	0.31712		0.31859	VVW
153	0.32049		0.32069	VW
154	0.32276			
155	0.32547	0.32497	0.32490	VVW
156	0.32550)		0.32655	W
157	0.32786)			
158	0.32933			
159	0.33173		0.33125	VVW
160	0.33301			
161	0.33356			
162	0.33379			
163	0.33600		0.33502	VVW
164	0.34098		0.33810	VVW
165	0.34503			
166	0.34602			
167	0.34624			
168	0.34678			
169	0.34753	0.34715	0.34783	W
170	0.34844			
171	0.34894			
172	0.34967			
173	0.35207			
174	0.35284)			
175	0.35465)	0.35378	0.35524	MW
176	0.35597)			

n	$\sin^2\theta$ C2/m cell	$\sin^2\theta$ D/S	$\sin^2\theta$ G	I est
177	0.35747			
178	0.35921		0.35884	W
179	0.35934			
180	0.35976			
181	0.36050			
182	0.36232	0.36208	0.36172	W
183	0.36296			
184	0.36409)		0.36437	M
185	0.36442)			
186	0.36642			
187	0.36671			
188	0.36949	0.36827	0.36967	MW
189	0.37225	0.37156	END DATA	
190	0.37532			
191	0.37646			
192	0.37676			
193	0.37830			
194	0.37984			
195	0.38216			
196	0.38272			
197	0.38613			
198	0.38854			
199	0.38998			
200	0.39030			
201	0.39033	0.39080		
202	0.39216			
203	0.39219)	0.39259		
204	0.39245)			
205	0.39382			
206	0.39935			
207	0.40047)	0.40055		
208	0.40067)			
209	0.40140			
210	0.40149			
211	0.40181			
212	0.40278			

n	$\sin^2\theta$ C2/m cell	$\sin^2\theta$ D/S	$\sin^2\theta$ G	I est		n	$\sin^2\theta$ C2/m cell	$\sin^2\theta$ D/S	$\sin^2\theta$ G	I est
213	0.40317	0.40325								
214	0.40704									
215	0.40735									
216	0.40839	0.40860								
217	0.41071	END DATA								

3:3:2:2 $\underline{K_2U_2O_7}$

All the lines measured on both Debye-Scherrer and Guinier films for potassium diuranate(VI), $K_2U_2O_7$, were indexed according to the data generated for the reported $P2_1/m$ cell. These results are summarised in Table 3:12. Identical X-ray powder diffraction data were obtained for the potassium diuranate(VI) products from preparations 7, 8 and 9.

Two differently coloured products were obtained during Preparation 9 after firing potassium uranyl(VI) triacetate at 650°C for 2 hours. The bulk of the product was dark yellow and gave X-ray powder diffraction data in agreement with the published data. However, there was a thin layer of orange material in the bottom of the crucible which gave an X-ray pattern matching that from the dta/tg experiment (Section 3:2). The extra diffraction lines, one of which was of medium to strong intensity, were eliminated by refiring the material. These findings agree with the suggestion in Section 3:2 that oxygen starvation or carbon dioxide poisoning results in the formation of a lower or substoicheiometric oxide.

Table 3: 12 X-Ray Powder Diffraction Data for $K_2U_2O_7$ (Preparation 7)

n	$\sin^2\theta$ P2₁/m cell	$\sin^2\theta$ D/S	$\sin^2\theta$ G	I est	n	$\sin^2\theta$ P2₁/m cell	$\sin^2\theta$ D/S	$\sin^2\theta$ G	I est
1	0.01370)	0.01428	0.01359	VS	37	0.11153			
2	0.01397)				38	0.11875			
3	0.01838				39	0.12088			
4	0.02305)		0.02319	VW	40	0.12110	0.12169	0.12167	W
5	0.02332)				41	0.12331			
6	0.02773				42	0.12343	0.12410	0.12347	MW
7	0.03696				43	0.12475			
8	0.03740				44	0.12476)		0.12512	W
9	0.04631				45	0.12555)			
10	0.05019				46	0.12570			
11	0.05099)	0.05183	0.05117	S	47	0.13266			
12	0.05110)				48	0.13278			
13	0.05136)				49	0.13411			
14	0.05480)	0.05531	0.05499	S	50	0.13433)	0.13538	0.13488	W
15	0.05577)				51	0.13505)			
16	0.05587	0.05633	0.05579	VS	52	0.13512)			
17	0.05954				53	0.13894			
18	0.06033				54	0.14001			
19	0.06415				55	0.14680)	0.14706	0.14742	MW
20	0.06522		0.06508	W	56	0.14784)			
21	0.07351		0.07386	M	57	0.14892			
22	0.07435	0.07479	0.07451	M	58	0.14958	0.14995	0.14956	M
23	0.08286				59	0.15718			
24	0.08735				60	0.15765			
25	0.08758)	0.08812	0.08932	W	61	0.16071			
26	0.08815)				62	0.16082			
27	0.08838)				63	0.16215			
28	0.09220				64	0.16310			
29	0.09326				65	0.16328			
30	0.09670				66	0.16355	0.16349	0.16374	M
31	0.09750				67	0.16515			
32	0.09784				68	0.16539			
33	0.09811				69	0.16728			
34	0.10252				70	0.16796			
35	0.10940				71	0.17149			
36	0.11090				72	0.17229			

Table 3:12 Continued

n	$\sin^2\theta$ P2₁/m cell	$\sin^2\theta$ D/S	$\sin^2\theta$ G	I est	n	$\sin^2\theta$ P2₁/m cell	$\sin^2\theta$ D/S	$\sin^2\theta$ G	I est
73	0.17450				109	0.23625			
74	0.17474				110	0.23693			
75	0.17662				111	0.23740			
76	0.18523				112	0.23773			
77	0.18654				113	0.23815		0.23911	VW
78	0.19354				114	0.24134			
79	0.19567				115	0.24277			
80	0.19602				116	0.24427			
81	0.19977				117	0.24463			
82	0.20000				118	0.24560			
83	0.20057				119	0.24742			
84	0.20075	0.20121	0.20140	W	120	0.24769			
85	0.20255				121	0.24929			
86	0.20278)		0.20341	W	122	0.24953			
87	0.20394)				123	0.25141			
88	0.20439				124	0.25210			
89	0.20467				125	0.25661			
90	0.20537	0.20522	0.20522	M	126	0.25898			
91	0.20545				127	0.26086			
92	0.20745				128	0.26111			
93	0.20757				129	0.27035			
94	0.20890				130	0.27068			
95	0.20935)				131	0.27082			
96	0.20984)	0.20958	0.21050	W	132	0.27232		0.27228	W
97	0.21010)				133	0.27268			
98	0.21329	0.21408	0.21419	VW	134	0.27289			
99	0.21922	0.21960	0.21996	W	135	0.27301			
100	0.22309				136	0.27365)			
101	0.22347	0.22384	0.22391		137	0.27433)	0.27332	0.27428	MW
102	0.22857				138	0.27434)			
103	0.23198				139	0.27528			
104	0.23282				140	0.27970			
105	0.23341				141	0.28016			
106	0.23342	0.23387	0.23387	W	142	0.28368			
107	0.23492				143	0.28391			
108	0.23528				144	0.28414			

Table 3:12 Continued

n	$\sin^2\theta$ P2₁/m cell	$\sin^2\theta$ D/S	$\sin^2\theta$ G	I est
145	0.28471			
146	0.28489			
147	0.28808			
148	0.28852			
149	0.28959			
150	0.29403			
151	0.29742	0.29843	0.29871	VW
152	0.30336			
153	0.30337			
154	0.30548			
155	0.30723			
156	0.30761)			
157	0.30774)	0.30796	0.30907	VW
158	0.31004)			
159	0.31106			
160	0.31173			
161	0.31473			
162	0.31483			
163	0.31497			
164	0.31641			
165	0.31686			
166	0.31756			
167	0.31906			
168	0.31939			
169	0.31942			
170	0.32039			
171	0.32041			
172	0.32107			
173	0.32187			
174	0.32576			
175	0.32886			
176	0.33142			
177	0.33263			
178	0.33311			
179	0.33656			
180	0.33821			

n	$\sin^2\theta$ P2₁/m cell	$\sin^2\theta$ D/S	$\sin^2\theta$ G	I est
181	0.34198			
182	0.34246			
183	0.34253			
184	0.34288			
185	0.34312		0.34402	VW
186	0.34525			
187	0.34560			
188	0.34743			
189	0.34846			
190	0.34917			
191	0.34941			
192	0.34958			
193	0.35026			
194	0.35034			
195	0.35052)	0.35045	0.35189	W
196	0.35188)			
197	0.35260			
198	0.35352			
199	0.35381			
200	0.35449			
201	0.35493)	0.35496	0.35644	W
202	0.35703)			
203	0.35715			
204	0.35847			
205	0.35848			
206	0.35852			
207	0.35876			
208	0.35942			
209	0.36195			
210	0.36626)	0.36705	0.36798	VW
211	0.36880)			
212	0.37003			
213	0.37050	0.36996	0.37136	VW
214	0.37305			
215	0.37352	0.37415	0.37524	VW
216	0.37817	END DATA		

Table 3: 12 Continued

n	$\sin^2\theta$ P2₁/m cell	$\sin^2\theta$ D/S	$\sin^2\theta$ G	I est		n	$\sin^2\theta$ P2₁/m cell	$\sin^2\theta$ D/S	$\sin^2\theta$ G	I est
217	0.37992									
218	0.38017									
219	0.38156									
220	0.38256									
221	0.38300									
222	0.38451									
223	0.38486									
224	0.38583)									
225	0.38656)		0.38641 END DATA	VW						

3:3:2:3 $\underline{Rb_2U_2O_7}$

The Debye-Scherrer data obtained for the rubidium diuranate(VI) products from Preparations 7, 8 and 9 were identical. As shown in the summary table of the X-ray powder diffraction results, Table 3:13, all the lines visible were indexed based on the reported $P2_1/m$ cell.

As with the potassium analogue, two distinct phases were observed during Preparation 9. The X-ray data for the main yellow sample matched those from the previous preparations with the exception of two additional weak lines. A thin layer of an orange product was found at the bottom of the main sample. The X-ray powder diffraction data for this material differed totally from previous data. Additionally, there was no similarity between these data and those obtained in the dta/tg experiment. After grinding and refiring a homogeneous yellow product was obtained. The Debye-Scherrer data for this material was in agreement with the previous and published values.

The Guinier films for the $Rb_2U_2O_7$ products from Preparations 8 and 9 were identical. However, there were weak extra lines which could not be indexed according to the published cell. The Guinier film recorded for the product from Preparation 7 exhibited further extra lines which could not be indexed. These data are tabulated, for comparison with those for the product from Preparation 9, in Table 3:14.

Table 3: 13 X-Ray Powder Diffraction Data for $Rb_2U_2O_7$ (Preparation 7)

n	$\sin^2\theta$ P2₁/m cell	$\sin^2\theta$ D/S	$\sin^2\theta$ G	I est	n	$\sin^2\theta$ P2₁/m cell	$\sin^2\theta$ D/S	$\sin^2\theta$ G	I est
1	0.01233	0.01239	0.01224	VS	37	0.10897			
2	0.01371				38	0.11082			
3	0.01773				39	0.11094	0.11124	0.11124	W
4	0.02157				40	0.11594			
5	0.02296				41	0.11662			
6	0.02696				42	0.11755			
7	0.03435				43	0.12006			
8	0.03698				44	0.12018)	0.12094	0.12052	W
9	0.04359				45	0.12078)			
10	0.04640				46	0.12287			
11	0.04931)	0.04970	0.04921	S	47	0.12342			
12	0.04931)				48	0.12518			
13	0.05056				49	0.12961			
14	0.05069	0.05113	0.05062	M	50	0.13212			
15	0.05471				51	0.13251			
16	0.05485	0.05507	0.05487	VS	52	0.13267			
17	0.05565				53	0.13377			
18	0.05855		0.05741	VW	54	0.13671			
19	0.05981		0.05964	W	55	0.13739	0.13736	0.13763	M
20	0.06410		0.06167 0.06410 0.06657	VW VW VW	56	0.13806			
21	0.07092				57	0.14664			
22	0.07133	0.07167	0.07152 0.07478	M VW	58	0.14780			
23	0.07964				59	0.14792)	0.14867	0.14885	S
24	0.08017				60	0.14792)			
25	0.08338		0.08342	VW	61	0.14958)			
26	0.08380				62	0.15292			
27	0.08629				63	0.15413		0.15387	VW
28	0.08754				64	0.15882			
29	0.08888				65	0.15958			
30	0.09183				66	0.15985			
31	0.09304				67	0.16025			
32	0.09553				68	0.16040			
33	0.09692				69	0.16067			
34	0.09973				70	0.16163	0.16101	0.16153	M
35	0.10094				71	0.16284			
36	0.10790				72	0.16565			

Table 3:13 Continued

n	$\sin^2\theta$ P2₁/m cell	$\sin^2\theta$ D/S	$\sin^2\theta$ G	I est	n	$\sin^2\theta$ P2₁/m cell	$\sin^2\theta$ D/S	$\sin^2\theta$ G	I est
73	0.16700				109	0.22489			
74	0.16882				110	0.22756			
75	0.16992	0.17012	0.17028	VW	111	0.22866			
76	0.17438				112	0.23018			
77	0.17770				113	0.23065	0.23098		
78	0.18227				114	0.23172			
79	0.18293				115	0.23182			
80	0.18561				116	0.23278			
81	0.18656				117	0.23420			
82	0.18695	0.18696	0.18753	W	118	0.23548			
83	0.19403				119	0.23923			
84	0.19414				120	0.23989			
85	0.19432				121	0.24278			
86	0.19485				122	0.24345			
87	0.19656				123	0.24388			
88	0.19722				124	0.24417			
89	0.19723				125	0.24484	0.24484		
90	0.19765)				126	0.24765			
91	0.19848)	0.19814	0.19799	S	127	0.24886			
92	0.19850)				128	0.25263			
93	0.19914				129	0.25342			
94	0.20225				130	0.25639			
95	0.20277	0.20361	0.20401	M	131	0.25792			
96	0.20608				132	0.25874			
97	0.20647				133	0.25886)			
98	0.20663				134	0.25956)	0.25955	0.26033	W
99	0.20775				135	0.26091)			
100	0.21149				136	0.26386			
101	0.21468				137	0.26498			
102	0.21565				138	0.26548			
103	0.21885				139	0.26763			
104	0.21941				140	0.26881			
105	0.22060	0.22023	0.22038	M	141	0.27079			
106	0.22094				142	0.27134			
107	0.22258				143	0.27422			
108	0.22259				144	0.27753			

Table 3:13 Continued

n	$\sin^2\theta$ P2₁/m cell	$\sin^2\theta$ D/S	$\sin^2\theta$ G	I est
145	0.27993			
146	0.28033			
147	0.28043			
148	0.28043			
149	0.28115			
150	0.28169			
151	0.28171			
152	0.28370			
153	0.28532			
154	0.28545			
155	0.28598)	0.28691	0.28801	VW
156	0.28917)			
157	0.28958			
158	0.29294			
159	0.29750			
160	0.29885			
161	0.30196			
162	0.30205			
163	0.30262			
164	0.30414			
165	0.30578			
166	0.30695			
167	0.30750			
168	0.30816			
169	0.30859			
170	0.30905			
171	0.30914			
172	0.31076			
173	0.31362			
174	0.31385			
175	0.31493			
176	0.31619			
177	0.31691			
178	0.31731)			
179	0.31741)			
180	0.31830)			

n	$\sin^2\theta$ P2₁/m cell	$\sin^2\theta$ D/S	$\sin^2\theta$ G	I est
181	0.31838)	0.31764	0.31999	VW
182	0.31855)			
183	0.32068)			
184	0.32286			
185	0.32562			
186	0.32738			
187	0.32779			
188	0.32914			
189	0.33085			
190	0.33282			
191	0.33353			
192	0.33519	0.33487		
193	0.33838			
194	0.34195			
195	0.34207			
196	0.34283			
197	0.34393			
198	0.34444			
199	0.34514)			
200	0.34515)			
201	0.34515)			
202	0.34603)			
203	0.34612)	0.34581	0.34688	M
204	0.34643)			
205	0.34654)			
206	0.34707)			
207	0.34818			
208	0.35017			
209	0.35055			
210	0.35060)			
211	0.35208)	0.35194	0.35309	W
212	0.35400)			
213	0.35455			
214	0.35553			
215	0.36140			
216	0.36313			

n	$\sin^2\theta$			I est		n	$\sin^2\theta$			I est
	$P2_1/m$ cell	D/S	G				$P2_1/m$ cell	D/S	G	
217	0.36342									
218	0.36354									
219	0.36357									
220	0.36612									
221	0.36690									
222	0.36717									
223	0.36734									
224	0.36852)									
225	0.36886)	0.36794	0.36967	W						
226	0.37050)									
		END DATA	END DATA							

Table 3:14 Comparison of Guinier Data for $Rb_2U_2O_7$ from Preparations 7 and 9

$P2_1/m$ Cell Data		Experimental Data			
		Prep 7		Prep 9	
n	$\sin^2\theta$	$\sin^2\theta$	I_{est}	$\sin^2\theta$	I_{est}
1	0.01233	0.01224	VS	0.01229	VS
11,12	0.04931	0.04921	S	0.04921	VS
14	0.05069	0.05062	M	0.05073	M
				0.05239	W
16	0.05485	0.05487	VS	0.05465	VS
18	0.05855	0.05741	VW		
19	0.05981	0.05964	W		
		0.06167	VW	0.06179	W
20	0.06410	0.06410	VW	0.06435	VW
		0.06657	VW		
21	0.07092			0.07113	M
22	0.07133	0.07152	M	0.07139	MS
		0.07478	VW		
				0.07663	W
25	0.08338	0.08342	VW	0.08287	W
33	0.09692			0.09688	VW
39	0.11094	0.11124	W	0.11092	M
40	0.11594			0.11568	VW
42	0.11755			0.11712	VW
45	0.12078	0.12052	W	0.12069	M
48	0.12518			0.12529	VW
52	0.13267			0.13318	VW
53	0.13377				
54	0.13671	0.13763	M	0.13711	MS
55	0.13739				
59,60	0.14792	0.14885	S	0.14814	VS
63	0.15413	0.15387	VW		
67	0.16025				
68	0.16040	0.16153	M	0.16043	S
69	0.16067				
70	0.16163				
75	0.16992	0.17028	VW	0.16990	W
82	0.18695	0.18753	W	0.18675	M
90	0.19765	0.19799	S	0.19760	VS
95	0.20277	0.20401	M	0.20341	M
104	0.21941	0.22038	M	0.21955	M
105	0.22060				
113	0.23065			0.23084	VW
125	0.24484			0.24511	VW
134	0.25956	0.26033	W	0.25946	MW
155	0.28598	0.28801	W	0.28665	W
168	0.30816			0.30815	W
182	0.31855	0.31999	VW	0.31859	W
183	0.32068				
191	0.33353			0.33408	W
202	0.34603	0.34688	M	0.34569	S
211	0.35208	0.35309	W	0.35213	MS
225	0.36886	0.36967	W	0.36895	MW

3:3:2:4 $\underline{Cs_2U_2O_7}$

The Debye-Scherrer data obtained for caesium diuranate(VI) from Preparations 7, 8 and 9 were identical. The X-ray powder diffraction results generated by both the Debye-Scherrer and Guinier methods for the product of Preparation 7 are tabulated with the published data in Table 3:15. This summary shows that all the lines on the Debye-Scherrer film could be indexed based on the GENSTRUCK generated data for the reported cell. A COHEN refinement to an accuracy of 0.00083 $\sin^2\theta$ gave the experimental cell parameters,

$$a = 14.529\text{Å};\quad b = 4.315\text{Å};\quad c = 7.501\text{Å} \text{ and } \beta = 113.64^\circ.$$

However, there were many extra lines visible on the Guinier film which could not be indexed according to the published data. These are unexplained.

Table 3:15 X-Ray Powder Diffraction Data for $Cs_2U_2O_7$ (preparation 7)

n	$\sin^2\theta$ C2/m cell	$\sin^2\theta$ D/S	$\sin^2\theta$ G	I est	n	$\sin^2\theta$ C2/m cell	$\sin^2\theta$ D/S	$\sin^2\theta$ G	I est
			0.01059	W	28	0.11604		0.11664	MW
1	0.01273	0.01259	0.01274	VS	29	0.12124		0.12118	VW
2	0.01347		0.01342	VW				0.12331	VW
3	0.01564		0.01557	W	30	0.12738		0.12778	S
4	0.03521		0.03545	W	31	0.12924	0.12861	0.12980	S
5	0.03677		0.03694	M	32	0.13398		0.13488	VVW
6	0.04267	0.04305	0.04271	S				0.13763	VVW
7	0.04328		0.04343	MW	33	0.14012)			
			0.04435	W	34	0.14079)	0.14079	0.14092	M
8	0.04550		0.04559	W	35	0.14085)			
			0.04975	VW	36	0.14302			
9	0.05094	0.05087	0.05106	S	37	0.14478	0.14446	0.14513	MS
10	0.05323	0.05361	0.05340	VS	38	0.14708		0.14760	W
11	0.05389		0.05419	S	39	0.15143		0.15243	W
			0.05706	VW	40	0.15518	0.15465	0.15550	M
12	0.05905	0.05949	0.05917	VS	41	0.15977		0.16043	VVW
			0.06023	VVW	42	0.16415	0.16503	0.16504	M
13	0.06216				43	0.16567)		0.16635	MS
14	0.06257	0.06275	0.06264	S	44	0.16567)			
			0.06496	MW	45	0.17067		0.17141	M
			0.07191	VW	46	0.17264			
15	0.07559	0.07586	0.07597	M	47	0.17288)	0.17300	0.17349	S
			0.07904	VVW	48	0.17314)			
16	0.08141		0.08177	W	49	0.17387		0.17463	W
			0.08383	VVW	50	0.17498		0.17558	VVW
17	0.08554		0.08579	W	51	0.17832	0.17879	0.17902	S
18	0.08775		0.08790	W	52	0.18127	0.18212	0.18210	S
19	0.09074	0.09071	0.09104	M	53	0.18198		0.18268	W
20	0.09640)		0.09673	VVW	54	0.18603			
21	0.09671)				55	0.18995	0.19070	0.19087	S
22	0.10229)	0.10280	0.10258	S	56	0.19687	0.19703	0.19760	MS
23	0.10237)				57	0.19825		0.19919	M
24	0.10512		0.10517	VVW	58	0.20057	0.20059	0.20120	S
25	0.10881	0.10918	0.10920	MS	59	0.20254)		0.20341	VW
26	0.11417)	0.11422	0.11472	MS	60	0.20340)			
27	0.11461)				61	0.20376		0.20442	VW

Table 3: 15 Continued

n	$\sin^2\theta$ C2/m cell	$\sin^2\theta$ D/S	$\sin^2\theta$ G	I est	n	$\sin^2\theta$ C2/m cell	$\sin^2\theta$ D/S	$\sin^2\theta$ G	I est
			0.20826	VVW	96	0.29671	END DATA		
62	0.21292		0.21357	VVW	97	0.29743		0.29803	M
63	0.21417				98	0.30052			
64	0.21513				99	0.30130)		0.30216	
65	0.21554	0.21603	0.21624	W	100	0.30236)			M
66	0.21784		0.21831	M	101	0.30238		0.30331	M
67	0.21980				102	0.30464		0.30584	W
68	0.22378		0.22350	VVW	103	0.30799			
69	0.22430		0.22496	VVW	104	0.30936		0.30953	M
70	0.22967	0.23012	0.23020	MS	105	0.30988		0.31092	M
71	0.23188				106	0.31341			
72	0.23250		0.23295	MW	107	0.31381		0.31510	MS
73	0.23556				108	0.31692			
74	0.23619	0.23644	0.23719	MS	109	0.31827			
75	0.24199	0.24204	0.24275	MS	110	0.31837		0.31906	W
76	0.24658		0.24705	VW	111	0.32175			
77	0.24862)		0.24986	VVW	112	0.32266		0.32303	MS
78	0.25030)				113	0.32563		0.32678	M
79	0.25275		0.25355	VVW	114	0.32718			
			0.25617	VVW	115	0.32929)			
80	0.25948				116	0.32929)			
81	0.26010				117	0.33035)		0.33054	MS
82	0.26052	0.26104	0.26165	M	118	0.33039)			
83	0.26663		0.26717	VVW	119	0.33078)			
84	0.26817)		0.26916	VVW	120	0.33092)			
85	0.26985)				121	0.33114		0.33219	MS
86	0.27053		0.27183	VVW	122	0.33617			
87	0.27446		0.27540	MW	123	0.33679		0.33786	VVW
88	0.27666				124	0.34215			
89	0.27903				125	0.34293		0.34379	VVW
90	0.28117				126	0.34550		0.34736	VW
91	0.28210		0.28303	W	127	0.35099			
92	0.28715		0.28823	VW	128	0.35148			
93	0.28997				129	0.35713		0.35884	VW
94	0.29296				130	0.35926		0.36076	MW
95	0.29305	0.29308	0.29437	MS	131	0.36294			

Table 3:15 Continued

n	$\sin^2\theta$ C2/m cell	$\sin^2\theta$ D/S	$\sin^2\theta$ G	I est	n	$\sin^2\theta$ C2/m cell	$\sin^2\theta$ D/S	$\sin^2\theta$ G	I est
132	0.36491				169	0.42740			
133	0.36893				170	0.42863		0.42969	W
134	0.37080				171	0.43350)			
135	0.37411		0.37548	W	172	0.43433)		0.43489	VVW
136	0.37768				173	0.43522)			
137	0.37969				174	0.43936		0.44060	W
138	0.37999		0.38106	MW	175	0.44575		0.44682	W
139	0.38400				176	0.45004			
140	0.38466				177	0.45065			
141	0.38535		0.38569	M	178	0.45163			
142	0.38558				179	0.45176		0.45304	W
143	0.38686				180	0.45534			
144	0.38874				181	0.45667)			
145	0.38957)		0.39056	VW	182	0.45691)		0.45703	M
146	0.39109)				183	0.45730)			
147	0.39400				184	0.45830)			
148	0.39401		0.39545	W	185	0.45845)		0.45902	M
149	0.39797				186	0.45975)			
150	0.39954		0.40084	W	187	0.46198			
151	0.40234		0.40403	W	188	0.46417			
152	0.40619				189	0.46725)			
153	0.40641				190	0.46893)		0.46876	VW
154	0.40855				191	0.46953)			
155	0.40855				192	0.47260)		0.47425	VVW
156	0.40916				193	0.47456)			
157	0.40946				194	0.47789			
158	0.40948				195	0.47790			
159	0.40995)		0.41067	W	196	0.47836			
160	0.41073)				197	0.47837			
161	0.41605				198	0.47906		0.47975	W
162	0.42034				199	0.48498		END DATA	
163	0.42043)								
164	0.42049)		0.42177	MW					
165	0.42240)								
166	0.42409)								
167	0.42543)		0.42597	MW					
168	0.42554)								

3:3:2:5 $\underline{Na_2Np_2O_7}$

The Debye-Scherrer films for the sodium dineptunate(VI) products from Preparations 10, 11 and 12 were identical. The data also matched the analogous diuranate films from Preparations 7, 8 and 9. All the lines could therefore be indexed according to the generated data for sodium diuranate(VI). Parameters had previously been calculated[106] for $Na_2Np_2O_7$ based on a COHEN refinement of the data indexed in this way.

The data obtained from both Debye-Scherrer and Guinier films are summarised in Table 3:16. The individual lines have been assigned to theoretical lines generated for the parameters previously calculated for $Na_2Np_2O_7$.

Large discrepancies (up to 0.00400 $\sin^2\theta$) between these theoretical values and the experimental values were found when each line was assigned the index allocated to its analogue on the $Na_2U_2O_7$ films. This may simply reflect a need to recalculate the cell parameters for $Na_2Np_2O_7$ by refining the latest experimental data.

The extra lines on the Guinier films which can not be indexed from this data also feature on the films of $Na_2U_2O_7$.

Table 3: 16 X-Ray Powder Diffraction Data for $Na_2Np_2O_7$

n	$\sin^2\theta$ C2/m cell	$\sin^2\theta$ D/S	$\sin^2\theta$ G	I est	n	$\sin^2\theta$ C2/m cell	$\sin^2\theta$ D/S	$\sin^2\theta$ G	I est
1	0.01391				37	0.11815			
2	0.01440				38	0.12256		0.12397	VW
3	0.01681	0.01768	0.01709	VS	39	0.12523			
4	0.01982				40	0.12592			
5	0.02263				41	0.12646		0.12812	W
			0.02825	VVW	42	0.12855			
6	0.03401		0.03299	VW	43	0.12962			
7	0.03885				44	0.13150			
8	0.04259				45	0.13604			
9	0.04485				46	0.13785			
10	0.04753				47	0.13929)		0.14110	VVW
11	0.05165)	0.05389	(0.05306	S	48	0.14056)			
12	0.05325)		(0.05408	VS	49	0.14325	0.14540	(0.14477 (0.14583	MW MW
13	0.05566				50	0.14869			
14	0.05761				51	0.15113			
15	0.05868)				52	0.15125	0.15475	0.15459	VS
16	0.05886)	0.05976	0.05917	VS	53	0.15541	0.15665	0.15641	M
17	0.06014)				54	0.15671			
18	0.06722	0.06914	0.06884	S	55	0.15761			
19	0.07099				56	0.15900			
20	0.07900				57	0.16061)		0.16245	VVW
21	0.07930				58	0.16061)			
22	0.08144)	0.08258	(0.08177	M	59	0.16740			
23	0.08291)		(0.08259	S	60	0.16848			
24	0.09050				61	0.16981			
25	0.09162				62	0.17036)	0.17148	0.17160	S
26	0.09646				63	0.17037)			
27	0.09718				64	0.17221	0.17445	0.17406	VS
28	0.09771	0.09990	0.09807	S	65	0.17523			
29	0.10033				66	0.17840			
30	0.10069				67	0.17842			
31	0.10439				68	0.17941			
32	0.10608				69	0.18058			
33	0.11171				70	0.19010			
34	0.11225				71	0.19014			
35	0.11475				72	0.19245			
36	0.11544								

Table 3: 16 Continued

n	$\sin^2\theta$ C2/m cell	$\sin^2\theta$ D/S	$\sin^2\theta$ G	I est	n	$\sin^2\theta$ C2/m cell	$\sin^2\theta$ D/S	$\sin^2\theta$ G	I est
73	0.19315				109	0.25574		0.25573	W
74	0.19351				110	0.25980			
75	0.19800				111	0.26191			
76	0.19981				112	0.26515			
77	0.20171				113	0.26712			
78	0.20363				114	0.26713			
79	0.20417				115	0.26769			
80	0.20660)				116	0.26785			
81	0.20706)		0.20745	W	117	0.26889			
82	0.20922		0.20928	MW	118	0.26930			
83	0.20967)		0.21275	W	119	0.26983			
84	0.21302)				120	0.27121			
85	0.21427)	0.21558	0.21542	MW	121	0.27429)		0.27585	W
86	0.21558)				122	0.27661)			
87	0.21699				123	0.27717			
88	0.21728				124	0.27797			
89	0.21943				125	0.28064)			
90	0.22159				126	0.28394)	0.28341	0.28371	M
91	0.22263	0.22273	0.22308	M	127	0.28395)			
92	0.22568	0.22557	0.22538	MW	128	0.28503)			
93	0.22838				129	0.28666			
94	0.22928				130	0.28691			
95	0.23044				131	0.28737			
96	0.23136				132	0.29278			
97	0.23471				133	0.29325			
98	0.23532				134	0.29329			
99	0.23543				135	0.29597			
100	0.23670)				136	0.29929)			
101	0.23776)	0.23727	0.23826	MW	137	0.30077)	0.30079	0.30078	W
102	0.23832)				138	0.30338			
103	0.23866)				139	0.30400			
104	0.24057)		(0.24275	MW	140	0.30410			
105	0.24509)	0.24297	(0.24361	MW	141	0.30519			
106	0.24545				142	0.30608			
107	0.24703		0.24770	VVW	143	0.30666			
108	0.25259				144	0.30698			

Table 3: 16 Continued

n	$\sin^2\theta$ C2/m cell	$\sin^2\theta$ D/S	$\sin^2\theta$ G	I est		n	$\sin^2\theta$ C2/m cell	$\sin^2\theta$ D/S	$\sin^2\theta$ G	I est
145	0.30775)	0.30947	(0.30930	M						
146	0.30906)		(0.31115	M						
147	0.31212	END DATA								
148	0.31321									
149	0.31345									
150	0.31602									
151	0.31602									
152	0.31720									
153	0.31996									
154	0.32222									
155	0.32578)		0.32678	W						
156	0.32598)									
157	0.32883									
158	0.32975		0.33078	MW						
159	0.33164		END DATA							
160	0.33252									

3:3:2:6 $\underline{K_2Np_2O_7}$

The Debye-Scherrer data for $K_2Np_2O_7$ were indexed according to the GENSTRUCK generated data for the published monoclinic, $P2_1/m$, cell of $K_2U_2O_7$. The data did not agree with the reported[91] hexagonal, $R\bar{3}m$, cell for $K_2Np_2O_7$. The Debye-Scherrer films from Preparations 10, 11 and 12 were all in agreement. These data also matched the analogous diuranate films from Preparations 7, 8 and 9.

The Guinier data for the product from Preparation 11 were used to determine the cell parameters for $K_2Np_2O_7$. The data were first indexed according to the $P2_1/m$ cell for $K_2U_2O_7$. Cell paramaters calculated in a COHEN refinement to an accuracy of 0.00124 $\sin^2\theta$ were used in the GENSTRUCK programme to generate the theoretical lines for $K_2Np_2O_7$. The experimental data were then indexed again from these new generated data and refined a second time to an accuracy of 0.00124 $\sin^2\theta$. The following cell parameters were obtained:

$$a = 6.908\text{Å};\quad b = 7.977\text{Å};\quad c = 6.998\text{Å};\quad \beta = 109.67^\circ.$$

These parameters were used to generate the theoretical data presented in Table 3:17. Experimental Debye-Scherrer and Guinier data are also tabulated.

Table3: 17 X-Ray Powder Diffraction Data for $K_2Np_2O_7$

n	$\sin^2\theta$ P2₁/m cell	$\sin^2\theta$ D/S	$\sin^2\theta$ G	I est	n	$\sin^2\theta$ P2₁/m cell	$\sin^2\theta$ D/S	$\sin^2\theta$ G	I est
1	0.01369)	0.01414	0.01371	VS	37	0.11210			
2	0.01405)				38	0.11856			
3	0.01840				39	0.12111			
4	0.02302				40	0.12144		0.12196	W
5	0.02338				41	0.12318			
6	0.02774				42	0.12336)	0.12513	0.12453	M
7	0.03706				43	0.12481)			
8	0.03735				44	0.12516)			
9	0.04640				45	0.12589)			
10	0.05013				46	0.12641			
11	0.05104)	0.05249	0.05179	S	47	0.13251			
12	0.05120)				48	0.13270			
13	0.05140)				49	0.13417			
14	0.05475				50	0.13450			
15	0.05575	0.05569	0.05531	VS	51	0.13525)		0.13591	W
16	0.05618	0.05714	0.05643	S	52	0.13575)			
17	0.05946				53	0.13879			
18	0.06054		0.06035	VW	54	0.14023			
19	0.06408		0.06452	VW	55	0.14658			
20	0.06552				56	0.14826			
21	0.07360)	0.07505	0.07451	M	57	0.14941)	0.15112	0.15028	M
22	0.07442)		0.07530	M	58	0.14945)		0.15139	M
23	0.08294				59	0.15760			
24	0.08746				60	0.15764			
25	0.08748				61	0.16053			
26	0.08853)		0.08850	VW	62	0.16072			
27	0.08856)				63	0.16251			
28	0.09210				64	0.16310			
29	0.09354				65	0.16346			
30	0.09679				66	0.16376)	0.16487	0.16419	M
31	0.09773				67	0.16522)		0.16519	M
32	0.09787				68	0.16560			
33	0.09809				69	0.16781			
34	0.10244				70	0.16809			
35	0.10922				71	0.17150			
36	0.11095				72	0.17258			

Table 3:17 Continued

n	$\sin^2\theta$ P2₁/m cell	$\sin^2\theta$ D/S	$\sin^2\theta$ G	I est	n	$\sin^2\theta$ P2₁/m cell	$\sin^2\theta$ D/S	$\sin^2\theta$ G	I est
73	0.17456				109	0.23687			
74	0.17493				110	0.23715			
75	0.17743		0.17741	VW	111	0.23786			
76	0.18561				112	0.23795			
77	0.18648		0.18836	VW	113	0.23844			
78	0.19327				114	0.24217			
79	0.19570				115	0.24274			
80	0.19614		0.19776	VW	116	0.24469			
81	0.19954				117	0.24526			
82	0.20050				118	0.24649		0.24645	VW
83	0.20062				119	0.24714			
84	0.20109				120	0.24750			
85	0.20257				121	0.24926			
86	0.20295				122	0.24964			
87	0.20416)				123	0.25186			
88	0.20482)				124	0.25214)		0.25451	VW
89	0.20503)	0.20487	0.20559	S	125	0.25633)			
90	0.20545)				126	0.25864			
91	0.20560)				127	0.26151			
92	0.20722)				128	0.26208			
93	0.20741)	0.20826	0.20709	M	129	0.27036			
94	0.20921)				130	0.27052			
95	0.20984				131	0.27076			
96	0.21043				132	0.27259			
97	0.21046				133	0.27271			
98	0.21415				134	0.27278			
99	0.21898)				135	0.27327			
100	0.22301)		0.22158	W	136	0.27450			
101	0.22473		0.22600	VW	137	0.27457			
102	0.22832				138	0.27575)	0.27586	0.27558	MS
103	0.23230				139	0.27582)			
104	0.23305				140	0.27969			
105	0.23340				141	0.27974			
106	0.23407				142	0.28358			
107	0.23535				143	0.28455			
108	0.23592				144	0.28466			

Table 3: 17 Continued

n	$\sin^2\theta$ P2₁/m cell	$\sin^2\theta$ D/S	$\sin^2\theta$ G	I est	n	$\sin^2\theta$ P2₁/m cell	$\sin^2\theta$ D/S	$\sin^2\theta$ G	I est
145	0.28508				181	0.34216			
146	0.28513				182	0.34237			
147	0.28820				183	0.34268			
148	0.28886				184	0.34292			
149	0.28964				185	0.34367			
150	0.29439				186	0.34511			
151	0.29767				187	0.34556			
152	0.30303				188	0.34689			
153	0.30373				189	0.34982			
154	0.30502				190	0.34986			
155	0.30705				191	0.34992			
156	0.30771				192	0.34992			
157	0.30878				193	0.35022			
158	0.30954				194	0.35050			
159	0.31256				195	0.35114			
160	0.31310				196	0.35150			
161	0.31435				197	0.35414			
162	0.31463				198	0.35423			
163	0.31501				199	0.35440			
164	0.31745				200	0.35458			
165	0.31751				201	0.35552)			
166	0.31817				202	0.35663)	0.35793	0.35577	M
167	0.31888				203	0.35682)			
168	0.31940				204	0.35862)			
169	0.31996				205	0.35916			
170	0.32091				206	0.35979			
171	0.32120				207	0.35987			
172	0.32190				208	0.36048			
173	0.32199		0.32298	VW	209	0.36347			
174	0.32750				210	0.36593			
175	0.32858		0.32866	VW	211	0.36839			
176	0.33175				212	0.37093			
177	0.33358				213	0.37168)	0.37294	0.37253	M
178	0.33433				214	0.37324)			
179	0.33618				215	0.37414	END DATA	END DATA	
180	0.33792				216	0.37844			

3:3:2:7 $\underline{Rb_2Np_2O_7}$

The Debye-Scherrer films for $Rb_2Np_2O_7$ from Preparations 10, 11 and 12 were identical and were indexed using the GENSTRUCK listing for the monoclinic, $P2_1/m$, diuranate analogue, $Rb_2U_2O_7$. These data could not be indexed according to the published[91] $R\bar{3}m$ cell. Comparison of the films showed the dineptunate to be isostructural with the diuranate.

As with the potassium dineptunate, the Guinier data for the product from Preparation 11 were used to determine the cell parameters based on the unit cell of the uranium complex, $Rb_2U_2O_7$. The experimental Guinier X-ray diffraction data obtained for $Rb_2Np_2O_7$ were first indexed in accordance with the GENSTRUCK generated data for $Rb_2U_2O_7$. The data were then refined in the COHEN programme to an accuracy of 0.00166 $\sin^2\theta$. The resulting cell parameters were used to generate the theoretical listing from which the measured lines were re-indexed. A second COHEN refinement to an accuracy of 0.00166 $\sin^2\theta$ gave the cell parameters,

$$a = 7.027\text{Å};\quad b = 8.046\text{Å};\quad c = 7.430\text{Å};\ \text{and}\ \beta = 109.53^\circ.$$

The theoretical lines generated for these parameters for a $P2_1/m$ cell are tabulated with the experimental Debye-Scherrer and Guinier data in Table 3:18.

Table 3:18 X-Ray Powder Diffraction Data for $Rb_2Np_2O_7$

n	$\sin^2\theta$ P2₁/m cell	$\sin^2\theta$ D/S	$\sin^2\theta$ G	I est	n	$\sin^2\theta$ P2₁/m cell	$\sin^2\theta$ D/S	$\sin^2\theta$ G	I est
1	0.01212		0.01240	VS	37	0.10610			
2	0.01355				38	0.10838			
3	0.01710				39	0.10906			
4	0.02130				40	0.11187		0.11218	M
5	0.02273				41	0.11588			
6	0.02628				42	0.11685			
7	0.03424				43	0.11756			
8	0.03672				44	0.11824			
9	0.04342				45	0.11903			
10	0.04489				46	0.12017			
11	0.04847				47	0.12105		0.12150	M
12	0.04884				48	0.12196			
13	0.04919	0.05080	0.04975	VS	49	0.12751			
14	0.05027		0.05162	W	50	0.12821			
15	0.05382	0.05219	0.05318	S	51	0.13109			
16	0.05407				52	0.13114			
17	0.05420	0.05610	0.05533	S	53	0.13181			
18	0.05765				54	0.13363		0.13454	W
19	0.05837		0.06059	VW	55	0.13682			
20	0.06338				56	0.13694			
21	0.06841				57	0.14509			
22	0.07095	0.07224	0.07243	VW	58	0.14578			
23	0.07759				59	0.14612			
24	0.07916				60	0.14688			
25	0.08161				61	0.14831			
26	0.08345				62	0.14859)	0.15063	0.15028	VS
27	0.08519				63	0.15103)			
28	0.08591				64	0.15392			
29	0.08834				65	0.15575			
30	0.09092				66	0.15749			
31	0.09263				67	0.15868			
32	0.09474				68	0.15899			
33	0.09617				69	0.15977			
34	0.09692				70	0.16043			
35	0.09972				71	0.16177)	0.16233	0.16264	S
36	0.10513				72	0.16310)			

Table 3:18 Continued

n	$\sin^2\theta$ P2₁/m cell	$\sin^2\theta$ D/S	$\sin^2\theta$ G	I est
73	0.16398			
74	0.16607			
75	0.16895)		0.17160	W
76	0.17318)			
77	0.17366			
78	0.17953			
79	0.17956			
80	0.18111			
81	0.18236			
82	0.18503			
83	0.18874			
84	0.19064			
85	0.19099			
86	0.19168			
87	0.19177			
88	0.19389			
89	0.19449			
90	0.19466			
91	0.19535			
92	0.19606			
93	0.19649			
94	0.19675)			
95	0.20108)	0.20037	0.20019	VS
96	0.20165)			
97	0.20307)			
98	0.20384)		0.20381	VW
99	0.20457)			
100	0.20593	0.20685	0.20583	VW
101	0.20990			
102	0.21305			
103	0.21467			
104	0.21529			
105	0.21628			
106	0.21681			
107	0.21956			
108	0.22183			
109	0.22223	0.22276	0.22266	VW
110	0.22308	END DATA		
111	0.22385			
112	0.22599			
113	0.22603			
114	0.23033			
115	0.23061			
116	0.23093			
117	0.23101			
118	0.23138			
119	0.23226			
120	0.23347			
121	0.23654			
122	0.24161			
123	0.24171			
124	0.24239			
125	0.24304			
126	0.24379			
127	0.24660			
128	0.24977			
129	0.25089			
130	0.25139			
131	0.25353			
132	0.25525			
133	0.25579			
134	0.25594			
135	0.25855			
136	0.25874			
137	0.25980)		0.26187	M
138	0.26218)			
139	0.26320			
140	0.26373			
141	0.26591			
142	0.26883			
143	0.27149			
144	0.27238			

Table 3: 18 Continued

n	$\sin^2\theta$ P2₁/m cell	D/S	G	I est
145	0.27364			
146	0.27367			
147	0.27438			
148	0.27651			
149	0.27728			
150	0.27797			
151	0.27843			
152	0.27868			
153	0.27937			
154	0.28067			
155	0.28282			
156	0.28285			
157	0.28370			
158	0.28382			
159	0.29519			
160	0.29567			
161	0.29642			
162	0.29728			
163	0.29790			
164	0.29943			
165	0.29991			
166	0.30080			
167	0.30158			
168	0.30296			
169	0.30445			
170	0.30560			
171	0.30570			
172	0.30665			
173	0.30805			
174	0.30812			
175	0.30821			
176	0.30865			
177	0.31036			
178	0.31039			
179	0.31076			
180	0.31214			

n	$\sin^2\theta$ P2₁/m cell	D/S	G	I est
181	0.31295			
182	0.31663			
183	0.31723			
184	0.31730			
185	0.31934			
186	0.32005			
187	0.32433			
188	0.32581			
189	0.32641			
190	0.32644			
191	0.32852			
192	0.33047			
193	0.33313			
194	0.33382			
195	0.33787			
196	0.33830			
197	0.33856			
198	0.33877			
199	0.33968			
200	0.34077			
201	0.34136			
202	0.34154			
203	0.34259			
204	0.34300			
205	0.34363			
206	0.34402			
207	0.34477			
208	0.34484			
209	0.34581			
210	0.34757			
211	0.34795			
212	0.34844)			
213	0.34852)		0.34998	S
214	0.35145)			
215	0.35335			
216	0.35411)			

Table 3: 18 Continued

n	$\sin^2\theta$			I est		n	$\sin^2\theta$			I est
	$P2_1/m$ cell	D/S	G				$P2_1/m$ cell	D/S	G	
217	0.35605)		0.35548	W						
218	0.35626)									
219	0.35629)									
220	0.35762		END DATA							

3:3:2:8 <u>$Cs_2Np_2O_7$</u>

The Debye-Scherrer films for the $Cs_2Np_2O_7$ products of Preparations 10, 11, 12 and 13 were identical. These data were indexed from the GENSTRUCK listing for the published[91] C2/m cell parameters,

$$a = 14.300\text{Å};\quad b = 4.330\text{Å};\quad c = 7.400\text{Å};\ \beta = 113.58^{\circ}.$$

The films were similar but not identical to those obtained for the analogous diuranate, $Cs_2U_2O_7$.

As with β-$Cs_2U_2O_7$ extra lines, which could not be indexed according to the reported cell, were found on the Guinier films. There were only two such lines found for $Cs_2Np_2O_7$ and these matched two of the extra lines found on the β-$Cs_2U_2O_7$ films. These extra lines remain unresolved.

The Debye-Scherrer and Guinier data are summarised in Table 3:19 with the theoretical $\sin^2\theta$ values for the C2/m cell.

Table 3: 19 X-Ray Powder Diffraction Data for $Cs_2Np_2O_7$

n	$\sin^2\theta$ C2/m cell	$\sin^2\theta$ D/S	$\sin^2\theta$ G	I est	n	$\sin^2\theta$ C2/m cell	$\sin^2\theta$ D/S	$\sin^2\theta$ G	I est
			0.01080	W	34	0.14063			
1	0.01292	0.01304	0.01302	S	35	0.14285			
2	0.01384		0.01465	VW	36	0.14455			
3	0.01606		0.01563	VW	37	0.14661	0.14735	0.14778	W
4	0.03516		0.03517	VW	38	0.14983			
5	0.03746	0.03774	0.03770	W	39	0.15423			
6	0.04273	0.04268	0.04282	M	40	0.15786		0.15896	VW
7	0.04412	0.04439	0.04414	W	41	0.16221			
8	0.04688		0.04497	VW	42	0.16424		0.16504	VW
9	0.05168	0.05197	0.05206	M	43	0.16748			
10	0.05343	0.05373	0.05385	M	44	0.16957			
11	0.05536	0.05588	0.05579	M	45	0.17091	0.17025	0.17141	VW
12	0.05971	0.05974	0.05988	S	46	0.17367			
13	0.06283	0.06295	0.06300	MW	47	0.17649			
14	0.06424	0.06449	0.06447	MW	48	0.17670			
			0.06607	VW	49	0.17776	0.17791	0.17787	W
15	0.07614		0.07636	W	50	0.17802			
16	0.08242				51	0.17847		0.17902	W
17	0.08691				52	0.18214	0.18184	0.18268	W
18	0.08967				53	0.18752		0.18871	VW
19	0.09180		0.09263	VW	54	0.19103	0.19062	0.19146	W
20	0.09753				55	0.19155			
21	0.09802				56	0.20123			
22	0.10437		0.10502	VW	57	0.20289	0.20198	0.20260	W
23	0.10538	0.10578	0.10610	W	58	0.20518)	0.20483	0.20603	W
24	0.10745				59	0.20536)			
25	0.11204	0.11199	0.11281	W	60	0.20672			
26	0.11628				61	0.20933			
27	0.11638)	0.11734	0.11745	W	62	0.21370			
28	0.11819)				63	0.21646			
29	0.12455				64	0.21793			
30	0.12679	0.12661	0.12728	M	65	0.22048			
31	0.13097	0.13127	0.13148	MW	66	0.22143		0.22162	VVW
32	0.13539				67	0.22336			
33	0.13971	0.13944	0.14005	W	68	0.22481			

n	$\sin^2\theta$ C2/m cell	$\sin^2\theta$ D/S	$\sin^2\theta$ G	I est
69	0.22725			
70	0.23216	0.23225	0.23295	VW
71	0.23423			
72	0.23582			
73	0.23883	0.23781	0.23932	VW
74	0.24042			
75	0.24307	0.24297	0.24425	VW
76	0.25134			
77	0.25159			
78	0.25698			
79	0.25817			
80	0.26327			
81	0.26335			
82	0.26734	0.26617	0.26894	VW
83	0.27134			
84	0.27137			
85	0.27661			
86	0.27672			
87	0.27714			
88	0.28335			
89	0.28379			
90	0.28708			
91	0.28873			
92	0.28900			
93	0.29068			
94	0.29630)	0.29635	0.29757	VW
95	0.29635)			
96	0.30179			
97	0.30328			
98	0.30455			
99	0.30541			
100	0.30560			
101	0.30700)		0.30768	VW
102	0.30746)			
103	0.31194			

n	$\sin^2\theta$ C2/m cell	$\sin^2\theta$ D/S	$\sin^2\theta$ G	I est
104	0.31328	0.31314	0.31394	VW
105	0.31431			
106	0.31471			
107	0.31641			
108	0.31834			
109	0.32300			
110	0.32609			
111	0.32779			
112	0.32968)			
113	0.32971)	0.32931	0.33007	VW
114	0.33046)		END DATA	
115	0.33141			
116	0.33350			
117	0.33374			
118	0.33599			
119	0.33612			
120	0.33701			
121	0.33711	0.33722		
122	0.33874			
123	0.34537			
124	0.34598			
125	0.34766			
126	0.34821			
127	0.35111			
128	0.35794			
129	0.35869			
130	0.36261	0.36325		
131	0.36721			
132	0.36995			
133	0.37176			
134	0.37300)	0.38343		
135	0.38376)			
136	0.38433	END DATA		

3:3:3 Spectroscopic Properties of the Alkali Metal Dineptunates(VI)

As discussed in Section 3:1:3 an increasing level of Np(V) contamination with time was found in the alkali metal neptunyl(VI) triacetates. This was also found to be the case for the alkali metal dineptunates(VI).

Following the measurement of the enthalpy of solution in 1 mol dm^{-3} HCl by calorimetry the resulting solution was monitored for Np(V) contamination by uv/visible spectrophotometry. The results obtained are summarised in Table 3:20. The level of Np(V) contamination in the starting triacetates at the time of decomposition was unknown.

Samples from these preparations surplus to calorimetry requirements were left in storage and monitored at a later date for Np(V) content. All the samples showed an increasing level of contamination with time. Exclusion of light from the samples did not affect the increase.

Table 3:20 Percentage Np(V) Contamination in Neptunyl(VI) Solutions Following Calorimetry

Starting Complex	Preparation	Time From Preparation (Days)	Np(V) Contamination[a] (%)
$Na_2Np_2O_7$	10	142	
	12	41	<1.0
$K_2Np_2O_7$	10	121	<2.0
	11	99	<2.7
	12	35	<4.0
$Rb_2Np_2O_7$	10	120	6.5
	11	95	5.0
	12	45	2.5
$Cs_2Np_2O_7$	10	99	9.1
	11	88	9.6
	12	48	21.0

a determined by sodium nitrite reduction (Section 2:4:1)

Owing to the high levels of Np(V) contamination of 9.1, 9.6 and 21% in the caesium dineptunate samples from Preparations 10, 11 and 12, respec-

rively, a further sample was prepared for calorimetry. However, the starting acetate (Preparation 6) showed a neptunium(V) content of 2.7% only 18 hours after its preparation. The decomposition of this triacetate, Preparation 13, was carried out when the acetate was 5 days old. Using the Beer-Lambert method (Section 2:4:2) the Np(V) content of the oxide was determined as 3.6% on the day of preparation. After a further 290 days storage in total darkness this had risen to 15%. The sample was not used for calorimetric measurements.

3:3:4 Stability of Alkali Metal Diuranates(VI) in Air

It is known that sodium uranates other than $NaUO_3$ and the uranates(VI) with Na/U $\leq$ 1 are hygroscopic[93] and therefore have to be handled in dry atmospheres. In a study of the Cs-U-O systems[98] only Cs_2UO_4 was described as being hygroscopic. In the analogous potassium and rubidium systems the complexes K_2UO_4 and Rb_2UO_4 were likewise the only compounds identified as being hygroscopic.[94] However, all the oxides in this particular investigation were handled in a dry box.

As a precaution, therefore, and to gain experience in glove-box handling techniques prior to the neptunate work, all the uranate handling was performed in dry atmosphere boxes.

The investigation of the stability of the alkali metal diuranates(VI) was limited to the decomposition of the alkali metal uranyl(VI) triacetates in the laboratory atmosphere and the exposure of the products from dry oxygen preparations to the laboratory air. All the materials were monitored by Debye-Scherrer X-ray powder diffraction and the samples exposed to the laboratory atmosphere were checked for weight changes. Within the limits of detection of these techniques the results (see Section 2:10:2:2) suggest that the diuranates, $M^I_2U_2O_7$ (M^I = Na, K, Rb, Cs), are indeed stable with respect to moist air. This is perhaps not unexpected in view of the fact that in a previous study of alkali metal uranates[189] $Na_2U_2O_7$

and $K_2U_2O_7$ prepared by heating U_3O_8 with alkali metal chloride were washed in water to remove excess alkali metal chloride.

3:4 THERMODYNAMIC RESULTS

3:4:1 Auxiliary Data

Enthalpy of solution measurements were obtained by calorimetry at 298K, for the dissolution reaction,

$$M_2^{I}M_2^{VI}O_7(s) + \{aHCl, bH_2O\} \rightarrow \{2M^{I}Cl, 2M^{VI}O_2Cl_2, (a-6)HCl, (b+3)H_2O\}; \quad \Delta H_1.$$

In the experiments the ratio b/a was 54.4 and the molar ratio of HCl to $M_2^{I}M_2^{VI}O_7$, a, ranged from ca 600 to 2200.

The enthalpies of formation of the alkali metal diuranates(VI) and dineptunates(VI) at 298K,

$$2M^{I}(s) + 2M^{VI}(s) + \tfrac{7}{2}O_2(g) \rightarrow M_2^{I}M_2^{VI}O_7(s); \quad \Delta H_f^{\ominus},$$

were calculated from the enthalpies of solution, ΔH_1, and the following relationships, ΔH_2 to ΔH_7.

$$M^{I}(s) + \tfrac{1}{2}Cl_2(g) \rightarrow M^{I}Cl(s); \quad \Delta H_2$$

$$M^{I}Cl(s) + \{aHCl, bH_2O\} \rightarrow \{M^{I}Cl, aHCl, bH_2O\}; \quad \Delta H_3$$

$$M^{VI}(s) + O_2(g) + Cl_2(g) \rightarrow M^{VI}O_2Cl_2(s); \quad \Delta H_4$$

$$M^{VI}O_2Cl_2(s) + \{aHCl, bH_2O\} \rightarrow \{M^{VI}O_2Cl_2, aHCl, bH_2O\}; \quad \Delta H_5$$

$$H_2(g) + \tfrac{1}{2}O_2(g) + \{aHCl, bH_2O\} \rightarrow \{aHCl, (b+1)H_2O\}; \quad \Delta H_6$$

$$\tfrac{1}{2}H_2(g) + \tfrac{1}{2}Cl_2(g) + \{aHCl, bH_2O\} \rightarrow \{(a+1)HCl, bH_2O\}; \quad \Delta H_7$$

These relationships complete the thermochemical cycle such that,

$$\Delta H_f^{\ominus}(M_2^{I}M_2^{VI}O_7, s) = 2\Delta H_2 + 2\Delta H_3 + 2\Delta H_4 + 2\Delta H_5 + 3\Delta H_6 - 6\Delta H_7 - \Delta H_1.$$

The enthalpy data for these reactions are summarised in Tables 3:21 to 3:25. The appropriate discussion accompanies each table.

Table 3:21 Enthalpy of Formation of $M^{I}Cl(s)$ [165] (ΔH_2)

Alkali Metal Chloride	$\Delta H_f^{\ominus}(M^{I}Cl, s)$ (kJ mol^{-1})
NaCl	-411.258 ± 0.109
KCl	-436.467 ± 0.138
RbCl	-435.019 ± 0.201
CsCl	-442.688 ± 0.201

Table 3:22 Heat of Solution of $M^{I}Cl(s)$ in 1 mol dm^{-3} HCl (ΔH_3)

Alkali Metal Chloride	Heat of Solution, Literature Data (kJ mol^{-1})	Ref	Heat of Solution, Value Used (kJ mol^{-1})
NaCl	+ 4.60 ± 0.40	190	
	+ 4.31 ± 0.40	90	+ 4.46 ± 0.40
KCl	+18.02 ± 0.06	191	
	+18.13 ± 0.22	*a*	+18.08 ± 0.23
RbCl	+17.36 ± 0.33	191	+17.36 ± 0.33
CsCl	+16.48 ± 0.08	192	
	+16.92 ± 0.04	193	+16.69 ± 0.40

a This work - see accompanying text

The experimental results for the measurement of the heat of solution of NBS SRM999(KCl) in 1 mol dm^{-3} HCl are summarised in Table 3:23. The material had been treated in the recommended manner[151] by drying at 760°C for 18 hours followed by regrinding to a fine powder. The powder was stored over P_2O_5 for the hour before use. The calorimetry was performed on an LKB calorimeter using a 25ml reaction vessel. The data were corrected to allow for a Relative Humidity of 50% in the ampoules.

Table 3:23 Heat of Solution of KCl in 1 mol dm^{-3} HCl

Experiment	Sample Weight (mg)	Concentration of Compound in Soln (10^{-3} mol dm^{-3})	Enthalpy Effect (J)	ΔH_{soln} (kJ mol^{-1})
1	13.80	7.404	3.4161	18.46
2	11.45	6.143	2.7986	18.22
3	12.40	6.653	3.0031	18.06
4	12.49	6.701	2.9988	17.90
5	12.33	6.615	2.9674	17.94
6	13.57	7.281	3.3163	18.22
Average				18.13 ± 0.22

Two measurements of the heat of solution of the same batch of SRM999 in water were also made. The average result of 17.49 ± 0.25 kJ mol^{-1} for a final solution *ca* 7 x 10^{-3} mol dm^{-3} compares well with the IUPAC recommended[194] value of 17.55 ± 0.04 kJ mol^{-1} for the reaction,

$$KCl(s) + 200\ H_2O(l) \rightarrow \{KCl,\ 200\ H_2O\}(l),$$

and a value of 17.22 ± 0.03 kJ mol^{-1} at infinite dilution[195].

Table 3:24 Enthalpy of Formation of $M^{VI}O_2Cl_2$ in 1 mol dm^{-3} HCl (ΔH_4 and ΔH_5)

Compound	$\Delta H_f^{\ominus}(M^{VI}O_2Cl_2,\ 1\ mol\ dm^{-3}\ HCl)$ (kJ mol^{-1})
UO_2Cl_2	-1345.2 ± 2.1
NpO_2Cl_2	-1187.1 ± 4.9

The value for UO_2Cl_2 was calculated as the sum of the enthalpy of formation, $\Delta H_f^{\ominus}(UO_2Cl_2,s)$ = -1243.5 ± 1.2 kJ mol^{-1}[196] (ΔH_4), and the heat of solution in 1 mol dm^{-3} HCl, ΔH_{soln} (UO_2Cl_2,s, 1 mol dm^{-3} HCl) = -101.7 ± 1.7 kJ mol^{-1}[196,174] (ΔH_5).

Solid NpO_2Cl_2 does not exist as a stable compound hence an alternative method of calculation, as published elsewhere[137], was used. The value for the heat of formation of NpO_2Cl_2 in 1 mol dm^{-3} HCl was taken as the sum of the heat of formation of NpO_2^{2+} in aqueous solution and the difference between the heats of formation of UO_2^{2+} in aqueous solution and in 1 mol dm^{-3} HCl, respectively,

$$\Delta H_f(NpO_2^{2+},\ 1\ mol\ dm^{-3}\ HCl) = \Delta H_f(NpO_2^{2+},\ aq) + \Delta H_f(UO_2^{2+}, 1\ mol\ dm^{-3}\ HCl) - \Delta H_f(UO_2^{2+},\ aq)$$

This assumes that the enthalpy of solution in 1 mol dm^{-3} HCl of NpO_2Cl_2 would be the same as that of UO_2Cl_2. The values for $\Delta H_f^{\ominus}(NpO_2^{2+},\ aq)$ = -860.6 ± 4.6 kJ mol^{-1} and $\Delta H_f^{\ominus}(UO_2^{2+},\ aq)$ = -1018.8 ± 1.7 kJ mol^{-1} were taken from the literature[167].

Table 3:25 Enthalpy of Formation of Water and Hydrochloric Acid in 1 mol dm^{-3} HCl (ΔH_6 and ΔH_7)

Reaction	Enthalpy (kJ mol^{-1})	Ref
$\Delta H_f^{\ominus}(H_2O, l)$	-285.830 ± 0.042	15
$\Delta H_{dil}(H_2O, l, 1 \text{ mol } dm^{-3} HCl)$	-0.017	197
$\Delta H_6\{\Delta H_f(H_2O, 1 \text{ mol } dm^{-3} HCl)\}$	-285.85 ± 0.04	
$\Delta H_f^{\ominus}(Cl^-, aq)$	-167.080 ± 0.088	15
$\Delta H_{dil}(Cl^-, aq, 1 \text{ mol } dm^{-3} HCl)$	+2.175	165
$\Delta H_7\{\Delta H_f(HCl, 1 \text{ mol } dm^{-3} HCl)\}$	-164.36 ± 0.10	

The two values, ΔH_6 and ΔH_7, represent the partial molar enthalpy of formation of water and hydrochloric acid, respectively.

3:4:2 Enthalpy of Solution Results

3:4:2:1 Alkali Metal Diuranates(VI)

All the calorimetric data for the alkali metal diuranates(VI), $Na_2U_2O_7$, $K_2U_2O_7$, $Rb_2U_2O_7$ and $Cs_2U_2O_7$, were measured on an LKB calorimeter using a 100ml reaction vessel. These enthalpy of solution in 1 mol dm^{-3} HCl results are summarised in Table 3:26.

3:4:2:2 Alkali Metal Dineptunates(VI)

The enthalpies of solution in 1 mol dm^{-3} HCl of the alkali metal dineptunates(VI), $Na_2Np_2O_7$, $K_2Np_2O_7$, $Rb_2Np_2O_7$ and $Cs_2Np_2O_7$, were measured using the microcalorimeter with its 8.5ml reaction vessel. The results are summarised in Table 3:27.

The enthalpy of solution of caesium dineptunate(VI) from Preparation 12 was measured. A result of -184.9 ± 2.7 kJ mol^{-1} obtained from three experimental runs is not included in Table 3:27 because of the high level

(21%) of Np(V) contamination in the material. The product from Preparation 13 was not used for calorimetry due to the 15% Np(V) contamination.

Table 3:26 Calorimetry Results for the Alkali Metal Diuranates(VI) (ΔH_1)

Compound	Preparation	Experiment	Sample Wt (mg)	Concentration of Compound in Soln (10^{-3} mol dm^{-3})	Enthalpy Effect (J)	ΔH_{soln} (kJ mol^{-1})
$Na_2U_2O_7$	7	1	41.61	0.656	11.194	-170.6
		2	48.84	0.770	13.329	-173.0
		3	39.16	0.618	10.571	-171.2
	8	1	46.53	0.734	12.585	-171.5
		2	40.14	0.633	10.923	-172.5
	9	1	60.87	0.960	16.480	-171.6
		2	49.57	0.782	13.504	-172.7
		3	53.63	0.846	14.519	-171.7
					Average:	-171.8 ± 0.7
$K_2U_2O_7$	7	1	38.78	0.582	8.7132	-149.7
		2	33.63	0.505	7.4140	-146.9
	8	1	32.12	0.482	7.1358	-148.0
		2	67.17	1.008	14.620	-145.0
	9	1	46.42	0.682	10.171	-149.2
		2	53.34	0.801	11.888	-148.7
		3	50.49	0.758	11.270	-148.7
		4	57.87	0.869	12.981	-149.4
					Average:	-148.2 ± 1.3
$Rb_2U_2O_7$	7	1	49.36	0.650	10.770	-165.6
	8	1	56.22	0.741	12.267	-165.6
		2	48.22	0.635	10.575	-166.4
		3	44.65	0.588	9.6942	-164.8
		4	53.16	0.700	11.637	-166.1
	9	1	59.84	0.788	13.111	-166.3
		2	51.01	0.672	11.109	-165.3
		3	52.17	0.687	11.351	-165.1
					Average:	-165.6 ± 0.5
$Cs_2U_2O_7$	7	1	38.52	0.451	8.5527	-189.6
		2	39.15	0.459	8.6970	-189.7
	9	1	48.68	0.570	10.577	-185.5
		2	43.62	0.511	9.4762	-185.5
		3	40.62	0.476	8.8916	-186.9
		4	43.44	0.509	9.5345	-187.4
					Average:	-187.4 ± 2.0

Table 3:27 Calorimetry Results for the Alkali Metal Dineptunates(VI) (ΔH_1)

Compound	Preparation	Experiment	Sample Wt (mg)	Concentration of Compound in Soln (10^{-3} mol dm^{-3})	Euthalpy Effect (J)	ΔH soln (kJ mol^{-1})
$Na_2Np_2O_7$	10	1	8.846	1.647	2.3168	-165.5
		2	7.346	1.368	1.9201	-165.2
		3	7.962	1.482	2.0813	-165.2
		4	5.672	1.056	1.4733	-164.2
	12	1	8.452	1.573	2.2177	-165.8
		2	8.634	1.607	2.2712	-166.2
					Average:	-165.4 ± 0.7
$K_2Np_2O_7$	10	1	8.066	1.429	1.8121	-149.2
		2	7.784	1.379	1.7523	-149.5
		3	7.831	1.387	1.7568	-149.0
		4	9.328	1.652	2.1050	-149.9
		5	7.201	1.275	1.6289	-150.2
	11	1	7.009	1.241	1.5601	-147.8
		2	8.803	1.559	1.9735	-148.9
		3	8.651	1.532	1.9477	-149.5
	12	1	7.911	1.401	1.8127	-152.2
		2	7.589	1.344	1.7465	-152.9
		3	7.546	1.337	1.7199	-151.4
					Average:	-150.0 ± 1.0
$Rb_2Np_2O_7$	10	1	8.301	1.287	1.8803	-171.9
		2	7.504	1.163	1.6519	-167.1
		3	7.592	1.177	1.6130	-161.2
		4	6.881	1.067	1.4941	-164.8
		5	6.984	1.083	1.5110	-164.2
	11	1	7.813	1.211	1.7117	-166.3
		2	7.630	1.183	1.6589	-165.0
		3	6.136	0.951	1.3514	-167.1
	12	1	6.491	1.006	1.4350	-167.8
		2	9.822	1.523	2.2079	-170.6
		3	8.391	1.301	1.8498	-167.3
		4	7.603	1.179	1.7116	-170.9
		5	9.212	1.428	2.0337	-167.5
					Average:	-167.0 ± 1.8
$Cs_2Np_2O_7$	10	1	7.155	0.988	1.6756	-199.5
		2	5.402	0.746	1.2829	-202.3
		3	5.094	0.704	1.1912	-199.2
	11	1	6.614	0.913	1.5487	-199.5
		2	7.441	1.028	1.7421	-199.4
					Average:	-200.0 ± 1.6

3:4:3 Standard Enthalpy of Formation of Alkali Metal Diuranates (VI) and Dineptunates(VI)

Using the data from Tables 3:21, 3:22, 3:24, 3:25, 3:26 and 3:27 the standard enthalpies of formation of the alkali metal diuranates(VI) and dineptunates(VI) have been calculated. These results are tabulated in Table 3:28.

Table 3:28 Standard Enthalpy of Formation of Alkali Metal Diuranates (VI) and Dineptunates(VI) at 298.15 ± 0.10K

Oxide	$\Delta H_f^{\ominus}(M_2^{I}M_2^{VI}O_7,s)$ (kJ mol^{-1})	Remarks
$Na_2U_2O_7$	-3203.6 ± 4.4	
$K_2U_2O_7$	-3250.4 ± 4.5	
$Rb_2U_2O_7$	-3231.5 ± 4.3	
$Cs_2U_2O_7$	-3226.4 ± 4.8	
$Na_2Np_2O_7$	-2893.8 ± 9.9	< 1% Np(V)
$K_2Np_2O_7$	-2932.4 ± 9.9	< 2%, 2.7% and 4% Np(V)
$Rb_2Np_2O_7$	-2913.9 ± 10.0	6.5%, 5% and 2% Np(V)
$Cs_2Np_2O_7$	-2897.6 ± 10.0	9.1% and 9.6% Np(V)

The result for $Na_2U_2O_7$ is in excellent agreement with that obtained by T C Tso[90] (-3203.5 ± 4.4 kJ mol^{-1}) using the same calorimeter. It is also in reasonable agreement with results obtained elsewhere. A value of -3194.5 ± 2.1 kJ mol^{-1} was the result based on a cycle involving 6 mol dm^{-3} HCl[93]. Utilising a cycle based on 1.505 mol dm^{-3} H_2SO_4 a value of -3194.8 ± 1.8 kJ mol^{-1} was obtained[198]. The slight discrepancy in the results may be due to unidentified inconsistencies in the auxiliary data used in the various thermodynamic cycles. This is supported by the fact that a value of -172.4 ± 2.0 kJ mol^{-1} was obtained [199] for the enthalpy of solution in 1 mol dm^{-3} HCl using part of the sample employed in the determination in 1.505 mol dm^{-3} H_2SO_4[198]. This value is in excellent agreement with the result of 171.8 ± 0.7 kJ mol^{-1}

obtained in this work.

The value of -3226.4 ± 4.8 kJ mol^{-1} obtained for β-$Cs_2U_2O_7$ is in fair agreement with the recalculated result of -3220.8 ± 1.5 kJ mol^{-1} published in the literature[11].

The previously reported[106] value for $Na_2Np_2O_7$ of -2887 ± 12 kJ mol^{-1} was based on three experimental runs from only one preparation. The data presented here are based on six experimental runs using material from two separate preparations. As there was good agreement between the two samples the value of the enthalpy of formation included in Table 3:28 was calculated based on these latest experimental data only. In combining all the data the overall enthalpy of solution in 1 mol dm^{-3} HCl becomes, ΔH_{soln} ($Na_2Np_2O_7$, s, 1 mol dm^{-3} HCl) = -165.9 ± 1.0 kJ mol^{-1}. This yields a value for the enthalpy of formation of, ΔH_f^o ($Na_2Np_2O_7$, s) = -2894.3 ± kJ mol^{-1}.

Apart from the result for $Na_2Np_2O_7$ the data for the alkali metal dineptunates (VI), particularly that for $Cs_2Np_2O_7$, must be considered as preliminary results because of the varying levels of Np (V) contamination found in the solutions following calorimetry.

3:4:4 Enthalpy of Binary Oxide Complexation

The standard enthalpy of formation, ΔH_f^o ($M^I{}_2M^{VI}{}_2O_7$, s), values given in Section 3:4:3 can be combined with additional auxiliary data in order to calculate the enthalpy of complexation of binary oxides to form the alkali metal diuranates (VI) and dineptunates (VI). These complexation reactions are between alkali metal monoxide and either actinide trioxide or dioxide.

The two reactions to be considered therefore are,

(1) $M^I{}_2O$ (s) + $2M^{VI}O_3$ (s) → $M^I{}_2M^{VI}{}_2O_7$ (s) and,

(2) $$M_2^{I}O(s) + 2M^{IV}O_2(s) + O_2(g) \rightarrow M_2^{I}M_2^{VI}O_7(s).$$

Thermodynamic data are also available for chromium, molybdenum and tungsten complexes such that the enthalpy of complexation, based on reaction (1) above, can be calculated to compare with the results for the actinide compounds.

The thermodynamic data required for the calculations are presented in Table 3:19.

Table 3:29 Additional Thermodynamic Data

Complex	ΔH_f° (kJ mol^{-1})	Ref
Na_2O (s)	-414.22	20
K_2O (s)	-361.50	20
Rb_2O (s)	-338.90	20
Cs_2O (s)	-345.77	20
γ-UO_3 (s)	-1223.82 ± 1.26	11
NpO_3 (s)[a]	-1070 ± 6	200
CrO_3	-589.53	201
MoO_3	-745,09	201
WO_3 (s)	-842.87	201
$Na_2Cr_2O_7$	-1978.61	20
$Na_2Mo_2O_7$	-2245.05	20
$Na_2W_2O_7$	-2404.96	20
$K_2Cr_2O_7$	-2061.46	20
$K_2Mo_2O_7$	-2291.66	20
$Rb_2Cr_2O_7$	-1992.84	20
$Cs_2Cr_2O_7$	-2088.82	20
$Cs_2Mo_2O_7$	-2302.87	20

[a] NpO_3 does not exist as a stable solid complex

The calculated enthalpy of complexation results for the reaction involving actinide or transition metal trioxide are summarised in Table 3:30.

Table 3:30 $\Delta H_{complex}$ $(M^{I}_2O(s) + 2M^{VI}O_3(s) \rightarrow M^{I}_2M^{VI}_2O_7(s))$ (kJ mol^{-1})

M^{I} \ M^{VI}	U[a]	Np[a]	Cr	Mo	W
Na	-341.7 ± 6.6	-340 ± 16	-385.3	-340.6	-305.0
K	-441.3 ± 6.7	-431 ± 16	-520.9	-440.0	
Rb	-445.0 ± 6.5	-435 ± 16	-474.9		
Cs	-433.0 ± 6.9	-412 ± 16	-564.0	-466.9	

[a] An estimate of ± 4.2 kJ mol^{-1} was applied as the uncertainty for the alkali metal dioxide data

With the complexation reactions involving neptunium it is more realistic to consider reaction (2) above, which involves actinide dioxide, due to the instability of solid NpO_3. This reaction is also valid for the complexes of uranium.

The auxiliary data required are the standard enthalpies of formation of $UO_2(s)$ and $NpO_2(s)$ which are -1085.0 ± 1.0 kJ mol^{-1}[15] and -1074.0 ± 2.5 kJ mol^{-1}[31], respectively. The enthalpies of complexation of alkali metal monoxide and actinide dioxide to form the alkali metal diuranates (VI) and dineptunates(VI) are tabulated in Table 3:31.

Table 3:31 $\Delta H_{complex}$ $(M^{I}O_2(s) + 2M^{IV}O_2(s) + O_2 \rightarrow M^{I}_2M^{VI}_2O_7(s))$ (kJ mol^{-1})[a]

M^{I} \ M^{IV}	U	Np
Na	-619.4 ± 6.4	-332 ± 12
K	-718.9 ± 6.5	-423 ± 12
Rb	-722.6 ± 6.3	-427 ± 12
Cs	-710.6 ± 6.7	-404 ± 12

[a] An estimate of ± 4.2 kJ mol^{-1} was applied as the uncertainty for the alkali metal dioxide data

With reference to the Lux[79]-Flood[80] theory of an acid-base reaction between the binary oxides it would be expected that the enthalpy of complexation would become more exothermic (a more favourable reaction) with the increasing basicity of the alkali metal monoxide (ie $Na_2O \rightarrow Cs_2O$). This is, in fact, the case for both uranium and neptunium with the alkali metals Na, K and Rb (Tables 3:30 and 3:31). However, there is the anomaly of the enthalpy of complexation to form $Cs_2U_2O_7$ and $Cs_2Np_2O_7$ regardless of whether actinide dioxide (Table 3:31) or actinide trioxide (Table 3:30) is considered. In the case of the dineptunate(VI) this could be conveniently explained by the uncertainty in the accuracy of the standard enthalpy of formation resulting from the high level (∿ 9%) of Np(V) contamination. The result for the diuranate(VI) can not be so readily explained. Even allowing for a possible impurity suggested by the unindexed lines on the Guinier X-ray powder diffraction films the standard enthalpy of formation is so close to previously reported values [93,198,199] that this can not be the reason for the anomaly. It appears, therefore, that this is a real effect not observed previously in other alkali metal actinide oxide series[12]. An explanation might be that steric hinderance between the large caesium and uranium or neptunium atoms renders the formation of $Cs_2U_2O_7$ and $Cs_2Np_2O_7$ less favourable than would otherwise be expected.

The anomaly in the caesium complex is not found in the two series $M^I_2Cr_2O_7$ and $M^I_2Mo_2O_7$ where the enthalpy of complexation is more exothermic for the caesium complex than for the potassium complex, unlike in the uranium and neptunium series. However, since chromium and molybdenum are much smaller than uranium and neptunium, the concept of steric hinderance still holds.

It should be noted that in the series $M^I_2Cr_2O_7$ the enthalpy of complexation to form $Rb_2Cr_2O_7$ is lower than expected and may be worthy of further study.

In considering the series $Na_2Cr_2O_7$, $Na_2Mo_2O_7$, $Na_2W_2O_7$ it can be seen in Table 3:30 that a decrease in the acidity of the trioxide on going down the group renders the complexation reaction less exothermic.

4. SUMMARY

An alternative method of preparation to the classical methods has been used successfully to prepare samples of alkali metal diuranates(VI) and dineptunates(VI) for enthalpy of solution measurements. This route involves the controlled decomposition of well-characterised alkali metal actinyl(VI) triacetates.

The two series of alkali metal actinyl(VI) triacetates with uranium and neptunium were prepared for decomposition to the ternary oxides. With the exception of the two lithium salts, $LiUO_2(CH_3COO)_3$ and $LiNpO_2(CH_3COO)_3$, and caesium uranyl(VI) triacetate, unit cell parameters have been determined for these acetate complexes from X-ray powder diffraction data. In the case of the alkali metal uranyl(VI) triacetates with sodium, potassium and rubidium good agreement was found with published results. However, the β-phase of $KUO_2(CH_3COO)_3$ was not observed. In the analogous neptunyl(VI) series no such data had previously been reported for the potassium, rubidium and caesium salts. A sample of sodium neptunyl(VI) triacetate prepared in this work was used by other researchers for single crystal X-ray diffraction measurements[182]. Unlike the uranium series, two phases of $KNpO_2(CH_3COO)_3$ were observed during this work and these were identified as the α- and β-modifications based on the published data for the uranyl analogue. The X-ray powder diffraction data for $CsUO_2(CH_3COO)_3$ could not be fully interpreted. However, most reflections could be indexed based on a tetragonal cell similar to the neptunyl analogue. The data obtained for the two lithium salts have simply been presented as $\sin^2\theta$ listings to indicate the complexes being isostructural.

A disadvantage of this route to the dineptunates(VI) was found to be the occurence of Np(V) contamination in the alkali metal neptunyl(VI) triacetates which was carried through to the oxides. However, $NaNpO_2(CH_3COO)_3$

was prepared without any such contamination and subsequently decomposed to uncontaminated $Na_2Np_2O_7$. It is felt, therefore, that more careful control in the preparations might result in the isolation of purer samples of the triacetates and thence, oxides. The level of Np(V) contamination in both the triacetate complexes and the ternary oxides has been found to increase gradually with time. The unavoidable delay between sample preparation and measurement of the enthalpy of solution undoubtedly gave rise to higher levels of contamination at the time of the calorimetry. This increasing Np(V) level requires further examination. The mechanism may involve self-radiolysis but this requires confirmation.

Some discrepancies have been found between the experimental X-ray powder diffraction results and the published data for the alkali metal diuranates(VI) and dineptunates(VI). The two dineptunates, $K_2Np_2O_7$ and $Rb_2Np_2O_7$, were found to be isostructural with their diuranate analogues and as such were indexed based on a monoclinic, $P2_1/m$, cell. It was not possible to index all the reflections based on the reported[91] hexagonal, $R\bar{3}m$, cell. Weak reflections which could not be indexed according to literature data were found on the films of $Na_2U_2O_7$, $Rb_2U_2O_7$, $Cs_2U_2O_7$ and $Cs_2Np_2O_7$. However, a listing for $Na_2U_2O_7$ which had been prepared by the classical method of heating stoicheiometric amounts of uranium oxide and sodium carbonate also shows the unindexed reflections found for $Na_2U_2O_7$ during this research. Exact equivalents to some of these unindexed reflections were also visible in the data collected for $Na_2Np_2O_7$. Similarly, unindexed reflections were found to be common to both β-$Cs_2U_2O_7$ and $Cs_2Np_2O_7$. These results indicate that these unindexed weak reflections for all the ternary oxides are a feature of the structure and do not represent any impurity. The experimental listings from this work require comparison with complete listings from previous research.

The enthalpy of formation results obtained for $Na_2U_2O_7$ and β-$Cs_2U_2O_7$ show good agreement with the previously reported data. This is a further indication of the absence of impurities and illustrates the success of the method of preparation. When considering the enthalpy of complexation of binary oxides to form the alkali metal diuranates(VI) and dineptunates(VI), the data show good agreement between the two series. The higher (ie less negative) values obtained in the neptunium series reflect the lower thermal stability[6] of the neptunates(VI) compared with the uranates(VI). There is also general agreement with the results for similar complexes of chromium, molybdenum and tungsten. The enthalpy of formation results for $Na_2Np_2O_7$ confirm the results for the one previous determination[106] for this complex. The results for $K_2Np_2O_7$, $Rb_2Np_2O_7$ and $Cs_2Np_2O_7$ are new data. However, these data should be considered as preliminary results due to the varying levels of Np(V) contamination found following calorimetry.

No further evidence was found for the existence of the controversial ternary oxide, $Li_2U_2O_7$. Similarly, $Li_2Np_2O_7$ was not the product of the decomposition of $LiNpO_2(CH_3COO)_3$.

5. REFERENCES

1. Katz J J and Seaborg G T (eds) — *The Chemistry of the Actinide Elements* Methuen, New York (1957)

2. Fee D C and Johnson C E — *Journal of Nuclear Materials* 99, 107 (1981)

3. Lindemer T B, Besmann T M, and Johnson C E — *Journal of Nuclear Materials* 100, 178 (1981)

4. Mignanelli M A — *The Reactions of Sodium with Urania, Urania-Plutonia and Urania-Plutonia Containing Fission Product Simulants* PhD Thesis, University of Nottingham (1983)

5. Keller C — *Gmelin Hbh Anorg Chem* 8th Edn, (*Thorium*), Erganzungsband, Teil C2, Springer-Verlag, Berlin (1976)

6. Keller C — *MTP International Review of Science (Inorg Chem)* K W Bagnall (Ed), Series 1, Vol 7, 47, Butterworths, London (1972)

7. Keller C — *Gmelin Hbh Anorg Chem* 8th Edn (*Uran*) Erganzungsband, Teil C3, Springer-Verlag, Berlin (1975)

8. Fujino T — *Nihon Genshiryoku Gakkaishi* 20, 19 (1978)

9. Tagawa H and Fujino T — *Nihon Genshiryoku Gakkaishi* 22, 871 (1980)

10. Keller C — *Gmelin Hbh Anorg Chem* 8th Edn (*Transurane*), Band C, 40, Springer-Verlag, Berlin (1972)

11. Cordfunke E H P and O'Hare P A G — *The Chemical Thermodynamics of Actinide Elements and Compounds*, Part 3, *Miscellaneous Actinide Compounds* IAEA, Vienna (1978)

12. Morss L R — *Complex Oxide Systems of the Actinides* Invited Paper for Actinides - 1981, Asilomar Conference Grounds, Pacific Grove, California (1981)

13. Fried S, Hagemann F and Zachariasen W H — *J Am Chem Soc* 72, 771 (1950)

14. Hund F — *Ber Deut Keram Ges* 42, 251 (1965)

15. CODATA (1977) — *J Chem Thermodyn* 10, 903 (1978)

16. Sellers P A, Fried S M, Elson R E & Zachariasen WH — *J Am Chem Soc* 76, 5935 (1954)

17. Roberts L E J & Walter A J *Physico-Chimie du Protactinium* Colloques Internationaux du Centre National de la Recherche Scientifique, No 154, 51, Paris (1966)

18. Winslow G H *High Temp Sci* 3, 361 (1971)

19. Belbeoch B & Boivineau J C *Bull Soc Mineral Cristallogr* 90, 558 (1967)

20. Wagman D D, Evans W H, Parker V B, Schumm R H and Nuttall R L *NBS Tech Note* 270-8, US Dept of Commerce, Washington DC (1981)

21. Hoekstra H R, Santoro A and Siegel S *J Inorg Nucl Chem* 18, 166 (1961)

22. Nakayama Y *J Inorg Nucl Chem* 33, 4077 (1971)

23. Loopstra B O *Acta Cryst* B26, 656 (1970)

24. Siegel S & Hoekstra H R *Inorg Nucl Chem Lett* 7, 455 (1971)

25. Loopstra B O and Cordfunke E H P *Rec Trav Chim Pays-Bas* 85, 135 (1966)

26. Debets P C *Acta Cryst* 21, 589 (1966)

27. Wait E *J Inorg Nucl Chem* 1, 309 (1955)

28. Kovba L M, Vidavskii L M and Lavat E G *Zhur Strukt Khim* 4, 627 (1963)

29. Siegel S, Hoekstra H R and Sherry E *Acta Cryst* 20, 292 (1966)

30. Zachariasen W *Transuranium Elements, Natl Nuclear Energy Ser* Div IV, 14B, II, 1489 (1949)

31. Huber E J Jr and Holley C E Jr *J Chem Eng Data* 13, 545 (1968)

32. Cohen D and Walter A J *J Chem Soc* 2696 (1964)

33. Roberts L E J and Walter A J *AERE Report* R 3624 (1963)

34. Coffinberry A S and Ellinger F H *International Conference on the Peaceful Uses of Atomic Energy* A/CONF/8P/826 USA (1955)

35. Chereau P, Dean G, deFranco M & Gerdanian P *J Chem Thermodyn* 9, 211 (1977)

36. Eyring L — *High Temperature Oxides* A M Alper (Ed), II, 41, Academic Press, New York (1970)

37. Pardue W M and Keller D L — *J Am Ceram Soc* 47, 610 (1964)

38. Flotow H E, Osborne D W, Fried S M and Malin J G — *J Chem Phys* 65, 1124 (1976)

39. Chikalla T D & Eyring L — *J Inorg Nucl Chem* 30, 133 (1968)

40. Asprey L B, Ellinger F H, Fried S and Zachariasen WH — *J Am Chem Soc* 77, 1707 (1955)

41. Morss L R and Fuger J — *J Inorg Nucl Chem* 43, 2059 (1981)

42. Mosley W C — *J Inorg Nucl Chem* 34, 539 (1972)

43. Morss L R, Fuger J, Goffart J and Haire R G — *Actinides - 1981, Lawrence Berkeley Laboratory Report* LBL-12441, 263 (1981)

44. Groh H J, Huntoon R T, Schlea C S, Smith J A and Springer F H — *Nucl Appl* 1, 327 (1965)

45. Baybarz R D — *J Inorg Nucl Chem* 35, 4149 (1973)

46. Baybarz R D — *J Inorg Nucl Chem* 30, 1769 (1968)

47. Green J L & Cunningham BB — *Inorg Nucl Chem Lett* 3, 343 (1967)

48. Copeland J C and Cunningham B B — *J Inorg Nucl Chem* 31, 733 (1969)

49. Turcotte R P and Haire RG — *Proceedings of the 4th International Transplutonium Element Symposium, Baden-Baden, 1975* W Muller and R Lindner (Eds), 267, North Holland/American Elsevier (1976)

50. Baybarz R D, Haire R G and Fahey J A — *J Inorg Nucl Chem* 34, 557 (1972)

51. Ackermann R J & Rauh E G — *J Inorg Nucl Chem* 35, 3787 (1973)

52. Lorenz R, Scherff H L and Toussaint N — *J Inorg Nucl Chem* 31, 2381 (1969)

53. Brown D and Jones P J — *J Chem Soc A* 719 (1967)

54. Bagnall K W, Brown D and Easey J F — *J Chem Soc A* 288 (1968)

55. Keller C — *Gmelin Hbh Anorg Chem Protactinium* Erganzungsband 2, 6, Springer-Verlag, Berlin (1977)

56. Latta R E and Fryxell R E — *J Nucl Mat* 35, 195 (1970)

57. Gronvold F — *J Inorg Nucl Chem* 1, 357 (1955)

58. Roberts L E J and Walter A J — *J Inorg Nucl Chem* 22, 213 (1961)

59. Blank H and Ronchi C — *Acta Cryst* A24, 657 (1968)

60. Hoekstra H R, Siegel S and Gallagher F X — *J Inorg Nucl Chem* 32, 3287 (1970)

61. Hoekstra H R and Siegel S — *J Inorg Nucl Chem* 18, 154 (1961)

62. Bagnall K W & Laidler J B — *J Chem Soc* 2696 (1964)

63. Katz J J and Gruen D M — *J Am Chem Soc* 71, 2106 (1949)

64. Battles J E, Reiskus J W and Shinn W A — *ANL Report* ANL-7575, 77 (1969)

65. Skavdahl R E — *USAEC Report* HW-77906 (1964)

66. Sari C, Benedict U and Blank H — *EUR Report* EUR-3563e (1967)

67. Akimoto Y — *J Inorg Nucl Chem* 29, 2650 (1967)

68. Chikalla T D and Eyring L — *J Inorg Nucl Chem* 29, 2281 (1967)

69. Chikalla T D and Eyring L — *J Inorg Nucl Chem* 31, 85 (1969)

70. Haug H O — *Angew Chem* 79, 993 (1967)

71. Gibby R L, McNeilly C E and Chikalla T D — *J Nucl Mat* 34, 299 (1970)

72. Foex M and Traverse J P — *Rev Int Hautes Temper et Refract* 3, 429 (1966)

73. Wallmann J C — *J Inorg Nucl Chem* 26, 2053 (1964)

74. Haug H O — *J Inorg Nucl Chem* 29, 2753 (1967)

75. Cunningham B B and Wallmann J C — cited in D K Fujita *Thesis, USAEC Report* UCRL-19507 (1969)

76. Peterson J R and Cunningham B B — *Inorg Nucl Chem Lett* 3, 327 (1967)

77. Haire R G and Baybarz R D — *J Inorg Nucl Chem* 35, 489 (1973)

78. Haire R G — *Annual Progress Report, Oak Ridge National Lab* ORNL-5297, 35 (1977)

79. Lux H — *Z Elektrochem* 45, 303 (1939)

80. Flood H and Forland T — *Acta Chem Scand* 1, 592, 781, 790 (1947)

81. Paletta E and Hoppe R — *Naturwissenschaften* 53, 611 (1966)

82. Hagenmuller P, Devalette M and Claverie J — *Bull Soc Chim France* 1581 (1966)

83. Hoppe R and Seeger K — *Z Anorg Allgem Chem* 375, 264 (1970)

84. Keller C, Koch L and Walter K H — *J Inorg Nucl Chem* 27, 1225 (1965)

85. Keller C — *J Inorg Nucl Chem* 27, 321 (1965)

86. Cordfunke E H P and Ouweltjes W — *J Chem Thermodynamics* 13, 187 (1981)

87. Marcon J P, Pesine O and deFranco M — *Rev Internat Hautes Temper et Refract* 9, 193, (1972)

88. Kemmler-Sack S and Rüdorff W — *Z Anorg Allgem Chem* 354, 255 (1967)

89. Gebert E, Hoekstra H R, Reis A H Jr and PetersonSW — *J Inorg Nucl Chem* 40, 65 (1978)

90. Tso T C, Brown D, Judge AI, Holloway J H and Fuger J — *J Chem Soc, Dalton Trans* 1853 (1985)

91. Hoekstra H R and Gebert E — *J Inorg Nucl Chem* 39, 2219 (1977)

92. Kovba L M — *Soviet Radiochem* 14, 746 (1972)

93. Cordfunke E H P and Loopstra B O — *J Inorg Nucl Chem* 33, 2427 (1971)

94. Van Egmond A B and Cordfunke E H P — *J Inorg Nucl Chem* 38, 2245 (1976)

95. Van Egmond A B — *J Inorg Nucl Chem* 38, 2105 (1976)

96. O'Hare P A G, Flotow H E and Hoekstra H R — *J Chem Thermodynamics* 13, 1075 (1981)

97. Kovba L M and Trunova V I — *Soviet Radiochem* 13, 796 (1971)

98. Cordfunke E H P, Van Egmond A B and Van Voorst G — *J Inorg Nucl Chem* 37, 1433 (1975)

99. Kovba L M — *Russ J Struct Chem* 13, 428 (1972)

100. Hauck J — *Z Naturforschung* 28b, 215 (1973)

101. Hauck J and Rosenhauer M — *Z Naturforschung* 31b, 1053 (1976)

102. Kovba L M — *Russ J Inorg Chem* 16, 1639 (1971)

103. Van Egmond A B — *J Inorg Nucl Chem* 38, 1649 (1976)

104. Pages M, Nectoux F and Freundlich W — *Radiochem Radioan Lett* 7, 155 (1971)

105. Keller C and Seiffert H — *Angew Chem Intern Ed* 8, 279 (1969)

106. Tso T C, Brown D, Judge A I, Holloway J H and Fuger J — *11eme Journee des Actinides* Jesolo Lido, Italy, Paper 6, May 25-27 (1981)

107. Keller C and Seiffert H — *Inorg Nucl Chem Lett* 5, 51 (1969)

108. Keller C, Koch L and Walter K H — *J Inorg Nucl Chem* 27, 1205 (1965)

109. Hoekstra H R and Gebert E — *Inorg Nucl Chem Lett* 14, 189 (1978)

110. Keller C — *Gmelin Hbh Anorg Chem, Protactinium* Erganzungsband 2, 17, Springer-Verlag, Berlin (1977)

111. Iyer P N and Smith A J — *Acta Cryst* B27, 731 (1971)

112. Bartram S F and Fryxell R E — *J Inorg Nucl Chem* 32, 3701 (1970)

113. Ippolitova E A, Kovba L M, Simanov Yu P, and Muraveva S A — *ANL-Trans-33* 53 (1961)

114. Chamberland B L — *Inorg Chem* 8, 1183 (1969)

115. Efremova K M, Ippolitova E A and Simanov Yu P — *ANL-Trans-33* 59 (1961)

116. Hoekstra H R and Siegel S — *J Inorg Nucl Chem* 26, 693 (1964)

117. Bachelet M, Cheylan, Douis and Goulette — *Bull Soc Chim France* 441 (1955)

118. Vidavskii L M, Kovba L M, Ippolitova E A & SpitsynVI — *ANL-Trans-33* 70 (1961)

119. Allpress J G, Anderson J S and Hambley A N — *J Inorg Nucl Chem* 30, 1195 (1968)

120. Vidavskii L M, Kovba L M and Ippolitova E A — *ANL-Trans-33* 75 (1961)

121. Val'tsev V K — *Soviet Radiochem* 9, 694 (1967)

122. Spitsyn V I, Ippolitova E A, Efremova K M and Simanov Yu P — *ANL-Trans-33* 142 (1961)

123. Jayadevan N C, Singh Mudher K D and Chackraburtty D M — *BARC-726* (1974)

124. Toussaint C J and Avogadro A — *J Inorg Nucl Chem* 36, 781 (1974)

125. Prins G and Cordfunke EHP — *J Less-Common Metals* 91, 177 (1983)

126. Kovba L M — *Soviet Radiochem* 12, 486 (1970)

127. Kovba L M — *Russ J Inorg Chem* 16, 1639 (1971)

128. Hauck J — *J Inorg Nucl Chem* 36, 2291 (1974)

129. Chernyaev I I (Ed) — *Complex Compounds of Uranium* 97, Oldbourne Press, London (1966)

130. Kovba L M and Golubenko AN — *Russ J Struct Chem* 1, 367 (1960)

131. Efremova K M, Ippolitova E A and Simanov Yu P — *ANL-Trans-33* 65 (1961)

132. Greaves C, Cheetham A K and Fender B E F — *Inorg Chem* 12, 3003 (1973)

133. Anderson J S — *Chimia* 23, 438 (1969)

134. Efremova K M, Ippolitova E A and Simanov Yu P — *ANL-Trans-33* 44 (1961)

135. Ippolitova E A, Efremova KM Orlinkova O L and Simanov Yu P — *ANL-Trans-33* 52 (1961)

136. Van Egmond A B — *J Inorg Nucl Chem* 37, 1929 (1975)

137. Morss L R, Fuger J and Jenkins H D B — *J Chem Thermodynamics* 14, 377 (1982)

138. Lorenz A (Ed) — *IAEA Report* INDC(NDS)-127/NE (1981)

139. Walton G N — *Glove Boxes and Shielded Cells for Handling Radioactive Materials* Butterworths, London (1958)

140. D'Eye R W M and Wait E — *X-Ray Powder Photography in Inorganic Chemistry* 43, Butterworths, London (1960)

141. Bagnall K W and Freeman JH — *J Chem Soc* 4579 (1956)

142. Marples J A C and Shaw J L — *UKAEA Report* AERE-R5210 (1966)

143. Nelson J B and Riley D P — *Proc Phys Soc* 57, 160 (1945)

144. Guinier A — *X-Ray Crystallographic Technology* 113, Hilger and Watts, London (1952)

145. Guinier A — *X-Ray Diffraction in Crystals, Imperfect Crystals and Amorphous Bodies* 2, Freeman, San Francisco and London (1963)

146. Hindman J C, Magnusson L B and LaChapelle T J — *The Transuranium Elements, G T Seaborg, J J Katz and W M Manning (Eds)* Paper 15.2, 1039, McGraw-Hill, New York (1949)

147. Hagan P G and Cleveland JM — *J Inorg Nucl Chem* 28, 2905 (1966)

148. Knoll G F — *Radiation Detection and Measurement* Wiley, New York (1979)

149. Rogers F J G — *UKAEA Report* AERE-R 8005 (1976)

150. Chanda R N and Deal R A — *Idaho Nuclear Corp, Catalogue of Semiconductor Alpha-Particle Spectra* IN-1261, Physics TID-4500 (1970)

151. Kilday M V — *J Research NBS (US)* 85, 467 (1980)

152. Fuger J — *1965, 1966 Annual Reports EURATOM - University of Liege Research Contract* 011-64-6 TPUB (1965) (1966)

153. — *LKB 8700-1 Precision Calorimetry System, Instruction Manual* LKB-Produketer AB, Sweden

154. US Bureau of Standards — *Certificate and Recommendations for Use of Tris (Hydroxymethyl) Aminomethane (Batch 724a) as Calorimetric Standard* Provisional Draft (1971)

155. Fuger J, Spirlet J C and Muller W — *Inorg Nucl Chem Lett* 8, 709 (1972)

156. Fuger J, Brown D and Easey J F — *J Chem Soc A* 2995 (1969)

157. Sanner S and Wadso I — *Science Tools* 13, 1 (1966)

158. Hill J O, Jeklund G O and Wadso I — *J Chem Thermodynamics* 1, 111 (1969)

159. Gunn S R — *J Chem Thermodynamics* 2, 535 (1970)

160. Morss L R — *J Phys Chem* 75, 392 (1971)

161. — *Atomic Weights of the Elements 1979* N E Holden (Ed) *Pure Appl Chem* 52, 2349 (1980)

162. Youden W J — *Statistical Methods for Chemists* 18-20, Wiley, New York (1968)

163. Faires R A and Boswell GGJ — *Radioisotope Laboratory Techniques* 108, Butterworths, London (1981)

164. CODATA — *Recommended Key Values for Thermodynamics, CODATA Bull* 28, (1978)

165. Parker V B, Wagman D D and Garvin D — *NBS Report* NBSIR 75-968 (1976)

166. Oetting F L, Rand M H and Ackermann R J — *The Chemical Thermodynamics of Actinide Elements and Compounds, The Actinide Elements* IAEA, Vienna

167. Fuger J and Oetting F L — *The Chemical Thermodynamics of Actinide Elements and Compounds* Part 2, *The Actinide Aqueous Ions* IAEA, Vienna (1976)

168. Holley C E, Rand M H and Storms E K — *The Chemical Thermodynamics of Actinide Elements and Compounds, The Actinide Carbides* IAEA, Vienna

169. Potter P E, Mills K C and Takahashi Y — *The Chemical Thermodynamics of Actinide Elements and Compounds, The Actinide Pnictides* IAEA, Vienna

170. Grønvold F, Drowart J and Westrum E F Jr — *The Chemical Thermodynamics of Actinide Elements and Compounds, The Actinide Chalcogenides* IAEA, Vienna

171. Flotow H E and Yamauchi S — *The Chemical Thermodynamics of Actinide Elements and Compounds, The Actinide Hydrides* IAEA, Vienna

172. Chiotti P, Akhachinskij V V, Ansara I and Rand M H — *The Chemical Thermodynamics of Actinide Elements and Compounds, The Actinide Alloys* IAEA, Vienna

173. Potter P E, Holleck H and Spear K E — *The Chemical Thermodynamics of Actinide Elements and Compounds, Selected Ternary Systems* IAEA, Vienna

174. Hubbard W N, Fuger J, Oetting F L and Parker V B — *The Chemical Thermodynamics of Actinide Elements and Compounds* Part 8, *The Actinide Halides* IAEA, Vienna (1982)

175. Rand M H, Ackermann R J, Grønvold F, Oetting F L and Pattoret A — *The Chemical Thermodynamics of Actinide Elements and Compounds, The Actinide Oxides* IAEA, Vienna

176. Wadso I — *Science Tools* 13, 33 (1966)

177. — *Int Crit Table* Vol III, McGraw-Hill, New York (1928)

178. Jackson N and Short J F — *UKAEA Memo* AERE-M 444 (1959)

179. Jones L H — *J Chem Phys* 23, 2105 (1955)

180. Koch G — *Gmelin Hbh Anorg Chem, Transurane* Band 4C, 235, Springer Verlag, Berlin (1972)

181. Ryan J L and Keder W E — *Advances in Chemistry, Series* 71, 335 (1967)

182. Alcock N W, Roberts M M and Brown D — *J Chem Soc, Dalton Trans* 33 (1982)

183. Meyer R J — *Gmelin Hbh Anorg Chem,* 24, *Rubidium* 228, Springer-Verlag, Berlin (1937)

184. Zachariasen W H and Plettinger H A — *Acta Cryst* 12, 526 (1959)

185. Fankuchen I, cited in Ferrari A, Cavalca L and Tani M E — *Gazz Chim Ital* 89, 1534 (1959)

186. Ferrari A, Cavalca L and Tani M E — *Gazz Chim Ital* 89, 1534 (1959)

187. Henry N F M, Lipson H and Wooster W A — *The Interpretation of X-Ray Diffraction Photographs* 179, Macmillan, London (1960)

188. Ibid — p 258

189. Hoekstra H R — *J Inorg Nucl Chem* 27, 801 (1965)

190. O'Hare P A G, Hoekstra H R, and Fredrickson D R — *J Chem Thermodynamics* 8, 255 (1976)

191. O'Hare P A G and Hoekstra H R — *J Chem Thermodynamics* 6, 1161 (1974)

192. Fuger J and Brown D — *J Chem Soc A* 841 (1971)

193. O'Hare P A G and Hoekstra H R — *J Chem Thermodynamics* 6, 251 (1974)

194. Herington E F G and Cox J D — *Pure Appl Chem* 40, 399 (1974)

195. Weintraub R, Apelblat A and Tamir A — *J Chem Thermodynamics* 14, 887 (1982)

196. Parker V B — *NBS Report* NBSIR 80-2029 (1980)

197. Parker V B — *NBS Report* NSRDS-NBS 2 (1965)

198. Cordfunke E H P, Muis R P, Ouweltjes W, Flotow H P and O'Hare P A G — *J Chem Thermodynamics* 14, 313 (1982)

199. O'Hare P A G — *Communication to J Fuger* (1984)

200. Fuger J — *Personal Communication* (1982)

201. Wagman D D, Evans W H, Parker V B, Halow I, Bailey S M and Schumm R H — *NBS Tech Note* 270-4, US Dept of Commerce, Washington DC (1969)